Departament de Psicologia Bàsica

Facultat de Psicologia, Universitat de Barcelona

TRACING FUNCTIONAL BRAIN ARCHITECTURE:

A COMBINED fMRI-DTI APPROACH

(Traçant l' arquitectura cerebral funcional combinant imatges de ressonància magnètica funcional i de difusió)

Resum Tesi Doctoral

Doctorant: Estela Càmara Mancha

Director: Dr. Antoni Rodríguez Fornells

Programa de Doctorat Ciència Cognitiva i Llenguatge

Bienni 2003-05

Barcelona, Juliol 2008

Visc la meva vida en cerceles creixents

que s' estenen sobre les coses

Tal volta l'últim no podré perder-lo;

Vull intentar-ho tanmateix.

(Rainer Maria Rilke*)*

Dels meus pares,

per a tu.

Agraïments

Per a tu Toni. Per a tu Cuni, per a tu QQ, per a tu Ruth. Pera a tu Anna, per a tu Josep, per a tu Lluís. Para ti Diana, para ti Núria, per a tu Julià, para ti Azadeh. Per a tu Irene, per a tu Xavi, para ti Jose. Für Dich Thomas. Für Dich Nils, für Dich Claus Tempelmann. Für Dich Ulrike, für Dich Wido. For David Norris. Per a tu Josep Maria, Sopena, per a tu Elizabeth Gilboy, per a tu Elisabet Tubau, per a tu Joan López, per a tu Joan Sansa, per a tu Josep Batista-Trobalón, per a tu José Antonio Aznar, per a tu Miquel Serra, per a tu Mònica Sanz, per a tu Salvador Soto, per a tu Núria Sebastián. Per a tu Agnès, per a tu Llorenç. Per a tu Jesús Pujol, per a tu Carles Soriano, per a tu Àngel Moreno. Per a tu Carles Falcón. Per a tu Thais, per a tu Mireia, per a tu Marta, per a tu Laia. Per a tu Dani, per a tu Vicenç. Per a tu Nia. Para ti Javi, per a tu Eli. Per a tu Sergio, per a tu Persi. Para ti Alberto, per tu Judit. Pour toi Mario. Para ti mama, para ti papa, per a tu Isra, per a tu Aida. Para ti yayo Antonio, para ti yayo Juan, para ti yaya Antonia, para ti yaya Maria. Para ti tita Maria José, para ti tita Antoñita, para ti Pepe. Per a tu Joan, para ti Eugenio. Para ti Sergio, para ti Jordi, para ti Virginia, para ti Hugo. Para ti Marta, per a tu Oriol, para ti Carol, para ti Jordi. Per a tu Vera, per a tu Koro.

Per l' amistat, per l' ajut, per la paciència, per la creença, perquè va ser possible. Per allò que és complicat, per allò que és fàcil, per les argumentacions científiques. Pels tes, pel vi, per les cerveses i les foundues, pels cafès. Pel que vam fer malament, pel que seguirem fent. Correcte. Per les desinhibicions. Per les nits sense dormir. Per Barcelona, perquè està Magdeburg, pels dies a New York. Pels viatges que compartirem. Per les mil tesis, per la sinapsi que comença i acaba igual. Per les anàlisi

exploratòries, per seguir descubrint. Perquè vull ser Val Val i també Met Met. Perquè vull ser com tu. Pel que vam deixar, pel que vam superar. Per l'optimisme. Pel rebut. Pels concerts de vibràfons. Pel caos i la planificació. Per intentar-ho. Por las setas de roble. Pels viatges, pels rejections, pel risk-seeking. Pel Matlab i el SPM. Perquè les probabilitats augmentin, però les significacions també. Per les mil feines i les rule violations amb underlying. Pels mils papers, perquè la biblioteca està plena de llibres. Pels dubtes, pels bailoteos, per les borratxeres, per les liades, pel carpe diem, pels connectors. For the marmotha 's day!. Pels dibuixos del Toni, pels mojitos i les illes desertes. Pels seminaris, pel donar sense esperar rebre. Per les beques alemanyes i les catalanes. Per les hores de biblioteca compartides. Pel cheese and wine i pel time to smile. Per les bones nits, pels sweet dreams. Per les coses importants, pels capritxos, per les coses especials. Per la funció, per l'estructura, per seguir somiant. Per la sort. Per les ressos.Per seguir construint. Per les noves agendes. Pel que som, pel que tenim. For the neurogenetic travel agency. Per la dispersió, pels gin-tònics i pels conflictes. Pel no saber escriure. Per seguir pescant, per les bogeries i pels moments tristos. Per les últimes oportunitats. Per les festes, per Rocafort, pels mil sopars. Per la integració. Pel tot és possible del papa i pels pastissos de la mama. Per tot el que he après, per comprendre. Per escoltar el mar i caminar com a fi i no com a medi, pels records de la caixa de les coses importants. Per les mirades.

Porque algo viene de antes, y sigue después y sigue...

Pel meu director de tesi, el Dr. Antoni Rodríguez-Fornells, pel Prof. Thomas Münte, pels meus amics, pels meus companys, per la meva família. Perquè sempre esteu allà.

Perquè m' encanta.

Per les dues tesis,

per la que llegeixen, i per la que llegim.

Moltíssimes Gràcies

Contents

Preface

Current views in cognitive neuroscience assume that many high level cognitive functions, such as learning, language, or memory are anatomically widely distributed across the whole brain, interacting and overlapping with different large-scale functional systems. These functional specific brain networks are believed to be implemented in the brain by the segregation of different brain regions, that is, groups of neurons or cortical columns with common functional properties. It is the integration of these distal segregated regions, which might define the different cognitive processes. Moreover, these regions are also connected by the presence of specific neural pathways, which permits the information flow between areas. The lack of an anatomical support of these networks makes a direct functional connection biologically impossible. Indeed, unique afferent and efferent connections might define the connectivity patterns used to convey information to other cortical and subcortical regions. In this framework, it is the integration of the distributed neural network, linked anatomically and functionally in a precise way, which largely may define the brain's function.

The present dissertation is devoted to the study of how functional and structural information is integrated in the human brain by using in vivo and non invasive magnetic resonance imaging (MRI). More concretely, by combining functional MRI and diffusion tensor imaging (DTI) information, this dissertation aims to examine possible functional and micro-structural interactions in the human brain in order to reach a better understanding of the organization and dynamics of the distributed neural systems that subserve neural functions and human behaviour.

In *Chapter 1* the current main approaches used to characterize brain function and brain micro-structure are described. Derived from this introduction, five main approaches are proposed to investigate different aspects of brain dynamic and organization. These are summarized in five experiments on which we will focus in the next chapters.

Chapter 2 responds to the standard univariate functional MRI approach, in which regionally specific effects are investigated. In this chapter, differences in functionally specialized areas are investigated using a reward-related task. This experiment is part of a big genetic project which has been developed in collaboration with the University of Magdebug and the Universtity of Tubingen (funded bv the VolkswagenStifftung Cognitive Neuroscience program). In this project, a large sample of 48 Spanish students (genetically characterized in several polymorphisms related to four dopaminergic genes) participated in a large neuroimaging protocol (including, electroencephalography, structural and functional MRI). MRI scanning was conducted in the Center of Advance Imaging (CAI, University of Magdeburg). In the first chapter, we report the effect interindividual variability in the dopaminergic system associated with genetic polymorphisms in reward processing.

Chapter 3 goes a step further. The sole consideration of local regional activation is not enough to understand brain dynamics, as brain regions do not work in isolation. Thus, the cortical brain supporting a single function may involve many specialized regions whose union is modulated by the functional integration among them. With this proposal in mind, *Chapter 3* introduces a new perspective to the reward processing question, revealing a differential pattern in the processing of positive and negative outcomes due to differences in interregional functional connectivity.

Chapter 4 presents the results of the work carried out during my research training in the Klinik für Neurologie II, Otto-von-Guericke-Universität Magdeburg, based on diffusion tensor imaging. This chapter aims to highlight the basics of the DTI technique. It brings new considerations to comparative longitudinal studies with voxel-based analysis by revealing the patterns of variation of white matter with age. More concretely, it proposes a new mask procedure in order to distinguish between micro-structural and global age-related changes.

Once diffusion is introduced as a potential technique to study micro-structural brain organization, the next point to investigate is the interrelation between functional and structural information. With this objective, *Chapter 5* is focused on the neurophysiological coupling between functional and structural properties by using a new combined functional MRI-DTI approach applied to the previously used reward-related task.

Nevertheless, it remains to be determined to what extent these functional-structural correlations interact with cognitive or behavioural performance measures. In particular, the similarity of the functional patterns observed with the micro-structural neural correlates associated suggests a tentative link for coupling neural activity at functional and structural level.

Chapter 6 is devoted to the study of the interrelation between micro-structural white matter and individual differences in performance. DTI has emerged as a potentially powerful method for describing anatomical connectivity. According to the functional-structural relationship, structural individual differences might also be able to explain differences in cognitive or behavioural performance measures. In this chapter, the correlation of true and false memory retrieval with micro-structural properties of

different white matter tracts is reported. The implication of white-matter structural differences is then highlighted as a fundamental key to the understanding of individual variations in cognitive functions.

Finally, *Chapter 7* gives an overview of the results presented. This chapter emphasizes the importance of integrating different brain levels in which functional and structural information interact with biological and performance variables. These levels include a combination of neurological, biological, psychological, physical and engineering factors, which, among others, are all necessary to the study of brain processing.

This dissertation should not be considered as a treatise on functional and structural integration but rather as a launching point in order to begin to understand human functional and structural brain connectivity.

Chapter 1

1. Introduction

1.1. From neural to hemodynamic Activity

Functional MRI (fMRI) is currently the most widely used neuroimaging method for brain mapping. The capacity to map brain functions non-invasively in vivo with fMRI has been critical for the success of cognitive neuroscience in the past decade. Nevertheless, the exact origin of the critical correlation between the physiological basis of the fMRI signal and neural activity still remains unclear.

The MR signal can be made sensitive to local changes in the oxygenation of the blood (Blood Oxygenation Level Dependent effect, BOLD), which increases in activated parts of the brain (Ogawa, Lee, Nayak, and Glynn, 1990). Because neural activity consumes energy substrates, maintaining an adequate energy supply requires that an increase of blood flow occurs in the regions of the brain that are active.

The energy demands of the brain, or the cerebral metabolic rate (CMR), is usually referred in terms of oxygen utilization ($CMRO_2$). This reduction is possible because nearly a ca. 90% of the glucose (5 mg $kg^{-1}min^{-1}$) is aerobically metabolized, and thereby the amount of oxygen consumption is practically proportional to the CMR of glucose utilization and proportional to the neural activity. Although the brain represents only 2% of the body weight, it receives 15% of the cardiac output, 20% of total body oxygen consumption, and 25% of total body glucose utilization (Buxton, 2002). Moreover, the oxygen consumption is four times greater in grey than in white matter. Accordingly, the

density of vascularization is not uniform across layers, in particular denser vascularization is observed where de highest concentrations of neural cell bodies are located.

Thus, activity dependent changes in local deoxyhemoglobin levels are thought to result from changes in oxygen extraction, blood flow and blood volume regulation within the brain, all of which change in relation to several types of neural activity (Buxton, Wong, and Frank, 1998) (Figure 1.1).

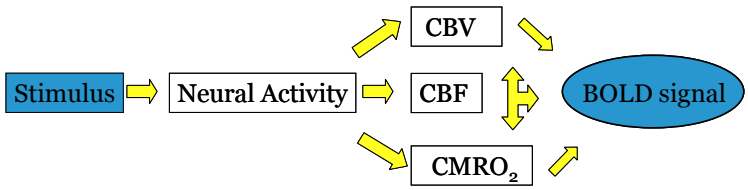

Figure 1.1: Neurovascular coupling. Schematic of the transformation of neural activity evoked by a stimulus to a hemodynamic response resulting in a BOLD signal.

Indeed, the intrinsic spatial sensitivity of the MR-signal to detect local changes in perfusion[1] and metabolism, provides the basis to map patterns of activation in the human brain. For a long time, the oxygen sensitivity of the MR signal from blood has been known. In particular, Thulborn et al. (Thulborn, Waterton, Matthews, and Radda, 1982) demonstrated that the T2 signal decay was strongly dependent on the oxygenation of the haemoglobin. Later, Ogawa et al. (Ogawa et al., 1990) observed that rodent brains at high-magnetic field strengths (7 Tesla) showed MR signal changes related to blood oxygenation in regions in the vicinity to local blood vessels. More importantly, the MRI signal around veins decreased when the oxygen content of the

[1] Perfusion is an indirect measure of the irrigation of the tissue via blood (the volume of blood that travels through a tissue mass over time).

inspired air was reduced, but the effect was inverted when the oxygen was returned to normal values. The reduction in the signal observed was extended in the tissue space around the vessels and not constrained to the blood itself. These results suggested that the T2* decay was affecting both intravascular and extravascular spaces.

Further experiments demonstrated that the same effects were found in an ischemia model, in which a reduction of T2* with decreasing oxygenation of the blood was observed (Turner, Le, Moonen, Despres, and Frank, 1991). It was in 1992 when the first functional MRI results in the human brain after visual stimulation were obtained, using both an inverted recovery and gradient-echo EPI sequence in 1.5 Tesla MRI scanner (Kwong et al., 1992; Turner et al., 1991).

Ogawa et al. (Ogawa et al., 1990) replicated these findings after observing changes in fMRI gradient-echo signal resulting from long duration visual stimulation. The fact that a signal increase was found after activation unexpectedly suggested that blood was more oxygenated with activation. Further experiments resolved this controversy. Deoxyhemoglobin produces magnetic field gradients around and through the blood vessels inducing a decrease in the MR signal. However, increases in the synaptic activity in the brain give rise to increase in the local cerebral blood flow, which increase much more than does the metabolic oxygen consumption. The result is that an increase in the oxygenated blood decreases the ratio of deoxyhemoglobin present and therefore the magnetic field distortions around the blood decrease. Thus, this change in susceptibility due to activity dependent changes in local deoxyhemoglobin levels, produces an increase in the local magnetic resonance signal and induces the BOLD signal in functional magnetic resonance imaging (Figure 1.2).

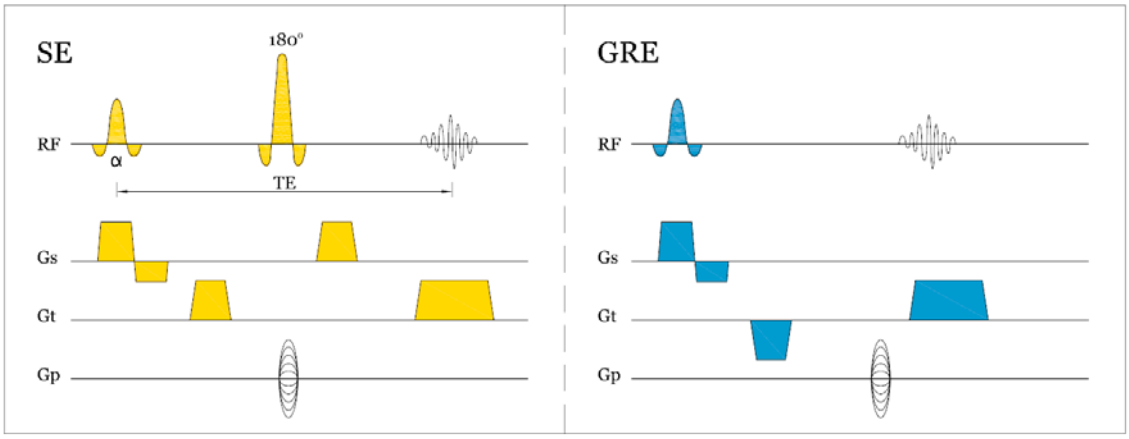

Figure 1.2: Schematic Spin-echo (SE) and gradient echo (GRE) pulse sequences. Both sequences are sensitive to BOLD signal changes. The GRE sequence does not include an 180° refocusing pulse or its accompanying slice selection gradient and therefore the TE (echo time) can be shorter.

The hemodynamic response begins with an initial short dip of the BOLD signal and then shows a steep increase, with a maximum between 4-6 s after the onset of neural activity. The hemodynamic response to a given stimulus can last between 20 and 30 s until complete return to a baseline level, but this pattern can vary between regions and subjects (Aguirre, Zarahn, and D'Esposito, 1998). The initial dip in the BOLD response is thought to reflect a local increase in oxygen consumption that likely reflects an increase in neural activity (Malonek et al., 1997). This effect should be spatially highly specific, but it is unfortunately quite inconsistent across studies. Such a discrepancy might be due to the fact that the amplitude of the initial dip is much smaller than the main BOLD signal. It is necessary to use high magnetic fields in order to enhance the signal-to-noise ratio and observe the effect (Yacoub et al., 2001).

Nevertheless, a major concern in the expanding field of functional MRI has been the absence of a quantitative link between BOLD signal and neural responses. Thus, Hegger et al. (Heeger, Huk, Geisler, and Albrecht, 2000) and Rees et al. (Rees, Friston, and Koch, 2000) provided the first direct evidence that fMRI responses were proportional to firing rates. Later, by simultaneously measuring and comparing local

field potential and multi-unit neural activity, Logothetis et al. (Logothetis, Pauls, Augath, Trinath, and Oeltermann, 2001; Logothetis, 2003) claimed that the local field potentials (LFP) were a slightly better predictor than multi-unit activity (MUA)[2] for the fMRI signal. From these results, Logothetis therefore concluded that the BOLD signal mainly measures the input and processing of neural activity within a region and not the output signal transmitted to other brain regions (Logothetis, 2003). Importantly, Mukamel et al. (Mukamel et al., 2005) after recording the single unit activity and local field potentials in auditory cortex of two neurosurgical patients and compared them with the functional MRI signals of eleven healthy subjects during the presentation of identical movie segment, demonstrated that functional MRI signals could provide a reliable measure of the firing rate of human cortical neurons (but see Goense and Logothetis, 2008).

1.2. Brain segregation and brain integration

Since the early anatomic theories of Gall, the identification of a particular brain region with a specific cognitive function has become a central topic in neuroscience. Indeed, the major goal of functional MRI analysis is to capture the BOLD signal associated with a particular task-related neural activity and maps it into a particular brain localization. Functional segregation is achieved by identifying brain regions that are more activated by one task than another.

[2] MUA and LFA reflect the dynamic interaction of different mechanisms. In particular, MUA reflects mostly the output of the neural population, while LFP provides a measure of the weighted average of synchronized dendro-somatic components of the input signal of a neural population.

Serial subtraction methods assume that the increase in neural activity observed in a region is elicited by the successive elaboration of a task by adding separable cognitive components. Based on the same subtraction logic first introduced to psychology by the Dutch scientist Donders, each cognitive component evokes an additional physiological activation that is the same irrespective of the cognitive or physiological activation context. However, it has been proposed that factorial designs are more powerful than subtraction designs in characterizing cognitive neuroanatomy, because they allow for interactions among the cognitive components of a task (Friston et al., 1996a; Mukamel et al., 2005).

Cognitive processes, however, cannot be understood only at the functional regionally specific level, because brain regions do not act in isolation (Mesulam, 1990). In many functional MRI experiments, multiple areas are found to be coactivated during a given task. It is common thus to report that a task evokes simultaneous activity in multiple brain regions. For example, a working memory task triggered activity in the prefrontal and parietal cortex or the classical finger tapping tasks respond to the precentral gyrus contralateral to the movement and to the cerebellum. However, coactivations do not imply that a single function is shared between regions. In a task thereby that involves pressing a button when a flashing light appears on the screen, the motor and the visual cortices should be activated concurrently, even though they perform very different functions. Thus, the cortical brain supporting a single function might involve many specialized regions whose union is modulated by the functional integration among them.

In light of this, two complementary fundamental principles of functional organization, functional integration and functional specialization, appear to be inherent to the human brain. This dissociation is observed in neurologically impaired patients. For

instance, studies of schizophrenic patients have shown an abnormal response in the frontal lobe in some contexts while they present normal activity in others (Price, Crinion, and Friston, 2006). Thus, abnormal functional integration in schizophrenia can be detected from the contextual activity pattern observed. Specifically, the frontal lobes might function normally when they interact with one set of regions but abnormally when they interact with another set (figure 1.3).

In this framework, a complete understanding of brain processing requires both regionally specific activations and regionally specific interactions (see for a review, Camara et al., 2008).

1.3. Functional brain connectivity

One of the fundamental questions in cognitive neuroscience therefore, is to determine how such functionally specialized areas are integrated in a known functional network, and how these interactions depend on the cognitive context. The inherently multivariate nature of functional MRI allows the investigation of how anatomically distant brain regions interact during a specific cognitive task.

Basically, it is assumed that those regions involved in a network should present strongly similar activity patterns among them. Indeed, correlation-based analyses are typically used to infer functional brain connections (Horwitz, Rumsey, and Donohue, 1998; McIntosh et al., 1994). Nevertheless, it is important to bear in mind that neural activity changes within milliseconds but the temporal scale of the hemodynamic response is in the order of seconds. Therefore, a significant correlation simply implies that activity goes up and down together in distant regions.

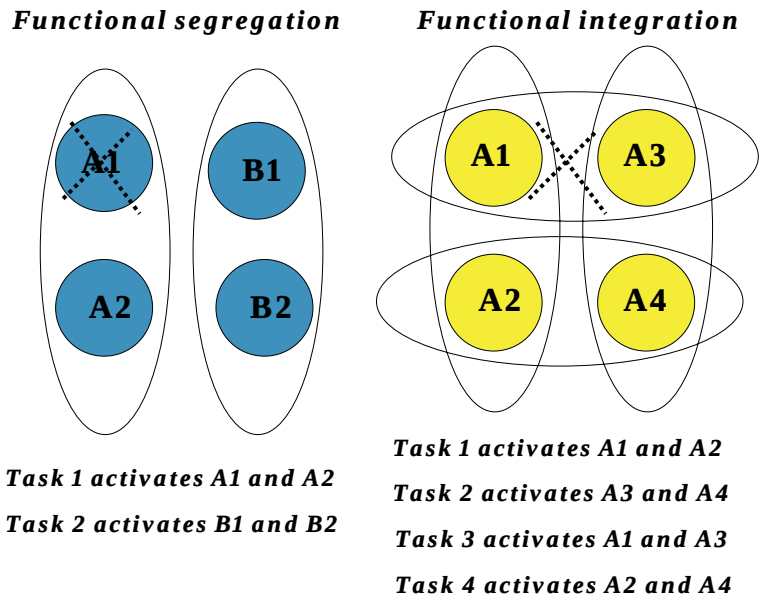

Figure 1.3: Functional segregation and integration. Functional segregation (left side) refers to the segregation of different brain regions according to their function. In this illustration, regions A1 and A2 are activated by task 1, while regions B1 and B2 are activated by task 2. Damage to one region (e.g. A1 indicated by dotted lines) impairs performance on task 1 but not on task 2. Functional integration refers to functions that depend on how regions interact with one another. In the illustration, region A1 is involved in two different tasks: one that depends on its interaction with region A3. Damage to the connections between regions A1 and A3 will disrupt responses in A1 when the task requires regions A1 and A3, but not when the task requires regions A1 and A2 (adapted from Price et al., 2006).

From such temporal correlations, the concepts of functional and effective connectivity were introduced by Friston et al. (Friston, Frith, Liddle, and Frackowiak, 1993) to identify functional networks. The important point of this distinction is based on the fact that functional connectivity refers simply to the presence of correlations between regions, but without considering what could be the causes. Contrary, effective connectivity according to some model of influences, describes differences between correlated regions based on the influences that one brain region exerts on another. Both concepts assume that temporal correlations in the BOLD signal reflect synchronous neural firing in the interacting regions.

1.3.1. Functional Brain Connectivity

Functional connectivity studies describe the patterns of neuronal connections by measuring the degree in which spatially remote neurophysiological events express similar behaviour or statistical independence. For example, in multi-unit electrode recordings, functional connectivity can result from stimulus-locked transient responses evoked by a common afferent input, or might reflect stimulus-induced phasic coupling of neural assemblies, mediated by synaptic connections among brain areas (Gerstein and Perkel, 1969). However, functional MRI connectivity analyses do not make any direct assumption about the nature of the neural activity that may have contributed to the BOLD signal. It could even reveal direct or indirect connections mediated by unknown areas.

Motivated by the idea that spontaneous firing of functional connected neurons might elicit correlation in the BOLD signal, several early explorations of functional connectivity were focused on inter-regional interactions during the resting states. The pioneering experiment in this field was reported by Biswal et al. (Biswal, Yetkin, Haughton, and Hyde, 1995), who demonstrated low frequency fluctuations between the left and right primary motor cortices, when the subject was not explicitly engaged in a cognitive task. Since then a number of resting state networks have been identified in humans (Salvador et al., 2005; Stein et al., 2000; Lowe, Mock, and Sorenson, 1998), and altered patterns of connectivity have been found in patients (Lowe et al., 2002). Then, studies began to investigate the correlation between two time series, during the continuous performance of a cognitive task as assessed in blocked design experiments.

Basically, classical *correlation analysis* assesses the correlation between a small number of pre-selected regions or between voxels of interest,

$$C = \frac{\sum_{i=1}^{n} X_i \cdot Y_i}{\sqrt{\sum_{i=1}^{n} X_i^2 \cdot \sum_{i=1}^{n} Y_i^2}}$$

where X_i and Y_i are two different voxels at the scanning volume i. The correlation field can be introduced as the matrix of all pair-wise correlation coefficients (auto-correlation matrix), indicating those regions coactivated with a particular activation pattern. The auto-correlation matrix can also be transformed and thresholded applying a *t*-statistic test with m = n-1 degrees of freedom:

$$T = \frac{\sqrt{m} \cdot C}{\sqrt{1 - C^2}}$$

If images have previously been smoothed, *p*-values can be obtained and thresholded by applying a random field approach. Those regions showing large correlations are considered functionally connected regions with regard to the specific cognitive task (Rogers, Morgan, Newton, and Gore, 2007). Simple correlation analyses, however are highly sensitive to the shape of the hemodynamic response function, such as onset-delay, time-to-peak, and width which are regional-dependent due to the individual differences in vascular properties across regions (Bandettini and Cox, 2000; Buckner et al., 1996). Due to this sensitivity, correlation analyses are often restricted to block paradigms, which are less sensitive to the shape of the hemodynamic response function.

Coherence-related parameters, in contrast, are invariant to differences in the hemodynamic response function, and consequently they provide a better approach for

studying connectivity in event-related paradigms, which can better exploit the temporal information provided by the signal. Thus, because the fMRI signal has a temporal dimension, the coherence BOLD-related information can be used to guide connectivity mapping. This approach has been used extensively in the measurement of high-frequency oscillations in the EEG waveform after the brain regular oscillatory electrical potential patterns discovered by Berger et al. (Berger et al., 1920; see Marco-Pallares et al., 2008 for a review of data analysis in EEG). Coherence provides a measure of frequency-specific association between two time series, *x* and *y*, at frequency λ domain. It is defined as the cross-spectrum of two time series (f*xy* (λ)), normalized by the power spectrum (f*xx* (λ)) of each time series:

$$Coh_{xy}(\lambda) = \frac{\left| f_{xy}(\lambda) \right|^2}{f_{xx}(\lambda) \cdot f_{yy}(\lambda)}$$

where the cross-spectrum f*xy* (λ) and the power spectrum f*xx* (λ) are defined as

$$f_{xy}(\lambda) = \sum_{u=1}^{n} Cov_{xy}[u] e^{-j \cdot \lambda \cdot u}$$

$$f_{xx}(\lambda) = \sum_{u=1}^{n} Cov_{xx}[u] e^{-j \cdot \lambda \cdot u}$$

and the cross-covariance function is then defined below for stationary time series, x and y as:

$$Cov_{xy}[u] = E\{(x[t] - \mu_x) \cdot (y[t+u] - \mu_y)\}$$

E denotes the expected value, while μ refers to the mean time series value, highlighting the link between the coherence and correlation function.

It is important to point out that the interregional covariance patterns do not allow a precise definition of functionally related networks. For example, two regions A and B may have a large correlation in activity, because they are directly linked anatomically and functionally. Alternatively, however, they might also both receive inputs from a third region C, which would also lead to high correlation values in spite of the fact that no direct interaction between the two regions takes place.

To account for this situation, another statistical approach adopted in functional connectivity studies is to compute partial correlation coefficients. Specific associations between two regions are estimated to control and remove the contributions of pair-wise correlations that might arise due to global or third-party effects (Hampson, Peterson, Skudlarski, Gatenby, and Gore, 2002). However, the selection of the appropriate connections is always model-dependent.

Partial coherence is a statistical parameter equivalent to the partial correlation, but in the time-domain (Sun, Miller, and D'Esposito, 2004), which can be calculated for each of the Fourier frequencies:

$$pcoh_{xy}(\lambda) = \left| \frac{f_{xy}^{-1}(\lambda)}{\sqrt{f_{xx}^{-1}(\lambda) \cdot f_{yy}^{-1}(\lambda)}} \right|^2$$

with f-1j,k (λ) corresponding to the (j,k)th element of the inverted spectral density matrix at frequency λ.

At this point, we have defined a general framework for the estimation of the main linear time/frequency-invariant relationship derived from the time series. In this context, coherence and partial coherence open a new perspective, which allows the detection of interactivity between the nodes of a selected task-related network and across tasks in blocked designs. The use of blocked design experiments clearly permits the distinction between task and rest periods. It has also the advantage of collecting a large number of temporally contiguous data points, which makes computations robust and sensitive to low frequency fluctuations. However, some cognitive processes could not be studied by block designs. For example, in action monitoring tasks aiming at the delineation of error-related activity, reward or in memory tasks trying to differentiate successfully and unsuccessfully remembered items, it is not possible to predict when an error or memory hit will be produced; hence, block-designs are not feasible.

A new approach to characterize functionally interacting regions using event-related functional MRI data was introduced by Rissman et al. (Rissman, Gazzaley, and D'Esposito, 2004) based on the parameter estimates obtained in the context of the general linear model. Parameter estimates reflect how much of the data is explained by each regressor (main regressors are the experimental conditions). Thus, Rissman et al. (Rissman et al., 2004), in accordance with previous electrophysiological and fMRI coherence studies, found that bimanual motor coordination elicited larger correlations between motor regions of the two hemispheres compared to simple motor tasks. The beta series method uses a standard general linear model approach but adapts the model in such a way that separate beta values (general linear model parameter estimates) are obtained in order to modulate activation changes for each component of each individual trial. With this approach, a series of parameter estimates can be extracted from a seed region, correlated across the brain and potentially identify specific networks. Statistical inferences can be made based on the correlation of the magnitude.

First, an arc-hyperbolic tangent transform is applied to normalize the correlation coefficients, which are therefore z- transformed. Finally, the z-tranformed correlation maps are spatially normalized and significance is inferred by applying a group level random effect *t*-test.

Subjects' brains (native space) differ markedly in their macroanatomical structure and consequently a direct comparison between brains is not possible. Normalization is a form of coregistration, which transforms all of the individual high-resolution images into a common stereotactic space (Ashburner and Friston, 1997). The most commonly used stereotactic space is the Talairach space (Talairach and Tournoux, 1988) derived from a single brain of an elderly woman. However, because it comes from a single brain, it is not representative of the population. Probabilistic stereotactic spaces which combine data from many individual brains provide a useful alternative. The Montreal Neurological Institute (MNI) template is the result of averaging 152 T1-weighted brain images after being transformed into the Talairach space.

Other approaches of assessing functional connectivity have been described; in particular, some of them have been focused on the reduction of the number of regions involved in the correlation analysis. As the number of regions that we are interested in comparing increases, the covariance matrix becomes larger and larger and thereby computations become more complex and more difficult to interpret. Indeed, different statistical multivariate approaches have been used to overcome and simplify the model, such as multidimensional scaling, principal component analysis, independent component analysis, or principal least squares. These methods are very attractive in the sense that they do not require any previous hypothesis about the connectivity links of interest.

Singular Value Decomposition, for instance, seeks to reduce the dimensions of the correlation structure to a small number of orthogonal modes, “principal components”, multiplied by weights that vary randomly over time or subject (Worsley, Chen, Lerch, and Evans, 2005). Eigenimages are usually extracted using singular value decomposition (SVD) or related techniques. SVD transforms the original time-series (X), where each column represents a voxel and each row a scan of mean-corrected data, into two sets of unitary orthogonal matrices (*v,u*), and a s diagonal matrix of decreasing singular values, (*t* denotes transposition).

$$[u, s, v] = SVD\{X\}$$

$$X = u \cdot s \cdot v^{t}$$

SVD allows the extraction of eigenvalues and eigenvectors of both $X \cdot X^t$ and $X^t \cdot X$. The first one is proportional to the voxel-by-voxel spatial covariance matrix, while the latter is equivalent to the scan-by-scan temporal covariance matrix. The eigenvalues are the same for both dimensions. That is, column of *v* defines the spatial components, representing a distributed brain system that can be displayed as an image (eigenimage). Column of *u* represents temporal or scan-order patterns accounting for the time-dependent profiles associated with each eigenimage (eigenvariate). Eigenvalues are the singular values squared of the *s* matrix, estimating the relative amount of variance accounted for each principal component, allowing a qualitative assessment of the importance of each eigenimage/eigenvariate. Thus, the first eigenimage expresses the pattern over voxels that accounts for the greatest variability across all the scans, while the first eigenvariate is the temporal pattern that reflects the greatest variability across all voxels. Thus, those voxels with high eigenimage values co-vary together and

consequently are positively correlated. In contrast, voxels with components differing in sign are negatively correlated.

When different methods used to compute functional connectivity are compared, slightly different results or information is obtained. Worsley et al. (Worsley et al., 2005) showed that in practice, correlations are highly sensitive and able to detect focal interactions while SVD are more prone to finding connections between more extensive regions. Nevertheless, the main drawback using SVD is to select the appropriate number of components involved, which should correspond to the number of networks that are of interest during a particular experiment. For instance, in the previously presented example, in which flashes of light were synchronized with hand squeezing, it is reasonable to suppose that two different networks (visual and motor) are playing a different role. More components will lead to a more complete but also more complex description of the system. Therefore, only a few principal components are typically selected and those components that only contribute minimally to the explained variance are neglected. The main advantage of correlation analysis over all other connectivity approaches is that it allows the quantification of the interactions by thresholding the correlations.

Many other studies also have reported the use of fMRI data to assess functional connectivity in healthy subjects during a specific task involving the motor system (Rogers, Carew, and Meyerand, 2004; He and Lian, 2002), language organization (Horwitz and Braun, 2004; Homae, Yahata, and Sakai, 2003; Hampson et al., 2002) and the visual and the auditory systems (Horwitz et al., 2004) or during resting conditions (Jiang, He, Zang, and Weng, 2004; Xiong, Parsons, Gao, and Fox, 1999; Biswal, Hudetz, Yetkin, Haughton, and Hyde, 1997), among others.

1.3.2. Effective connectivity

Effective connectivity refers explicitly to the influence of one neural system on another, either at synaptic (i.e. synaptic efficacy) or population level (Friston et al., 1993). More concretely, it has been proposed that "the [electrophysiological] notion of effective connectivity should be understood as the experiment- and time-dependent, simplest possible circuit diagram that would replicate the observed timing relationships between the recorded neurons" (Aertsen et al., 1991). Indeed, the concept of effective connectivity takes a step further than functional connectivity, because it seeks to describe and quantify the influence of one brain area upon another. Thus, constraining the regions and connections of interest with a theoretical causal model might explain the neural activity patterns. Then, considering the brain as a dynamic system, from which certain physiological parameters can be observed over time (BOLD signal for example) and given particular inputs (experimental perturbations of the system), it is possible to estimate those parameters that yield the dynamics of the underlying states. In the following, we will describe the main three approaches used to capture effective connectivity, namely (i) psychophysiological interactions (ii) structural equation modelling, and (iii) dynamic causal modelling.

In a *psychophysiological interaction* analysis (PPIs), the physiological response in one area of the brain is regressed on activity in all other voxels. Psychophysiological interactions can be understood as the modulation that one cerebral region exerts over another in a specific experimental context. That is, if we relate the activity of one region in terms of another, the slope of this regression reflects the influence of the second area over the first one. Friston et al. (Friston et al., 1997) illustrated this idea in a functional MRI study, in which participants were attending to a visual motion cue. Thus, by combining information about activity in the parietal region, which is assume that mediate attention to a particular stimulus, and information about the stimulus, they

identified regions that respond to that stimulus when activity in the parietal region was activated. Variations in the slope of such regressions model changes between experimental cognitive conditions. These regressors are used then to identify other regions in the brain where activity is significantly coupled with the specific psychological context.

One of the main problems in connectivity analysis is the large number of possible links among regions to be analyzed. It increases exponentially with the number of areas that are involved and it is thereby, extremely difficult to provide unique reliable solutions to connectivity analyses. In virtue of the assumption that the presence of a structural connection makes a functional connection biologically meaningful and more likely to occur, analyses of anatomical connectivity opens a useful tool for restricting the number of functional connections to be analyzed. Additional anatomical information has long been considered as a tool for helping in the analysis and interpretation of functional neuroimaging data. Accordingly, in contrast to psychophysiological interactions, structural equation modelling and dynamic causal modelling constrain the connectivity analysis to a limited number of regions, based on some known anatomical connections or functional systems.

Thus, *structural equation modelling* (SEM) is model-dependent, requiring the a priori specification of an aprioristic anatomical model, which graphically defines those anatomical connections considered functionally relevant (Goncalves and Hall, 2003). The connectivity model not only states which regions are connected one to another but also the direction of the connection. It is important to note that only a small number of regions can be included in such a model, because, otherwise, computational problems arise. Then, SEM estimates the connection strengths (path coefficients) that best predict the inter-regional covariances of the functional imaging data under the given

model. In practice, this is achieved by applying iterative methods that minimize the difference between the observed covariances ($\sum_{obs}$) and the predicted model ($\sum_{pred}$). Thus, the observed covariances are directly calculated by:

$$\sum_{obs} = \frac{X \cdot X^t}{N-1}$$

where X is a p x N matrix, where each column represents a voxel and each row a scan of mean-corrected data. One of the simplest models of effective connectivity is to consider the activation in a region as weighted sum of changes elsewhere. If we consider a model where the variables *X* reflect direct causal implications of a set of independent variables *z*, this can be defined as a set of variables *X* with residual influences *z*.

$$X \cdot I = X \cdot A + z$$

where I corresponds to the identity matrix, and A is a matrix of the unidirectional path coefficients imposed by the model. This reduces *X* to $X = z \cdot (I - A)^{-1}$ and the covariance matrix predicted by the model can be expressed as follows:

$$\sum_{pred} = (z \cdot (I - A)^{-1}) \cdot (z \cdot (I - A))^t = (I - A)^{-1} \cdot B \cdot (I - A)^t$$

where *B* corresponds to the covariance matrix of the residuals *z*. Different SEM approaches may differ in the precise method used for the calculation of the correlation matrix (Horwitz, 2003).

A variety of fitting functions can be applied such as maximum likelihood (ML) or generalized least squares (GLS), the latter is used when non-linear interaction terms are considered.

$$ML = \log(\det(\sum_{pred})) - \log(\det(\sum_{obs})) + trace(\sum_{obs} \cdot \sum_{pred}^{-1}) - p$$

where p corresponds to the number of free parameters. ML follows a $\chi 2$ distribution and can be used to infer statistical significance of the model.

Changes in effective connectivity are usually evaluated in SEM by comparing the fitting between two models. Thus, Mechelli et al. (Mechelli, Penny, Price, Gitelman, and Friston, 2002) for example, used a multisubject network to investigate intersubject variability in functional integration in the context of single word and pseudoword reading. They showed that differences between processing words and pseudowords do not simply lie in the degree of activation in one or more regions of the language system. Rather, such differences can be characterized in terms of context-sensitive interactions among brain areas. SEM also allows to compare changes in connectivity among different groups of subjects, such as patients and normal subjects.

Dynamic Causal Modelling (DCM) shifts the focus from regionally-specific activations to interregional path-specific activations using a dynamic deterministic nonlinear model, in which different expressions of effective connectivity can be derived as special cases of DCM. Unlike SEM, the characterization of the interregional connection between brain areas is based on the rate of change of neuronal activity, and therefore, it does not depend on the units of activity per se, but rather the speed or rate of interregional coupling and how this is modulated by experimental conditions. The basic aim is to model the brain as a dynamic system, which is subject to inputs and produces

outputs in terms of parameters that represent the coupling between unobserved brain states. Thus, inputs modulated by the experimental conditions can either induce neuronal responses in specific anatomical regions, but they might also change effective connectivity by influencing the coupling between nodes.

The main idea is to submit the system to different controlled experimental inputs, which directly generate variation in the outputs. By measuring the responses after perturbing the system, free model parameters can be estimated. Indeed, effective connectivity can be expressed following any nonlinear function characterizing the neurophysiological inputs related to a brain region in relation to other regions. DCM is also supported with a forward model, which transforms the neural responses to a measurable hemodynamic response, the output. The strength of the intrinsic connections infers the speed with which a change in activity in one region causes a change of activity in another region. A positive connection indicated that an increase in activity in one region results in an increase in activity in another region. In contrast, a negative connection assumes that an increase in activity in one region results in a decrease in activity in another. In general, DCM does not restrict the number of connections that can be modelled, consequently a large number of free parameters have to be estimated. Several constraints have to be imposed (for example, the neural activity cannot diverge exponentially to infinite values). A Bayesian framework is an appropriate approach to tackle such an analysis. A complete mathematical explanation of DCM can be obtained from Friston et al. (Friston, Harrison, and Penny, 2003).
Additional approaches for connectivity mapping include multidimensional scaling (Welchew, Honey, Sharma, Robbins, and Bullmore, 2002) and hierarchical clustering (Stanberry, Nandy, and Cordes, 2003). These methods use dissimilarities rather than partial correlations allowing the use of complementary multivariate techniques.

1.4. Anatomical connectivity

Currently, functional connectivity patterns have primarily been examined by using neurophysiological data collected from functional MRI. The pioneers who established structural–functional correlations by combining architectonic and neurophysiological observations in macaque and human brains were Brodmann (Brodmann, 1914) and Vogt et al. (Vogt and Vogt, 1919). Further studies have supported these findings, showing that the borders between cytoarchitectonic areas are functionally relevant. Thus, combining electrophysiological and architectonic studies in experimental animals has demonstrated that response properties of neurons are different at the border of two cytoarchitectonic regions (Luppino, Matelli, Camarda, Gallese, and Rizzolatti, 1991). In fact, currently cytoarchitectonic probabilistic maps represent the most appropriate tool for the precise localization of brain functions as obtained from functional imaging studies (Amunts, Schleicher, and Zilles, 2007).

Recent studies have proposed that at macroscale level, interregional statistical associations in cortical thickness can also reveal functional connectivity information in the human brain (Lerch et al., 2006). Cortical thickness is an indirect composite measurement, which includes the size, density, and arrangement of cortical neurons, neuroglia, and nerve fibers, among others. The human cerebral cortex is a highly folded sheet of neurons in which regionally specific variations exist (Brodmann, 1909; Zilles, zur, Schleicher, and Traber, 1990). Thus, the thickness of the cortex is of great interest in both normal development and neurodegenerative and psychiatric disorders (Fischl et al., 2002). Indeed, by examining a large cortical morphormetric database, Chen et al. (Chen et al., 2008) observed six different morphological patterns in cortical thickness that might be compatible with the intrinsic functional modularity of the brain network (visual, auditory, somatorsensory/motor, frontal/limbic). Importantly, this

study provides the first evidence of a modularized structural organization underlying the functional connectivity pattern of the human brain network and suggests a potential link between brain functional segregation and integration. This might result because cortical thickness and its interregional correlations may reflect the underlying cytoarchitecture and neural connectivity, conserving connections length (Sporns, Tononi, and Edelman, 2000), efficient recurrent processing within modules (Kotter and Stephan, 2003; Sporns et al., 2000), and efficient information exchange between modules (Latora and Marchiori, 2001).

Conversely, cortical thickness analysis is limited to the cortex and therefore cannot be used to examine non-cortical grey matter or white matter connections itself. Anatomical connectivity traditionally refers to the study of the white matter fiber tracks those connecting different brain regions. Importantly, the lack of an anatomical support of these networks makes a direct functional connection biologically impossible. A deeper understanding of white matter pathways is thereby relevant in order to characterize brain connectivity and dynamics.

Dendrites are the branched projections of a neuron that transmit the stimulation received from other neural cells to the cell body. In turn, axons act to conduct the signal to other neurons and allow greater extension of the connections. One neuron has only one axon but the axon may branch out to communicate with other brain regions. Axons with similar destinations frequently form bundles, which form the white matter tracts. According to the regions that these tracks connect, we distinguished U-fibers (connecting adjacent gyri), association fibers (between different lobes) or commissural fibers (between right and left hemisphere). Those connecting cortex and deep-brain regions are called projection fibers.

Long distance cortico-cortical connections for example, are particularly important in high level cognitive processes, such as attention, working memory or consciousness (Dehaene, Sergent, and Changeux, 2003), among others (Sporns et al., 2000). Briefly, cortico-cortico connections can be characterized based on their hierarchical organization, that is forward and backward connections. Forward connections (from a low to higher level), in particular, have sparse axonal bifurcations and are topographically constrained. They typically start in supragranular layers and finish in the layer VI. In contrast, backward connections, which are more abundant, present great axonal bifurcation and more diffused topography. Functionally, forward connections are more active, always eliciting a response given the appropriate pattern of inputs, while backward connections can also be modulatory showing slower dynamics (Salin and Bullier, 1995).

In addition, classical morphometry studies have demonstrated functional-dependent local structural changes in the adult human brain. In particular, Maguire et al. (Maguire et al., 2000; Maguire, Woollett, and Spiers, 2006) suggested anatomical correlates for navigation in the anterior and posterior hippocampus, after comparing taxi drivers with controls. Gaser et al. (Gaser and Schlaug, 2003) found gray matter volume differences in motor, auditory, and visual-spatial brain regions when comparing professional musicians (keyboard players) with a matched group of amateur musicians and non-musicians. On the other hand, Draganski et al. (Draganski, Winkler, Flugel, and May, 2004) showed that learning a complex visuomotor task (jungle training) induced changes in the adult human brain.

Traditionally anatomical connectivity has been studied using histological methods in animals. Different retrograde degeneration tracers, fluorescent retrograde tracers (Keizer, Kuypers, Huisman, and Dann, 1983) or trans-synaptic viral track tracing

techniques (Middleton and Strick, 2001) amongst others have long been used to trace individual axons with great precision. In contrast, the autoradiographic technique (Cowan, Gottlieb, Hendrickson, Price, and Woolsey, 1972) made it possible to delineate fiber pathways on a large scale. The main limitation of the autoradigrophaic technique is that it is restricted to animal experimentation (Beaulieu, 2002).

This has changed with the development in vivo of neuroimaging techniques. Unfortunately, an accurate description of these interactions is not possible to attain because of the complexity of the brain and the great difference in scale resolution between neural and neuroimaging data. Some aspects however, can be overcome by using diffusion tensor imaging.

1.5. Diffusion Tensor Imaging

Specifically, the introduction of diffusion tensor imaging (DTI), a non-invasive technique that is sensitive to water-diffusion properties in the tissue, opens a suitable method for monitoring micro-structural changes, neural architeacture (Beaulieu, 2002) and plasticity-related processes (Tovar-Moll et al., 2007). Diffusion of water molecules in the brain is characterized by random translational motion, (Brownian motion), as a direct consequence of the thermal energy carried by these molecules. This random motion is statistically well described by a diffusion coefficient, derived from Einstein's equation, which is related to the root mean square of the displacement of the molecules over a given time. However, the role of diffusion coefficient is that it depends only on the molecular weight, the temperature and the intermolecular interactions with the medium (actually, in MR imaging it depends also on diffusion acquisition parameters). In this way, knowing about diffusion-driven displacements, it is possible to assess a direct measure of micro-structure, in addition to a reflection of brain tissue integrity.

Nevertheless, it has to be considered that diffusivity is always a function of the window of time used. It means that only over a very short time diffusivity provides local intrinsic viscosity, and consequently local micro-structure patterns. Normally, diffusivity times are relatively long, and depend on the interactions of the diffusing molecules with the cellular micro-structure obstacles. The diffusion coefficient in MR imaging is mostly called apparent diffusion coefficient (ADC) because it is averaged over time and over a voxel volume.

In brain parenchyma structures there are clear boundaries on a microscopic scale, for example axon membranes and myelin sheaths, forcing the diffusion propagation of water molecules in certain preferential directions. In other words, some structures present greater molecular displacements in one direction than others, the diffusion is anisotropic. In contrast, there are molecules which travel almost freely across the medium and are unconstrained by micro-structures, such as in cerebrospinal fluid. In this case the diffusion is isotropic (Figure 1.4).

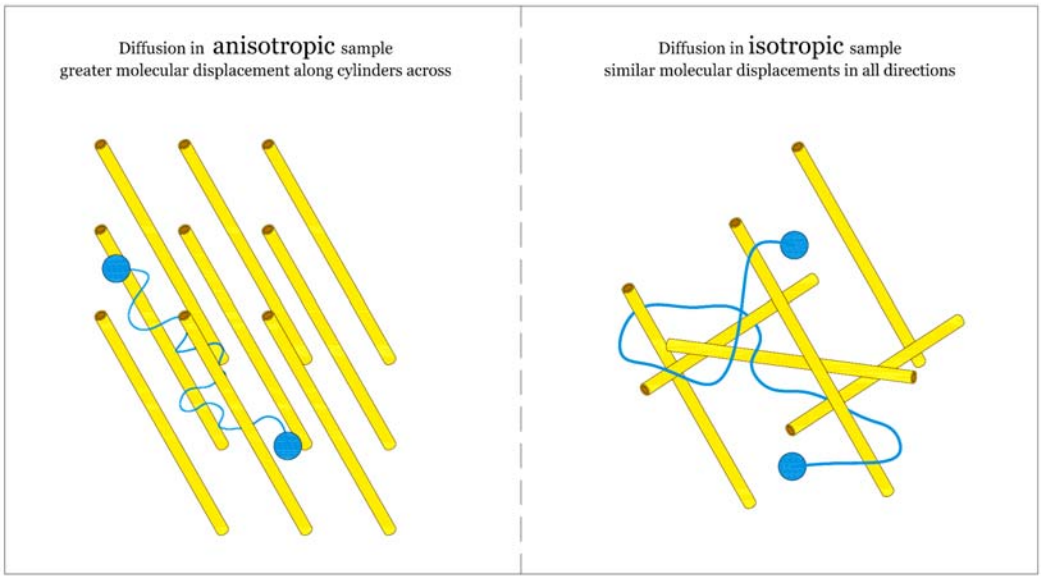

Figure 1.4: An illustration depicting diffusion in two different types of sample, one which has similar molecular displacements in all directions (isotropic diffusion) and the other which has greater diffusion along one direction over another (anisotropic diffusion). The structure surfaces are impermeable in this cartoon for illustrative proposes only (Adapted from Beaulieu et al. 2002).

Using the MR-signal-decaying effect of water diffusion in several directions, (Stejskal et al., 1965) it is possible to obtain diffusion images that allow the assessment of water diffusivity images and consequently obtain several diffusivity parameters (Figure 1.5). Thus, Apparent Diffusion Coefficient (ADC) for instance, expresses the directional average of the diffusion magnitude, and is related to the overall presence of obstacles to diffusion. Other scalar diffusivity indices have been used to characterize fibre architecture, describing how much molecular displacements vary in the space. That is, for instance, anisotropy indexes (e.g. fractional anisotropy (FA), relative anisotropy (RA) among others), which are related to the degree of directional dependency of the diffusion coefficient. These indexes reflect the presence and coherence of oriented structures, because of the dense packing of axons and their inherent axonal membranes that hinder water diffusion significantly perpendicular to the long axis of the fibers (Beaulieu, 2002).

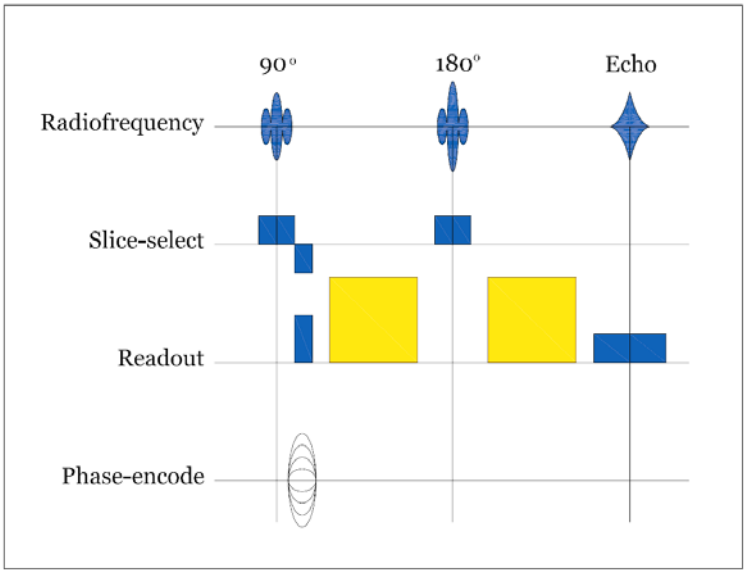

Figure 1.5: Schematic diffusion pulse sequences. Special diffusion weighted gradients (green) are used in order to increase the magnetic field in certain arbitrary directions. The phase of static spins is refocused by 180° RF pulse and the next diffusion weighted gradient. Diffusion spins stays diphase, and thereby diffusion-specific signal decay is obtained.

In particular, Moseley et al. (Moseley et al., 1990) reported the first systematic study of anisotropy water diffusion in the nervous system. They demonstrated that water diffusion was anisotropic in normal white matter of cat brain and spinal cord, while diffusion was isotropic in gray matter. The predominant direction of water diffusivity is linked with the orientation in the space of the structures. Thus, the axonal cytoskeleton of neurofilament and microtubes, and local susceptibility-difference-induced gradient, were confirmed to be the primary source of anisotropy in neural fibers (Beaulieu, 2002; Le, 2003). These explanations however, are clearly an oversimplification of the underlying biological complexity. The diversity of neurons, accompanied with the variability in axon dimensions, the thickness of myelin, extracellular axons, variable membrane permeability, amongst many others, may also play a specific role. In addition, multiple distinct compartments existing in an intra-voxel level where water can diffuse (intra-axonal, inter-axonal, extra-axonal, extra-cellular) and therefore similar diffusion patterns might mirror different tissue compositions.

Given the interest in white matter maturation and demyelinating disease, and because the numerous lipid bilayers of myelin might limit the permeability to water, the hypothesis of myelin related to water diffusion is tentative. Indeed, it has been shown that myelin constitutes a significant barrier to the diffusion of water, and therefore myelin may modulate the degree of anisotropy but its role is minor (Gulani, Webb, Duncan, and Lauterbur, 2001; Beaulieu, 2002). Indeed, volumetric or density white matter estimates can be used as a full-brain approach to measure white matter integrity and evaluate and compare the degree of connectivity in a particular region or in the whole brain between subjects.

1.5.1. Region-of-interest analysis (ROI)

Traditionally, the simplest approach used to compare local anatomical differences is commonly named region-of-interest analysis (ROI) in which a defined region is identified and statistical comparisons are made relating to its size or intensity value with a particular effect under study. Obviously, the crucial point is to delimit the studied region. Then, a mean value on the extension of such region can be extracted, compared between groups and then related to a particular effect.

Some limitations however have to be considered regarding ROI analyses. ROI analyses are restricted to the (few) regions selected for analysis, usually derived from a priori hypotheses. In turn, possible bias might be introduced due to manual or semi-automated definitions of the ROIs. Moreover, the additional averaging over a brain region also reduces spatial resolution, and some biologically meaningful differences that might be detected at the voxel-level might be missed (Virta, Barnett, and Pierpaoli, 1999). Given these concerns, a voxel by voxel comparison between groups of subjects might be an attractive method to investigate local changes.

1.5.2. Voxel-based morphometry (VBM)

Voxel-based morphometry (VBM) allows statistical inferences to be made at voxel-level for the whole brain, by estimating changes in local tissue concentrations and volumes. Some difficulties might appear in this procedure when micro-structural tissue properties are examined at a voxel level, as in structural diffusion data. In this case, identical brain coordinates have to be compared across the whole study population, discarding even mesoscopic structural differences. Thus, the main challenge facing voxel-based diffusion parameter analysis involves meeting the requirements for an optimal matching of the brains being compared. This is, however, usually quite difficult

to achieve. Indeed, traditionally, voxel-based analyses in diffusion data have only been treated as an exploratory tool. The development of complementary tools, bearing in mind the possible artifacts derived from these methodological constraints, converts voxel-based analysis into a very powerful approach also for diffusion data sets.

1.5.3. Fiber Tracking

DTI is currently the only approach that permits the tracking of white matter fibres, in a non-invasive way, through the human brain (Figure 1.6). Tractography is based on the assumption that the main diffusivity direction is aligned with the direction of the axonal fibre dominant within the imaging voxel (Pajevic and Pierpaoli, 1999). Elaborate fibre reconstruction algorithms manage to extrapolate the axonal fibre tracks, tracing the most favourable path between two predictable voxels. However, the complexities of connecting these macroscopic voxel-based vectors arise from the limitations imposed by using a microscopic technique to visualize macroscopic restrictions. Several approaches have been developed in order to make a continuous representation of the track. Many of them are focused on linear propagation algorithms (Conturo et al., 1999), distinguishing them from one another, by the way in which they incorporate the information of the neighbouring voxels. That is, the path is defined by smoothing trajectories or minimizing the noise contributions. In contrast, global energy minimization approaches have also been used in order to find the energetically most appropriate track (Poupon et al., 2000). More complex algorithms use multi cellular compartment models or insert aprioristic anatomical knowledge, in order to improve the connectivity patterns obtained (Mori and van Zijl, 2002). Nevertheless, the main problem in fiber reconstruction occurs when multiple fibre bundles are present within a voxel.

Normally one voxel does not contain only one axonal population and multiple axons from individual cells may merge into or branch out from one voxel (Beaulieu, 2002). Therefore, it is difficult to distinguish the direction of the fiber tracts due to the branching, crossing and kissing of fibres. This then might generate false positive connections. Indeed, recent high-angular resolution imaging such as Q-ball imaging (Tuch et al., 2005b) has been introduced to overcome these limitations (Fonteijn, Verstraten, and Norris, 2007).

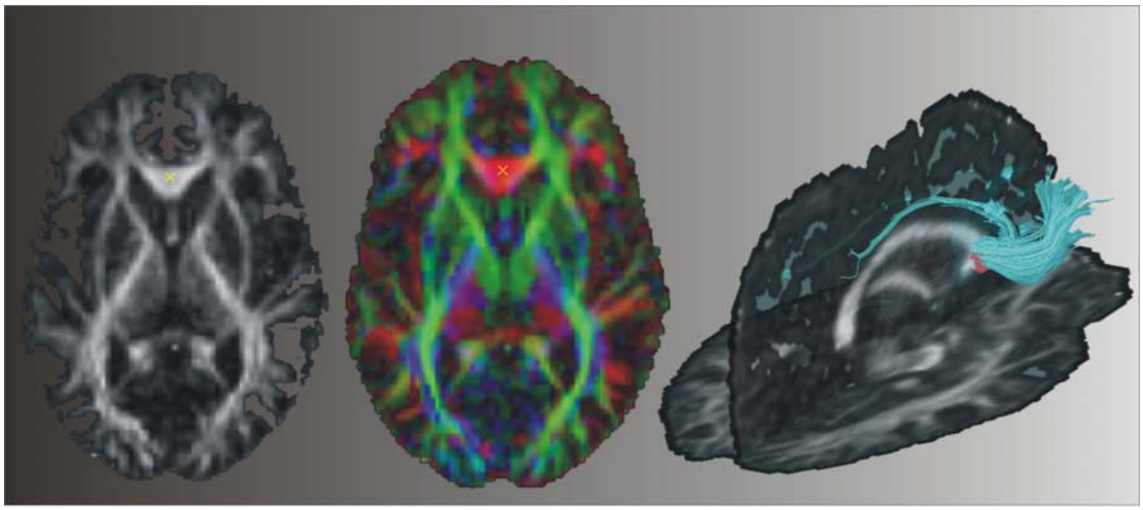

Figure 1.6: DTI anisotropy maps. Anisotropy images have sufficient resolution to segment white and gray matter (left). By incorporating DTI orientation information, white matter can be parcelled into various tract using colour-code maps (middle). The image resolution is sufficient to trace large white matter tracks using fiber-tracking algorithms (unpublished data).

Nevertheless, the exact pathway of the axonal fibers is of less interest in most of the cognitive studies than the degree of connectivity. This is the reason why the use of probabilistic methods (Behrens et al., 2003) to determine the degree of connectivity is preferred, instead of line streaming approaches that are focused on the anatomical pathways of the fibers.

At this time, fiber track reconstruction requires first the definition of a particular region of interest. Then, starting from points ("seed points") selected within this region, the

tracing is carried out basically by following the spatially interpolated direction of maximum diffusion in neighbouring voxels (Kubicki et al., 2002). In this way, the use of the foci of functional activity as initial and ending tracking points, allows the connection between regions. This appears to be a very promising approach to integrating structural and functional information, which might be used to model the underlying neural network in a specific task.

Indeed, some assumptions have to be made about how to link the neural functional focus detected by functional neuroimaging and the corresponding axonal pathways in white matter of the brain. Currently, it is not possible to follow axonal tracts into gray matter, the most common assumption is based on the hypothesis that the white matter adjacent to the gray matter is also connected to it.

1.6. Combining DTI and functional data

Structure–function relationships exist at many spatial scales and across different levels of brain organization in which anatomical, functional and effective connectivity become closely related to one another. On one hand, on a fine spatial scale, cytoarchitectonic mapping is relevant in the coupling of functional and structural properties. More concretely, changes in synaptic number (Anderson, Alcantara, and Greenough, 1996), dendritic volume (Green, Greenough, and Schlumpf, 1983), mitochondrial and vascular density (Anderson et al., 1996; Black, Zelazny, and Greenough, 1991), or glial volume (Sirevaag and Greenough, 1991) have been associated with motor skill learning among others. On the other hand, on a larger scale, functionally segregated cortical regions might be sustained by specific intrinsic (intracortical) and extrinsic (cortico-cortical) anatomical connections. More concretely, Passingham et al. (Passingham et al., 2002) have shown that each cortical region has a unique pattern of inputs and outputs called

connectional fingerprint, which represent the major determinant of the function of that region. Whereas the inputs provide the information on which the region operates, the outputs determine the areas on which it can exert an influence.

Historically, the first study that collected simultaneously fMRI and DTI data was Werring et al. (Werring et al., 1998) in which a case report of a patient after a traumatic internal capsule injury was investigated. Within, both fMRI and DTI data were collected and compared side by side, highlighting the potential value of combining fMRI and DTI data to monitor the mechanisms of recovery and persistent deficits in injury patients. Werring et al. (Werring et al., 1999) again reported the first study in healthy subjects that combined both techniques in a visual task. They demonstrated the feasibility of integrating fMRI and DTI information to investigate the structural properties of activated brain regions compared to the white matter tracts using photic stimulation. Basically, they concluded that BOLD responses were higher in areas with lower cortical grey matter than in white matter regions.

Since then, the number of studies where fMRI and DTI have been combined have rapidly increased. Most of them combine functional and structural measurement but only make qualitative inferences on single subjects based on clinical applications using fMRI block paradigms from either simple visual stimulation or motor activation (Au Duong et al., 2005; Walters et al., 2003). Others have been focused on studying the structural connectivity by creating the connectivity maps from the DTI images used as seed points the focus of the functional activations (Guye et al., 2003). In particular, Johansen-Berg et al. (Johansen-Berg et al., 2004) parcelled grey matter from the connectivity profiles associated with different functional-related cortical regions while Dougherty et al. (Dougherty, Ben-Shachar, Bammer, Brewer, and Wandell, 2005) studied how different fiber pathways projected from visual field maps within visual

cortex. From another perspective, very interesting results were reported by Toosy et al. (Tossy et al., 2004) who after segmenting the optic radiation using a probabilistic index from a connectivity tractography algorithm, found significant correlation between the mean fractional anisotropy of the estimated tracts and the BOLD signal evoked by the visual cortex. Interestingly, this result addresses the hypothesis that the BOLD response might be constrained by the external anatomical connections.

According to the previously presented ideas herein, function and structure become directly connected. Nevertheless, only considering the present results it is difficult to determine the physiological mechanisms underlying such coupling. Physiologically, oligodendrocytes, in the central neuron system (CNS) and Schwann cells, in the peripheral nervous system, have the unique capacity to synthesize large amounts of membranes that spiarilly wrap around the axons, and compact to form myelin, allowing the efficient and rapid propagation of action potentials. Although many of the factors affecting oligodendrocyte development are known, little is known about the mechanisms governing the onset of myelination. One factor that was suggested to induce the onset of myelination process by oligodendrocytes is electrical activity. Indeed, Demerens et al. (Demerens et al., 1996) investigated the influence of axonal electrical activity on myelinogenesis. They demonstrated that the inhibition of electrical activity in the optic nerve with the Na+ channel blocker tetrodotoxon prevented the initiation of myelinogenesis in a system of in vitro myelination using dissociated cultures from embryonic brain and in vivo. In contrast, simulation of neuronal activity by slowing Na+ channel inactivation increased myelination. Later, Stevens et al. (Stevens, Porta, Haak, Gallo, and Fields, 2002) showed that a release in adenosine at extrasynaptic after electrical stimulation of neurons, mediated by purinergic receptors in the oligodendrocyte progenitor cells induced the differentiation of the oligodendrocyte progenitor cells, eventually leading to an increase in myelination.

Ishibashi et al. (Ishibashi et al., 2006) went a step further by investigating whether neuronal activity influences the ability of more mature oligodendrocytes to myelinate. They found that the electrical activity of the neurons promoted myelination of mature oligodendrocytes through an activity-dependent release of ATP (Adenosine triphosphate). Adenosine, which regulated the proliferation and differentiation of oligodendrocyte progenitor cells, had no affect on the ability of mature oligodendrocytes to myelinate. Indeed, ATP only affected mature oligodendrocytes, not their precursors, suggesting that different signalling mechanisms are involved.

After experimenting with different ATP-receptor agonists, Ishibashi et al. (Ishibashi et al., 2006) found that members of the leukimia inhibitory factor family were crucial to promote oligodendrocyte myelination from astrocytes. Specifically, they concluded that the myelination of an axon does not only depend on the axon itself and the oligodendrocyte attached to it, but also on the presence of astrocytes in its proximity. In contrast, Bugga et al. (Bugga, Gadient, Kwan, Stewart, and Patterson, 1998) had previously reported that deficient leukimia inhibitory factor mice females exhibited reduced amounts of astrocytes, but myelin could nonetheless still be formed. This result pointed out that although astrocytes and astrocyted-derived LIF appear to have an important function in CNS myelination, their role is modulatory in the processing, at least at the onset of myelination.

Nevertheless, the possibility that the regulation of myelination in mature myelinated nerves is modulated by electrical activity is tempting (Spiegel et al., 2006). Astrocytes also have important functions in synapse, physiology, including synapses formation, the control of their number and in fine-tuning of synaptic strength (Volterra and Meldolesi, 2005). Although a variety of functions have been attributed to the

astrocytes, recent attention has focused on the role of astrocytes as a main intermediary between neural activity and increase of blood flow (Rossi, 2006).

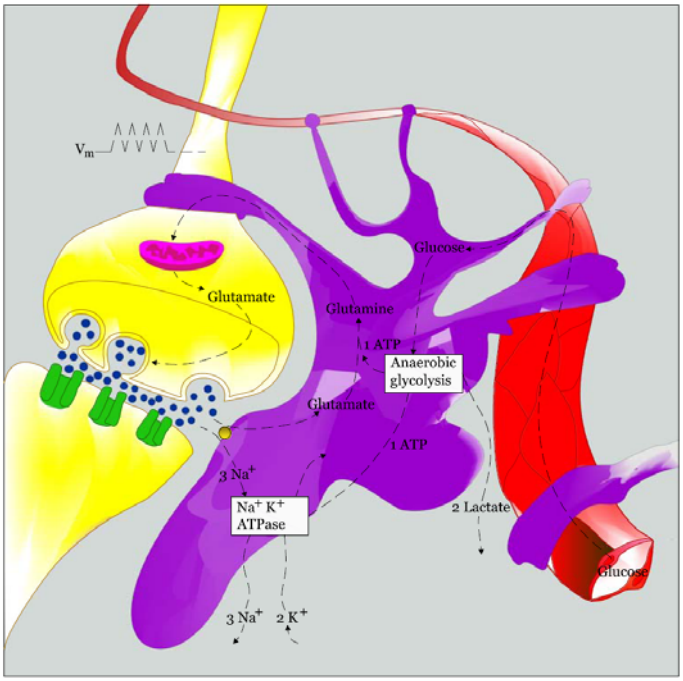

Figure 1.7: The astrocyte-neuron lactate model. In this model, glutamate released at the synapse following a change in membrane voltage (V_m) is quickly transported into an adjacent astrocyte where it is converted into glutamine for transport back to the neuron. The glutamate-glutamine conversion process is powered by one ATP from a fast anaerobic glycolysis process, which has two additional processes: lactate, which is realised into the extracellular space, and another ATP, which provides energy for the sodium-potassium pump at the astrocyte membrane (Adapted from Huettel, Song, and McCarthy, 2004)

In particular, it has been shown that the activation of astrocytes induces local vasodilations, which increase volume and blood flow (Takano et al., 2006). By sending specialized processes both to arterioles (astrocyte endfeet) and to glutamatergic synapses, cortical astrocytes trace an anatomical link between structure (neurons) and the blood supply (functional) (Figure 1.7). More concretely, this neurovascular coupling predicts changes in the deoxyhemoblogin in capillaries, arterioles, venules and veins due to glutamatergic synaptic activity, that might account for the observed changes in the BOLD signal recorded by functional MRI (Bennett, Farnell, and Gibson, 2008).

This last piece of information opens a clear physiological link between function and structure.

1.8. Research aims

By combining fMRI and DTI information, this dissertation pretends to examine possible functional and micro-structural interactions in the human brain in order to better understand the organization and dynamics of the distributed neural systems that subserve neural functions and human behavior. Five experiments are presented in this dissertation, each of which is independent in itself and pretends to give complementary approaches in the study of the human brain. Each section has the following specific objectives (Figure 1.8):

1.8.1. Experiment 1: Classical functional MRI approach.

An interesting open question is the degree to which the interindividual variability observed in the reinforcement learning system is due to differences in the response of the DA system. Genetic polymorphisms associated to dopamine function have been proposed as an interesting alternative in order to explain this variability. In particular, two specific genes, the Catechol-o-methyltransferase (COMT) and the DA D4 receptor (DRD4), are investigated due to the recently attention because of its involvement in DA regulation. The aim of this experiment is to evaluate the influence of COMT and DRD4 SNP-521 polymorphisms in reward processing by using a classical regional specific functional approach.

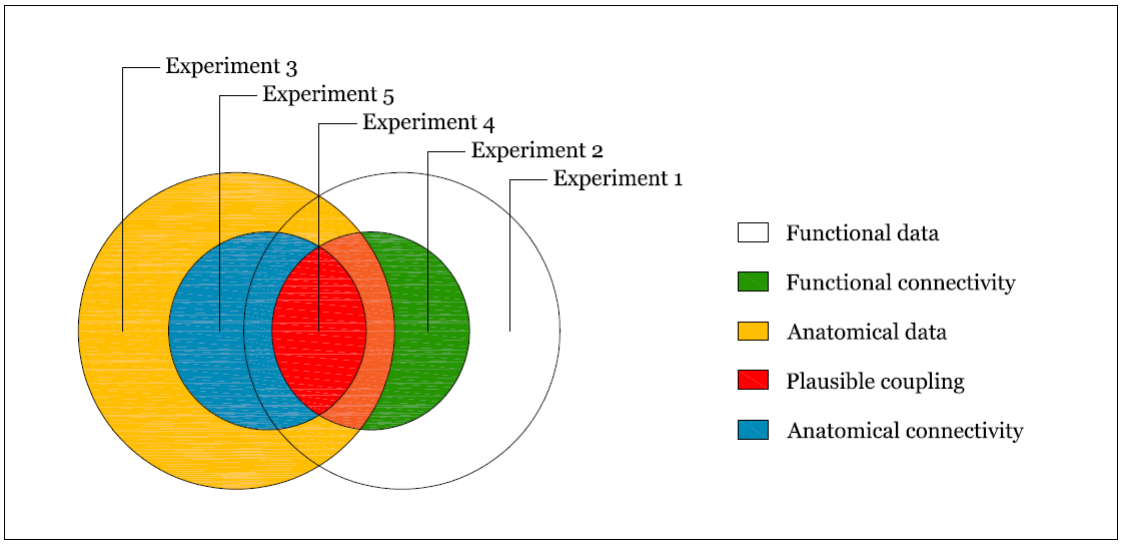

Figure 1.8: Venn diagram representing the different approaches adopted in this dissertation in order to combine functional and anatomical data.

1.8.2. Experiment 2: Functional connectivity approach

Whereas fMRI provides information about the cortical areas implicated in a given cognitive process, connectivity studies generate information on the structural/dynamic wiring that determines how the brain areas underlying a specific cognitive process are networked. There are controversial results about the neural mechanisms underlying reward and punishment processing. Broad evidence supports the fact that monetary gains and losses activate a similar fronto-subcortical-limbic network, but with a differential amount of activation. In contrast, recent studies also suggest that reward and punishment outcomes may be processed by different neural circuits. A complete understanding of the reward processing implies not only identifying the brain regions that are activated during a particular task, but also distinguishing how different regions interact with each other. We predict that the role of reward and punishment outcomes might be functionally differentiated by examining patterns of brain connectivity.

1.8.3. Experiment 3: Anatomical DTI approach

Functional networks should be anatomically segregated in specialised regions and sustained by the presence of specific neural pathways, which permits the information flow between areas. A deeper understanding of white matter pathways and diffusion imaging is relevant in order to characterize brain connectivity and dynamics. In that concern, the study of basic concepts such as diffusivity or anisotropy is absolutely necessary in order to interpret the DTI results. Methodological aspects on the data acquisition and analysis can critically affect the results on the analysis of diffusion tensor and with MRI technique. Accordingly, taking the proposal of learning about DTI and adding the novelty of the technique, we decided to concentrate our efforts in understanding this technique. This experiment result as a part of a DTI technique learning process, in which a sample of diffusion weighted images (of different ages) was analyzed in detail; this analysis slowly took form as a distinct project that could be of interest. This explains the methodological focus that can be seen in specific parts of the study, and the wide range of ages studied made it natural that white matter changes in ageing became the nucleus of the study. The study intends to show the importance of the methodology used when interpreting the results, and reflects some of the uses DTI might have in future studies of ageing, where the changes in white matter are of utmost importance.

1.8.4. Experiment 4: combined fMRI/DTI approach

The relationship between the function of the brain and its structure is still a fundamental open question. Structure–function relationships exist at many spatial scales and across different levels of brain organization. In particular, considering the relationship between functional and structural connectivity, it is reasonable to expect that the strength of an anatomical connection is correlated with that of a corresponding

functional connection. Concretely, we predict that individual regionally FA differences might be underlying individual functional related BOLD responses. This experiment pretends to evaluate the potential applications of a new combined fMRI-DTI methodology in reward processing.

1.8.5. Experiment 5: Anatomical connectivity approach.

Many fMRI studies are focused on discovering patterns of brain activity that are associated with specific cognitive processes or behaviours. In particular, the coupling between individual task performance and the evoked BOLD response has been one of the most outstanding measures in fMRI studies, since individual performance can be used to predict BOLD-related signal changes, and thereby indirectly relate psychometric parameters to neural activity. It remains to be determined however, to what extent these behavioural/(functional) correlations are interacting with structural measures. Previous described cognitive and neurobiological associations evidence that at least some of the individual differences observed in performance monitoring can be predicted both at functional and structural level. In this experiment, individual differences in true memory and false memory retrieval were studied and related to differences in the organization of white matter connections.

Chapter 2♣

2. Classical univariate MRI approach:

Double dissociation of the effects of COMT and dopamine receptor D4 genotypes on brain activations related to valence and magnitude of rewards

2.1. Introduction

Before making a decision, the consequences of our behaviour are weighted from the positive and negative outcomes from similar decisions made in the past. In order to adapt our behaviour, we try to increase the probability of the occurrence of positive reinforcements and suppress the recurrence of aversive events (Daw, O'Doherty, Dayan, Seymour, and Dolan, 2006). In this regard, the reinforcement learning theory Sutton and Barto (1998) has proposed the existence of an internal error-prediction signal which is amplified when the outcomes of the behaviour are unexpected or worse than expected ones. Therefore, this learning signal will influence subsequent decisions optimizing the possibility of obtaining positive rewards in response to changes in the environment.

♣ Camara E., Krämer UM., Cunillera T., Marco-Pallarés J, Cucurell D., Mestres-Missé, A., Nager W., Bauer P., Schüle-Freyer R., Schöls L., Tempelmann C., Rodriguez-Fornells A., Münte TF. **Reward-related fMRI responses in the ventral striatum are dependent of dopaminergic genetic differences (COMT)** (submitted).

In agreement with this theory, Schultz et al. (Schultz et al., 1998) has recorded phasic bursting activity of midbrain dopamine (DA) neurons from primates and showed that their signal amplitude changed according to the expectations of future salient and rewarding events. Specifically, phasic bursts of DA cell firing were associated with positive outcomes, whereas choices that did not lead to a reward evoked DA dips that fell below the baseline activity (Schultz, 2002). The projection from these mid-brain neurons through the mesocortical and mesolimbic DA tracts directly influences the function of several striatal-orbitofrontal and prefrontal regions involved in reward processing (Apicella, Ljungberg, Scarnati, and Schultz, 1991; Hikosaka and Watanabe, 2000; Wise, 2002). In particular, the mesocortical neurons project primarily to the medial prefrontal cortex (PFC), anterior cingulate (ACC) and entorhinal cortex. The mesolimbic pathway directly innervates the nucleus accumbens (NAcc), septum, olfactory tubercle, amygdala and piriform cortex. Several functional magnetic resonance imaging (fMRI) studies have provided convergent evidences about the involvement of this neural network in reward processing (Breiter, Aharon, Kahneman, Dale, and Shizgal, 2001; Delgado, Nystrom, Fissell, Noll, and Fiez, 2000b; Delgado, Locke, Stenger, and Fiez, 2003; Knutson, Momenan, Rawlings, Fong, and Hommer, 2001; Knutson, Fong, Bennett, Adams, and Hommer, 2003; McClure, York, and Montague, 2004; Tom, Fox, Trepel, and Poldrack, 2007; Yacubian et al., 2006). Moreover, a recent theory has highlighted the importance of the medial prefrontal cortex (ACC) and the ventral striatum in the adjustment of behaviour based on the reinforcement learning signals triggered from the midbrain regions (Holroyd and Coles, 2002).

In addition to this, the NAcc in the ventral striatum has emerged as a key region in reward processing and the regulation of addictive behaviors. The NAcc receives

synaptic inputs from the PFC [orbitofrontal cortex (OFC) and dorsolateral PFC, (DLPFC)] and limbic structures (hippocampus and the amygdala, (Groenewegen, Wright, Beijer, and Voorn, 1999) and is the target of dense dopaminergic innervations from the ventral tegmental area (Voorn, Jorritsma-Byham, Van, and Buijs, 1986), a region that has been repeatedly associated to learning and motivation (Schultz, 2007). Because of this rich interconnectivity, the NAcc has been proposed as an important region in the selection of appropriate responses and the modulation of goal-directed behaviour (Kelley and Berridge, 2002; Berridge and Robinson, 1998). This region shows increased blood oxygenation level-dependent (BOLD) activation in presence of positive reward outcomes (monetary gains) when compared to negative outcomes (monetary losses) (May et al., 2004; Delgado et al., 2003; Delgado et al., 2000b). These changes in NAcc BOLD signal have been interpreted as reflecting changes in postsynaptic D1 receptor activity due to dopamine release from DA neurons innervating this region (Knutson and Gibbs, 2007). Further experiments have also provided evidences for differential activation of the striatum for positive and negative feedback (Seger and Cincotta, 2005; Poldrack and Gabrieli, 2001; Elliott, Sahakian, Michael, Paykel, and Dolan, 1998). The ventral striatum activity has also been associated to the processing of the magnitude of rewards outcomes (Brown and Bowman, 1995) or the anticipation of larger rewards (Breiter et al., 2001; Gottfried, O'Doherty, and Dolan, 2003; Kirsch et al., 2003; Knutson, Adams, Fong, and Hommer, 2001; Knutson et al., 2003; O'Doherty, Deichmann, Critchley, and Dolan, 2002; Yacubian et al., 2007). In a similar vein, striatal neurons in monkeys show larger firing responses in presence of preferred rewards (Hassani, Cromwell, and Schultz, 2001).

Furthermore, one of the attributes that boost the impact of reward is the degree of uncertainty that exists in the estimation of the action's value. Indeed, reward

information becomes more relevant as the uncertainty of the reward prediction increases (Fiorillo, Tobler, and Schultz, 2003). In convergence with this idea, two recent fMRI studies have provided evidence that the NAcc response is larger when the reward obtained was less likely to occur (Abler, Erk, Herwig, and Walter, 2007; Yacubian et al., 2006).

In addition to the interaction between the midbrain-NAcc and medial prefrontal cortex in the regulation of the reinforcement learning system (Holroyd et al., 2002), several prefrontal regions have also been shown to be involved in regulating learning and action selection in the presence of reward signals. An interesting theory has been proposed in order to understand the crosstalk between cortical and sub-cortical systems in reward and learning, hereafter referred as phasic-tonic dopaminergic coupling (Bilder, Volavka, Lachman, and Grace, 2004; Grace, 1991; Grace, Floresco, Goto, and Lodge, 2007). This theory proposes that (i) burst (phasic)-firing DA responses are evoked in the NAcc and striatum which are associated to reward related cues or stimuli and (ii) a constant DA background firing exists in the striatum and is regulated by a baseline DA neuron firing and the prefrontal glutamatergic afferents to the striatum. This theory directly predicts that the sensitivity of the reinforcement learning system might depend on the amount of phasic DA release, which is necessary to react to salient rewarding stimuli. As this activity is regulated by prefrontal tonic afferents to the striatum, a decrease of this tonic regulatory system might increase the sensitivity of the reinforcement learning system. Interestingly, this prefrontal-striatal coupling could be used to influence the output of subcortical responses via a top-down regulating system. For example, increasing the tonic firing level of the PFC cortex could be used to modulate or dampen the effect of positive and negative rewards.

An interesting open question is to which degree the interindividual variability observed in the reinforcement learning system is due to differences in the response of the DA system. For instance, it has been proposed that reduced levels of D2 DA receptors, either genetically or as a result of life experiences, may determine vulnerability of abuse and addictive behaviors (Volkow et al., 1999). Besides, genetic polymorphisms associated to dopamine function have been proposed as an interesting alternative in order to explain this variability (Yacubian et al., 2007; Frank, Moustafa, Haughey, Curran, and Hutchison, 2007). In particular, two specific genes, the Catechol-o-methyltransferase (COMT) and the DA D4 receptor (DRD4), have recently received special attention because of its involvement in DA regulation.

COMT is an enzyme involved in DA degradation, mostly present in the prefrontal cortex (Chen et al., 2004). Specifically, as a result of a valine to methionine (Val/Met 158) substitution at codon 158/108 of a single nucleotide polymorphism (SNP) in the COMT gene, a three- to four- fold reduction of the enzymatic activity in the Met allele is obtained. Thus, Val alleles should express higher COMT activity in the prefrontal cortex, which presumably involves lower synaptic DA levels, and therefore an inhibition of the prefrontal functioning.

More importantly, based on the phasic-tonic dopaminergic hypothesis, low prefrontal tonic levels in the ValVal group would predict increased striatal phasic activity and thereby, an increase in phasic responses and sensitivity of the reinforcement learning system (Bilder et al., 2004). In addition, it has been recently been demonstrated that the presence of the methionine allele in COMT leads to decreases in the efficiency of dopamine synthesis in the midbrain (Meyer-Lindenberg et al., 2005). In a recent study, Yacubian et al. (Yacubian et al., 2007) investigated how COMT and DAT (DA

transporter) genetic differences influence reward probability and magnitude during anticipation of reward in a gambling task. In particular, ValVal homozygotes showed a relative deactivation in prefrontal and striatal (putamen) regions compared with MetMet homozygotes, presumably because of the elevated prefrontal DA levels in the Met allele carriers. Additionally, based on the hypothesis of top-down regulation of the prefrontal cortex on striatal DA levels, a similar effect was found in the ventral striatum encoding the expected value as an interaction between the COMT-DAT genotypes.

In a similar vein, a cytosine to timine (C/T 521) substitution in the DRD4 gene SNP-521 entails two homozygote alleles as well. The T-allele has been associated with 40% inferior transcriptional efficiency when it is compared with the C-allele (Okuyama, Ishiguro, Toru, and Arinami, 1999; but see for a different results Kereszturi et al., 2006). The -521 C/T SNP belongs to a series of polymorphisms identified in the promoter region of the DRD4 gene, including among others the 120 base pair duplication and other SNPs (-616 G/C, -615 A/G and -1217 G insertion/deletion). The D4 receptor, which is a D2-like receptor (Strange, 1993), have received special attention because its shows the highest affinity for the atypical antipsychotic clozapina (Seeman and Van Tol, 1994) and it is expressed in several brain regions related to planning, motivation and reward (Ariano, Wang, Noblett, Larson, and Sibley, 1997; Mrzljak et al., 1996; Meador-Woodruff, Damask, and Watson, Jr., 1994). Thus, compared to the distribution of COMT, DRD4 receptors are also present at mesolimbic (Matsumoto, Hidaka, Tada, Tasaki, and Yamaguchi, 1996) and at the striatum regions (Sanyal and Van Tol, 1997). However, the association of this polymorphism to psychological functions or traits remains elusive. Although some of the results in the literature are controversial (Mitsuyasu et al., 2007; Okuyama et al., 1999), the association between this DRD4 polymorphism and novelty seeking (Golimbet, Alfimova, Gritsenko, and

Ebstein, 2007; Okuyama et al., 1999; Ronai et al., 2001; Schinka, Letsch, and Crawford, 2002) or addictive behaviors seems to be well established (Rubinstein et al., 1997; Ronai et al., 2001; Geijer et al., 1997).

The aim of the present work is to evaluate the influence of COMT and DRD4 SNP-521 polymorphisms in reward processing. With that purpose in mind, selected volunteers participated in a simple gambling task (Gehring and Willoughby, 2002; Marco-Pallares et al., 2008) (adapted from Gehring and Willoughby, 2002; see Marco-Pallares et al., 2007), in which unexpected and larger monetary gains and losses (boost trials) were presented as well standard gain and loss trials (see experimental design at Figure 2.1). We specifically evaluated two predictions based on the phasic-tonic DA regulation model (Bilder et al., 2004). First, due to the reduced synaptic DA level in the PFC in ValVal homozygous, a diminished tonic activity is predicted and therefore, this group should show enhanced phasic DA activity in the striatum (NAcc) in the presence of rewards (standard and boost trials) (Bilder et al., 2004). In addition, considering the proposal that the medial prefrontal cortex (ACC) is involved in the evaluation of positive and negative feedback through the dopaminergic learning signals arising from the midbrain (Holroyd et al., 2002), we predicted that similar responses should be observed in the medial prefrontal cortex (ACC) coupled with the activation observed in the ventral striatum. More specifically, we expected that the medial prefrontal cortex and ventral striatum BOLD responses would show enhanced activation in the ValVal homozygous group during reward processing.

Second, for the DRD4, considering its association between novelty seeking and the possible role in addiction, we expected to encounter differences in the activation of the reward-related system for the different groups (CC vs. TT). In a recent fMRI feedback

learning study, the A1 allele of the polymorphism (DRD2-TAQ-IA, Klein et al., 2007), which is associated with a reduction in D2 receptor density and associated with addictive behaviours, showed reduced feedback negative BOLD response when compared to the higher receptor density allele. Based on these findings and the fact that D4 and D2 receptors belong to the same D2-like receptor family, we expected to encounter reduced BOLD response in the TT group (possible lower density of D4 receptors, Okuyama et al., 1999; but Kereszturi et al., 2006) compared to the CC group.

2.2. Materials and Methods

2.2.1. Participants

All procedures reported in this investigation were approved by the local ethical Institutional Review Board (IRB00003099) at the University of Barcelona.

An initial pool of 656 students from the University of Barcelona (491 women; age range from 18 to 56, mean = 21.7, S.D. = 3.5) was genotyped by preparing DNA using standard techniques from two independent EDTA blood samples of each participant. Genotyping of the -521 C/T polymorphism in the dopamine D4 receptor gene (DRD4) promoter (Okuyama et al., 1999) as well as the catecholamine-O-methyl transferase (COMT) G to A polymorphism at codon 108/158 (short/long isoform) resulting in valine to methionine substitution (Lachman et al., 1996) was carried out using real-time Fluorescence Resonance Energy Transfer (FRET) PCR. The region spanning the single nucleotide polymorphism (SNP) was amplified with the primers DRD4for (5' CTG AGG GCC AGA GGC TG 3') / DRD4rev (5' GAG GAT CAA CTG TGC AAC GG 3') and COMTfor (5' GGG CCT ACT GTG GCT ACT CA 3') / COMTrev (5' TTC AGT GAA CGT GGT GTG AAC A 3') respectively. The polymorphic nucleotide is covered by the

fluorescein labelled donor probe (DRD4sensor 5' CGG GCG TGG AGG GCG CG-Fl 3'; COMTsensor 5' ATT TCG CTG GCA TGA AGG ACA A-Fl 3'). The adjacent acceptor probe (DRD4anchor 5' LCRed610-GAC TCG CCT CGA CC--TCG T 3'; COMT anchor 5' LCRed610- GTG TGC ATG CCT GAC CCG TTG TCA-ph 3') was labelled with LCRed640). Melting curve analysis of the matrix-probe duplex is allele-dependent and allows discrimination of the two SNP alleles. Primers and probes were designed and synthesized by Tib Molbiol, Germany. Amplification and melting analysis were carried out on a LightCycler©480 instrument (Roche Diagnostics, Germany). For PCR amplification the LightCycler©480 genotyping master (Roche Diagnostics, Germany) was used in a 384-well format with 10 µL reaction volumes. Cycling conditions with touchdown annealing temperatures from 65°C to 55°C over the first 10 cycles were as following: 10 min 95°C, 45 cycles with 20 sec annealing temperature, 20 sec. 72°C and 20 sec 95°C followed by a high resolution melting curve from 50°C to 85°C with continuous fluorescence acquisition.

From the overall sample 53 participants (36 women; age range: 18 – 34 years, mean = 21.2) were selected for the fMRI experiment based on their DRD4 -521 and COMT alleles. Participants were homozygous for both polymorphisms to allow a two-by-two factorial design with the four groups TT-ValVal, TT-MetMet, CC-ValVal and CC-MetMet. Two participants had to be excluded due to a genotyping error (TC-MetMet instead of TT-MetMet and TC-ValVal instead of TT-ValVal), one TT-MetMet participant was excluded because of a morphological abnormality of the brain. In 4 participants (2 TT-ValVal, 2 CC-MetMet) were lost because of technical problems during their scanner session. This left 9 participants for the TT-ValVal group. The number of participants in the other groups was reduced to 9 as well in order to have ab

equal number of participants in each group. Therefore, the final sample comprised 36 right-handed Spanish students (n = 9 per group; 24 women).

Genotypes of participants selected for neuroimaging study were controlled in an independent second DNA sample by direct sequencing using the ABI PRISM BigDye Terminator v3.1 Cycle Sequencing Kit (Applied Biosystems, Foster City, USA). Sequencing products were resolved on an ABI 3100 automated sequencer (Applied Biosystems, Foster) and analyzed using the Staden Package (Bonfield, Smith, and Staden, 1995).

2.2.2. Design

Several important modifications were made to a monetary gambling task designed by (Gehring et al., 2002, see also Marco-Pallares et al., 2007). Each trial began with a warning signal ("*"; 500 ms duration) followed by the presentation of two numbers (5 and 25) displayed in white against a black background in the two possible combinations, [5 25] or [25 5]. Participants had to select one of the two numbers by pressing a spatially corresponding button with the left or right index finger (see Figure 2.1). One second after the choice, one of the numbers turned green while the other turned red. If the number selected by the participant changed to red, the participant incurred a loss of the corresponding amount of money in Euro cent. In contrast, if the number turned into green, this indicated a gain.

In addition to the standard trials described above (80%), two additional conditions were created to assess the brains responses to unexpected rewards and losses (see Figure 2.1). In 10 % of the trials ("boost unexpected trials"), an unexpected large gain or loss occurred: In these trials the number "125" appeared in either red or green signaling

the loss or gain of the corresponding sum in Euro cent (see Figure 2.1). This change in magnitude occurred equally often for "5" and "25" trial bets in order to avoid positive or negative biases in choosing "25" items. To control for the fact that boost trials were both, large and unexpected, in an additional 10 % of the trials ("similar unexpected") the chosen number turned to either 7 (instead of 5) or 27 (instead of 25). While these trials were unexpected, the magnitude of the gain or loss was virtually unchanged. Additionally, each run included 12 randomized fixation trials that lasted 20 seconds.

Participants were provided of an initial sum 10 € and were encouraged to gain as much as possible. Patients had performed a similar event-related potential task (without unexpected trials) several weeks to months earlier and thus were familiar with the task in general. They were informed about the potential occurrence of unexpected trials. The experiment comprised four blocks, each one comprising 140 trials. The four possible outcomes for the standard trials ([25 5] [5 25] [5 25] [25 5]; italics = red = loss, bold = green = gain), for the unexpected similar trials ([25 7] [5 27] [7 25] [27 5]), and for the unexpected boost trials ([25 125] [5 125] [125 25] [125 5]) were presented in random order. These combinations were counterbalanced by condition, making the statistically expected outcome zero on each trial in order to avoid confounds of differential probability of gains or losses. At the end of each run, participants were informed about their accumulated amount of money at this point. At the end of the experiment, the participants were paid the final amount obtained (bank transfer).

2.2.3. MRI scanning methods

fMRI data were collected using a 3T whole-body MRI scanner (Siemens Magnetom Trio, Erlangen, Germany). Visual images were back-projected onto a screen using an LED-projector and participants viewed the images through a mirror on the head coil.

Magnet- compatible response buttons were used. Conventional high resolution structural images [magnetization-prepared, rapid-acquired gradient echoes (MPRAGE) sequence, 192 slice sagittal, TR = 2500 ms, TE = 4.77 ms, TI = 1100 ms, flip angle = 7°, 1mm thickness (isotropic voxels)] were followed by functional images sensitive to blood oxygenation level-dependent contrast (echo planar T2*-weighted gradient echo sequence, TR=2000 ms, TE=30 ms, flip=80°). Each functional run consisted of 336 sequential whole-brain volumes comprising 32 axial slices aligned to the plane

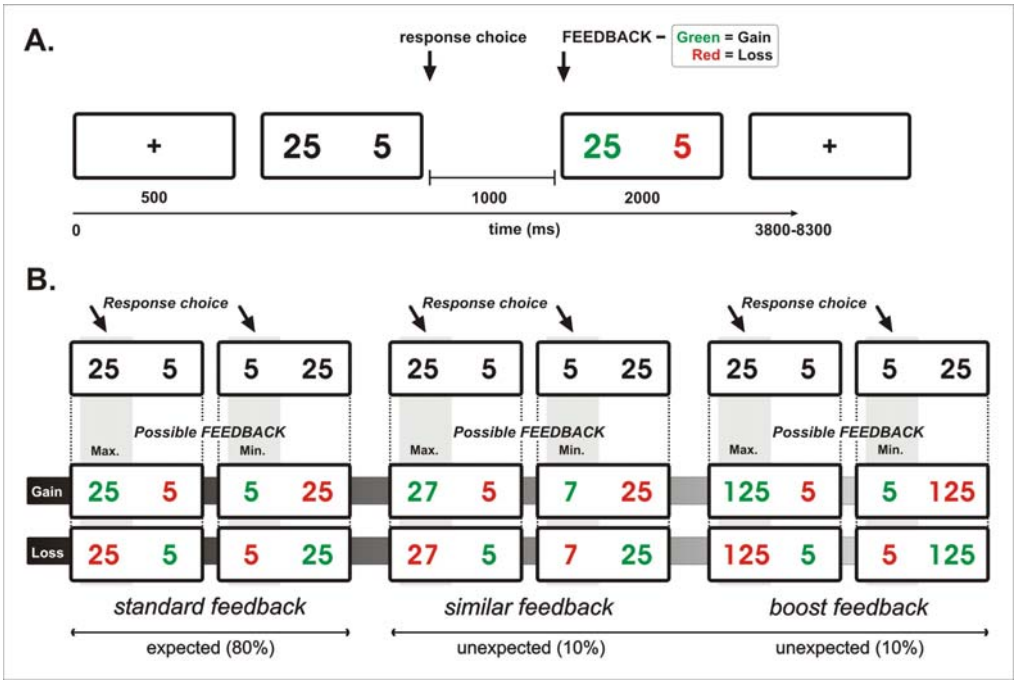

Figure 2.1: A. Sequence of stimulus and response events in the gambling task. After a warning signal, a pair or numbers ([5 25] or [25 5]) was presented and participants were forced to select one of the two numbers by pressing the corresponding button at left or right hand (response choice). One second after the choice, one of the numbers turned red and the other green (feedback) indicating a gain (green) or loss (red) of the corresponding amount of money in Euro cent. B. In the frequent *standard feedback* trials participants gained or lost the same amount of money they betted. By contrast, in the unexpected boost feedback condition, the magnitude of the reward was much larger than the expected one (10 % probability). In the *similar feedback* condition the magnitude was changed only slightly. This allowed us to dissociate the effects of reward magnitude and reward probability.

intersecting the anterior and posterior commissures, 3.5 mm in-plane resolution, 4 mm thickness, no gap, positioned to cover all but the most superior region of the brain and the cerebellum.

2.2.4. Image processing

Data were analyzed using standard procedures implemented in the Statistical Parameter Mapping software (SPM2, *http://www.fil.ion.ucl.ac.uk/spm*). The preprocessing included slice-timing, realignment, normalization and smoothing. First, functional volumes were phase shifted in time with reference to the first slice to minimize purely acquisition-dependent signal-variations across slices. Head-movement artifacts were corrected based on an affine rigid body transformation, where the reference volume was the first image of the first run (e.g., Friston, Williams, Howard, Frackowiak, and Turner, 1996). Functional data were then averaged and the mean functional image was normalized to a standard stereotactic space using the EPI derived MNI template (ICBM 152, Montreal Neurological Institute) provided by SPM2. After an initial 12-parameter affine transformation, an iterative non-linear normalization was applied using discrete cosine basis functions by which brain warps are expanded in SPM2 (Ashburner and Friston, 1999). Resulting normalization parameters derived for the mean image were applied to the whole functional set. Finally, functional EPI volumes were resampled into 4 mm cubic voxels and then spatially smoothed with an 8 mm full-width half-maximum (FWHM) isotropic Gaussian Kernel to minimize effects of inter-subject anatomical differences.

2.2.5. Data analysis

The statistical evaluation was based on a least-square estimation using the general linear model by modeling the different conditions with a regressor waveform convolved with a canonical hemodynamic response function (Friston et al., 1998). Thus, an event-related design matrix was created including the conditions of interest: Gain 5, Gain 25, Gain 7/27, Gain 125, Loss 5, Loss 25, Loss 7/27, Loss 125 and fixation.

The data was high-pass filtered (to a maximum of 1/90 Hz), and serial autocorrelations were estimated using an autoregressive model (AR(1) model). Resulting estimates were used for non-sphericity correction during the model estimation. Confounding effects in global mean were removed by proportional scaling, and signal-correlated motion effects were minimized by including the estimated movement parameters. The individual contrast images were entered into a second-level analysis using a one-sample *t*-test employing a random effects analysis within the general linear model.

2.2.5.1. Main contrasts of interest

First, in order to reveal brain regions responding selectively to gains and losses we created two contrasts: in standard trials the comparison Gain (25+5) vs. Loss (25+5) (and vice versa) reflected the effect of valence, while for the unexpected boost trials the corresponding contrast was Gain (125) vs. Loss (125) (and vice versa).

Second, to investigate whether differences in the previous contrasts could be explained in terms of reward magnitude (both contrasts differ with regard to magnitude and probability), magnitude-related effects were assessed by contrasting maximum vs. minimum feedback for standard [25 (Gain+Loss) vs. 5 (Gain+Loss)] and unexpected trials [125 (Gain+Loss) vs. 7/27 (Gain+Loss)] conditions separately. Notice that the last contrast is not confounded by probability as 125 and 7/27 trials appeared with equal

(low) probability. Finally, potential interactions between valence and magnitude were tested for both standard and unexpected boost trials.

The previous general contrasts were investigated in the entire sample (36 subjects) and were thresholded at $P < 0.05$, corrected for multiple comparisons at the whole-brain level by using a family-wise error (FWE) rate. The maxima of suprathreshold regions were localized by rendering them onto the mean volunteers' normalized T1 structural images on the MNI reference brain. Maxima and all coordinates are reported in MNI coordinates, as used by SPM and labeled in line with the Talairach atlas. The specific contrasts performed in order to investigate the influence of COMT, DRD4 and their interaction on valence and magnitude are detailed in the following sections.

2.3. Results

2.3.1. Behavioural Data

Overall, participants chose 25 more often than 5 (54.3 ± 11.8 % vs. 45.3 ± 11.7, $t(35) = -2.31$, $P < 0.05$). No differences were observed in choice (25 or 5) between the different genetic groups (main effects of COMT and DRD4, $F(1,32) < 1$ and COMT x DRD4, $F(1,32) = 1.7$, $P > 0.2$). On average, participants lost 0.5 ± 3.0 €.

Risk taking behaviour of participants was quantified by assessing the percentage of risky (25) decisions after unexpected boost trials. A significant interaction was encountered between DRD4 x condition (previous trial loss 125 vs. gain 125) ($F(1,32) = 4.5$, $P < 0.05$). After losses, no group differences in choosing 25 were seen (CC: 55.3 % vs. TT: 55.6, $t(34) < 1$), whereas the CC group had a greater preference for 25 after boost wins (CC: 59 % vs. TT: 46.3, $t(34) = -4.0$, $P < 0.001$). This pattern of increased risk taking after boost wins by CC-participants differs from other studies, in which risk-

aversive behaviour has been demonstrated after large wins (Gehring and Willoughby, 2002; Riba et al., 2008). No differences in risk-taking were observed for COMT.

2.3.2. Main effects of Valence and Magnitude in standard and boost trials

Main effects of Valence and Magnitude were assessed using the multiple comparison correction approach ($P < 0.05$; see Table 1). The contrast gain (5 + 25) vs. loss (5 + 25) led to activation in the ventral striatum (NAcc) bilaterally, with the activity extending to the amygdala (see Table 1a and Figure 2a). No significant differences were found for the inverse contrast (loss vs. gain trials) corroborating previous studies (Nieuwenhuis et al., 2005; Tom et al., 2007). With regard to the main effect of magnitude [i.e., 25 (Gain + Loss) vs. 5 (Gain + Loss)] there were no significantly activated brain regions at the specified threshold. Similarly, the assessment of the interaction between Valence and Magnitude did not reveal activated brain regions.

The valence effect for the analogous analysis on the boost trials [gain (125) vs. loss (125)] activated roughly the same region in the ventral striatum as the analysis for the standard trials (see Table 2.1b and Figure 2.2b). No effect was seen for the inverse comparison. In contrast to the standard trials, magnitude-related activations were found for the unexpected trials [i.e., 125 (Gain+Loss) vs. 7/27 (Gain+Loss)] located in the right insular cortex, the right inferior parietal lobe, the rACC and right cuneus (see Figure 2.3a and Table 2.1c). No significant regions were observed for the interaction between Valence and Magnitude for the boost trials.

2.3.3. COMT and DRD4 effects in the NAcc

At the locations of the peak activities observed in the contrasts mentioned above [valence effects: right and left ventral striatum (NAcc); magnitude effects only in boost trials: right insular cortex, inferior parietal lobe (IPL), rostral anterior cingulate cortex (rACC); see table 2.1], we reconstructed the BOLD event-related responses from the trial-specific evoked response depicted as a function of peristimulus time. First, peristimulus-time histograms were computed for each participant and voxel of interest within each session and then averaged over sessions and subjects. Finally the corresponding parameter estimates (β values) for each condition and individual were extracted and entered as dependent variables in various ANOVAs, using Valence or Magnitude as within-subjects factors and Genetic Group (COMT and DRD4) as a between-subjects factors.

In the *standard trials*, the corresponding ANOVA for the left NAcc showed no differential recruitment of the NAcc as a function of genetic group (main effect of Valence, $F(1,32) = 42.7$, $P < 0.001$; Valence x COMT, $F < 1$; Valence x DRD4, $F < 1$). The other main effects and interactions were not significant. For *boost trials*, the corresponding ANOVA showed a significant Valence x COMT interaction ($F(1,32) = 4.4$, $P < 0.05$). The interaction reflected the fact that the ValVal group showed a larger activation difference between gain and loss trials than the MetMet group (see Figure 2.2b). Further pairwise *t*-tests showed significant differences between COMT groups in loss ($t(34) = 2.1$, $P < 0.04$) but not in gain trials ($t < 1$). Indeed, Figure 2d shows a clear reduction in the BOLD response for the ValVal group in loss trials (left) resulting in an enhanced BOLD difference between gains and losses in this group (right). The remaining interactions or main effects, in particular those involving DRD4, were not significant.

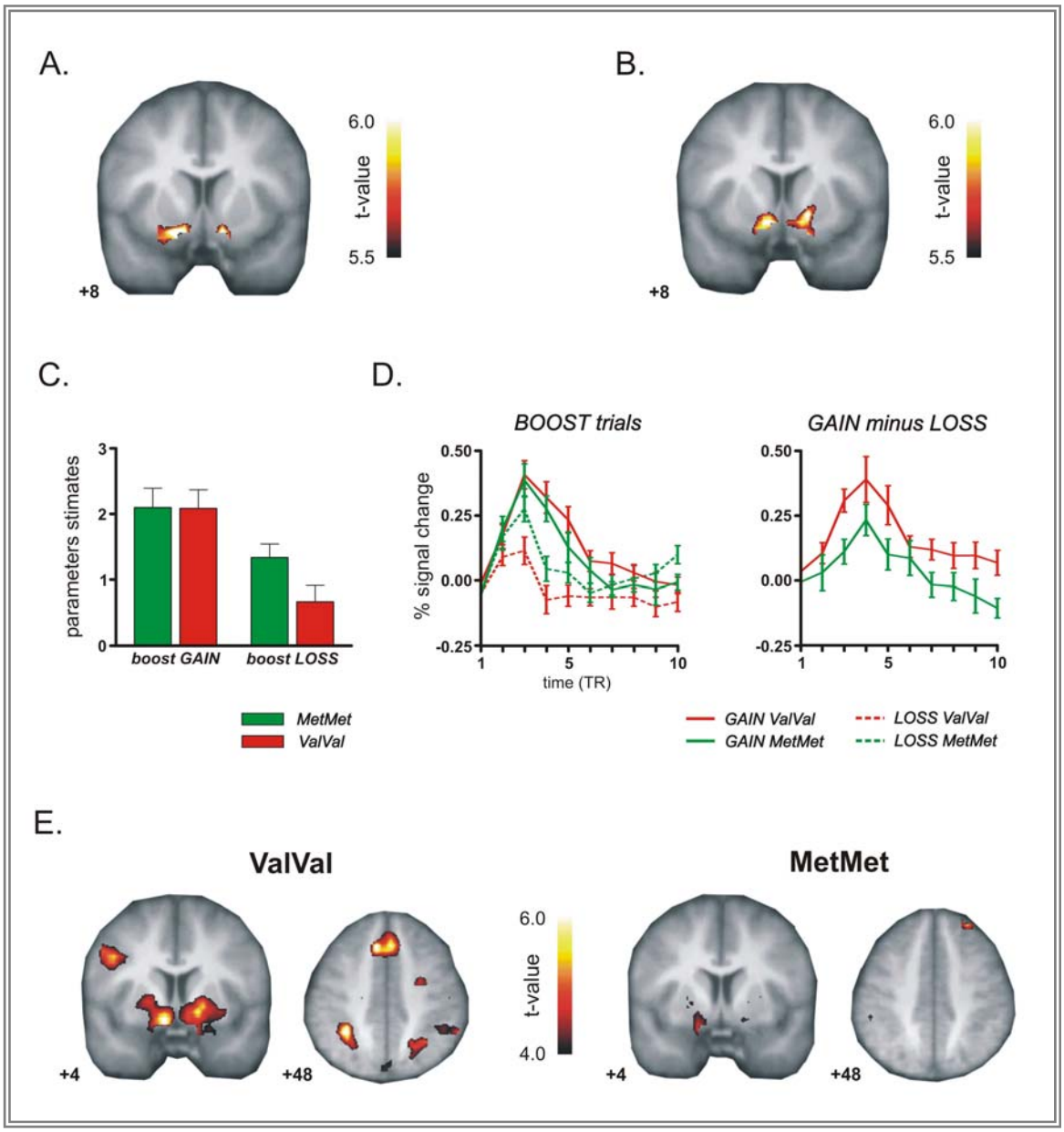

Figure 2.2: Valence effects. Coronal views of the group average Gain vs. Loss contrast superimposed on a group-averaged structural MRI image in standard stereotactic space (*t*-score overlays after multiple comparisons correction at the whole-brain level, $P < 0.05$). Both the standard trials (A) (peak *x*, *y*, *z*: -24, 4,-12 mm), and the boost trials (B), (peak, -8, 4, -8 mm), showed increased activity in the left and right ventral striatum. C. Reward-related activations for each boost condition (Gains and losses) and each COMT group. Notice the reduced activation in the boost loss condition for the ValVal group. D. BOLD time-course BOLD at the activation peak in the NAcc plotted separately for the COMT groups (left side). The difference between gain and loss boost conditions in each COMT group is shown on the right. E. Gain vs. Loss contrast for each COMT group (*t*-score overlays, $P < 0.001$ uncorrected). Notice the activation in this contrast in the NAcc, ACC and IPL in the ValVal which is largely missing in the MetMet group.

To follow up the *magnitude effect* reported in boost trials we performed separate ANOVAs for right cuneus, right insula, rACC and rIPL (see Table 2.1c). A significant DRD4 x Valence x Magnitude interaction was revealed in the right insular cortex (coordinates 24, 20, -16; $F(1,32) = 7.1$, $P < 0.012$)) and the rACC (8, 40, 24 mm; $F(1,32) = 5.02$, $P < 0.032$; see Figure 3b). The decomposition of this interaction showed that the DRD4 x Magnitude effects were restricted to gains (gains, DRD4 x Magnitude, right insular cortex, $F(1,34) = 12.26$, $P < 0.001$; rACC, $F(1,34) = 13.6$, $P < 0.001$; loss trials, DRD4 x Magnitude, $F < 1$, in both regions). For the insular cortex, further pairwise *t*-tests showed a significant difference between boost and similar gains in the CC genotype ($t(17) = 6.15$, $P < 0.0001$) but not in the TT group ($t(17) = 1.526$, $P > 0.1$). Also, CC and the TT groups differed for the boost gains condition ($t(34) = -2.9$, $P < 0.007$) but not for the similar gains trials ($t(34) < 1$) (see Figure 2.3c). In the rACC, a significant difference between boost and similar gains was also observed in both the CC genotype ($t(17) = 3.94$, $P < 0.0001$) and the TT group ($t(17) = 7.36$, $P > 0.0001$). In this region, CC and the TT groups differed in the boost condition ($t(34) = -2.8$, $P < 0.008$) but not in the similar gains ($t(34) = 1.3$) (see Figure 2.3c). Moreover, for the insular cortex a significant DRD4 main effect was observed ($F(1,32) = 4.3$, $P < 0.05$) reflecting greater overall activity in the CC group (see Figure 2.3c).

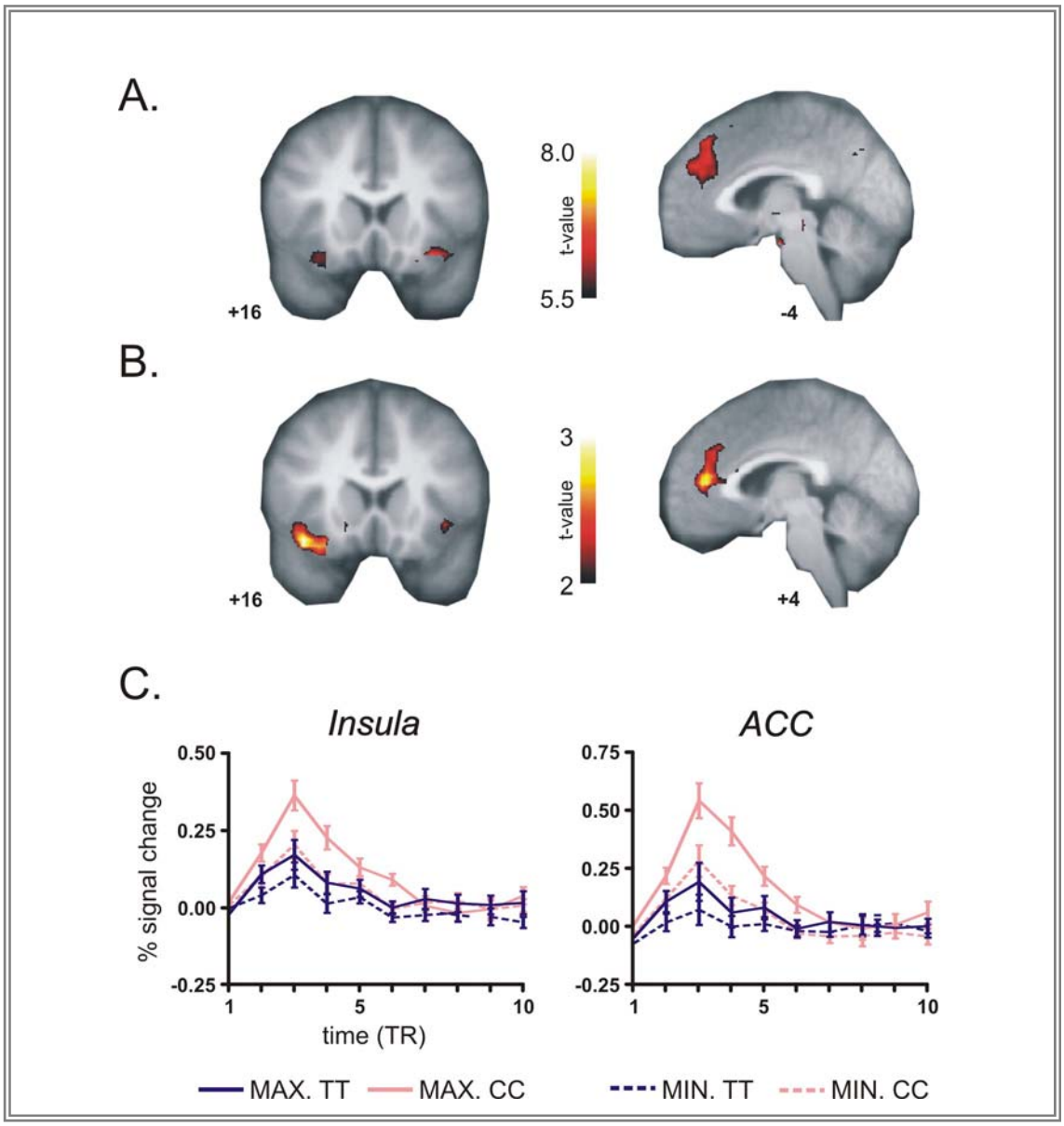

Figure 2.3: A. Magnitude effects, reward sensitivity contrast (boost trials, maximum vs. minimum values) (*t*-score overlays after multiple comparisons correction at the whole-brain level $P < 0.05$). The main effects of magnitude were observed in the right insula (x, y, z: 24, 20, -16 mm), the ACC (8, 40, 24 mm) and the right IPL (44, -48, 40 mm). B. DRD4 difference (CC vs. TT) in the Max (Gain+Loss) vs. Min (Gain+Loss) boost contrast at the whole-brain level (*t*-score overlays, $P < 0.01$, uncorrected). C. Left, time-course peak activation of the reconstructed hemodynamic response in the right insula (24, 20, -16 mm) in gain trials only. A larger amplitude of the response was observed in the CC group for maximum gains. A similar pattern was seen for the rostral ACC region (8, 40, 24 mm, right).

2.3.4. Exploratory analysis: COMT modulations in the ACC and IPL

The use of a very conservative threshold revealed only one significant region for the Valence contrast, i.e. the NAcc. In light of previous studies (e.g., Riba et al., 2008),

which have also found activity in medial prefrontal cortex, and because of theoretical accounts predicting a coupling between the ventral striatum (NAcc) and medial prefrontal cortex (ACC; Holroyd and Coles, 2002), we evaluated the SPM interaction contrast between COMT by Valence in boost trials (gain 125 > loss 125) at the whole-brain level. A less conservative threshold was applied for this analysis ($P < 0.001$ uncorrected, 20 voxels spatial extent; corrected for multiple comparisons at the cluster level, $P < 0.01$), which revealed two regions showing a COMT by Valence interaction (boost trials): the posterior medial prefrontal cortex (ACC) and the inferior parietal lobe (rIPL) (see Table 2.2a and Figure 2.4a-4b). We also reconstructed the corresponding BOLD event-related responses for both regions and carried out the corresponding ANOVAs. As expected, the ValVal group showed a greater difference between gains and losses (see difference BOLD response, Figure 2.4, right panel). For the ACC, the corresponding ANOVA showed a significant interaction between Valence and COMT ($F(1,32) = 22.3$; $P < 0.001$; Valence main effect, $F(1,32) = 10.3$, $P < 0.003$). Further pairwise group comparisons showed that while there were no differences in the MetMet group between gains and losses in this region ($t(17) < 1$), this difference was highly significant in the ValVal group ($t(17) = 6.2$, $P < 0.001$). Figure 4c illustrates the contrast between unexpected gain and loss boost trials for ValVal and MetMet groups separately. The MetMet group did not show differential activation (see also time course of the BOLD difference).

The pattern of activation observed in the rIPL was unpredicted but very reliable (see Figure 4b). A significant interaction was encountered in this region (Valence x Group, $F(1,32) = 15.3$, $P < 0.001$; Valence main effect, $F(1,32) = 9.9$, $P < 0.003$). Further pairwise comparisons showed that the COMT groups differed for the loss trials only (t

(34) = 2.6, $P < 0.012$; gains: $t < 1$; see Figure 2.4b). As it was the case for the ACC, no differential activation was seen in the MetMet group (see also Figure 2.4c).

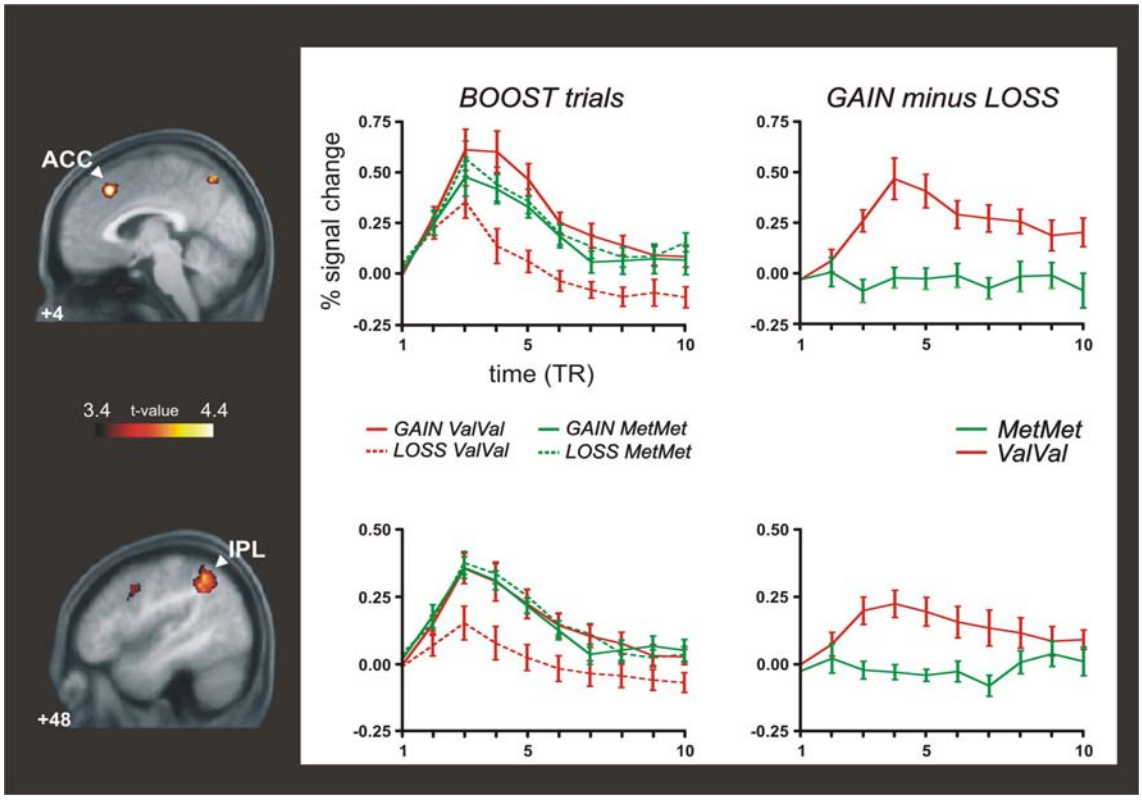

Figure 2.4: Sagittal views of the COMT difference (ValVal vs. MetMet) in the Gain vs. Loss contrast (boost trials) showing the main significant difference for the COMT alleles in the ACC (peak x, y, z: 4, 24, 48 mm) and left IPL (peak x, y, z: 44, -48, 40 mm) (*t*-score overlays, $P < 0.001$, uncorrected). The middle panel shows the BOLD time course for boost reward conditions separately for each COMT genotype in the two regions. On the right the corresponding gain minus loss difference waves are shown. A larger difference was present in the ValVal group in both regions.

Table 2.1: Main effects observed for Valence and Magnitude in standard and boost trials.

A. Valence standard trials: Gain (5+25) vs. Loss (5+25)

			Stereotactic coordinates				
Brain region	**~BA**	**n. voxels**	**x**	**y**	**z**	***T* peak**	***p* value**
L ventral striatum		59	-24	4	-12	6.52	<0.0001
			-12	8	-12	6.13	<0.0001
R ventral striatum			28	-8	-4	6.22	<0.0001

B. Valence boost trials: Gain (125) vs. Loss (125)

			Stereotactic coordinates				
L ventral striatum		79	-8	4	-8	6.68	<0.0001
R ventral striatum			16	8	-4	6.32	<0.0001
R cuneus	BA18	56	12	-88	16	6.81	<0.0001

C. Magnitude in boost trials: 125 (Gain + Loss) vs. 7/27 (Gain + Loss)

			Stereotactic coordinates				
R cuneus	BA18	43	20	-95	0	7.62	<0.0001
R INS		25	24	20	-16	7.01	<0.0001
Rostral ACC	BA32	80	8	40	24	6.65	<0.0001
R IPL	BA40	26	44	-48	48	6.02	<0.0001

Notes: MNI coordinates and T value for the peak location in a particular identified anatomical cluster. $p < 0.05$; 20 voxels spatial extent corrected for multiple comparisons at the whole-brain level by using a family-wise error (FWE) rate. Reported also the *p* value for the peak of activation at cluster level corrected for multiple comparisons and the number of voxels in each cluster (n. voxels)._BA = approximate Brodman's area; L = Left hemisphere; R = Right hemisphere; INS=Insular cortex; ACC=Anterior cingulate cortex; IPL=Inferior parietal lobe.

Table 2.2: Interactions between COMT and Valence effects in the corresponding boost trial contrasts

A. COMT x Valence [Gain (125) vs. Loss (125)]

			Stereotactic coordinates				
Brain region	**~BA**	**n. voxels**	**x**	**y**	**z**	***T* peak**	***p* value**
Posterior media PFC (ACC)	BA8/BA32	27	4	24	48	4.77	<0.01
R IPL	BA40	55	44	-48	40	3.84	<0.001

Notes: MNI coordinates and *T*-value for the peak location in a particular identified anatomical cluster. $P < 0.001$; 20 voxels spatial extent uncorrected for multiple comparisons at the whole-brain level. Reported also the *P* value for the peak of activation at cluster level the number of voxels in each cluster (n. voxels).

2.4. Discussion

Consistent with our working hypothesis derived from the phasic-tonic account (Bilder et al., 2004), we encountered a larger differential increase in the NAcc activity for ValVal homozygous participants after the delivery of large and unexpected monetary gains (boost trials) when compared to the MetMet group (Figure 2c,d). A similar pattern was also seen in the posterior medial prefrontal cortex (ACC) and the right inferior parietal lobe (Figure 2). This pattern was observed in the boost but not in the standard trials. This result is compatible with the idea that subtle genetic differences might manifest themselves only in extreme or demanding conditions and thus corroborates previous work on COMT and working memory in which genetic effects were found only in the most taxing conditions (Egan et al., 2001; Bertolino et al., 2006). Whereas the DRD4 polymorphism did not show an effect of valence, it modulated the brain's sensitivity to the magnitude of the feedback stimulus, i.e. the CC-group showed a larger activation in the boost (gain+loss) vs. unexpected similar

(gain+loss) contrast in two reward-related regions, the rostral ACC and the right insular cortex (Figure 2.3).

2.4.1. COMT effects on valence

Whereas monetary gains and losses activated a similar fronto-striatal network for standard and boost trials, monetary gains elicited greater activation which replicates previous studies (van Veen et al., 2004; Nieuwenhuis et al., 2005; Marco-Pallares et al., 2007). Additionally, BOLD activations were more sustained for gain, again replicating earlier studies (Delgado et al., 2000; Delgado et al., 2003; May et al., 2004). No modulation of valence effects by the DRD4 polymorphism was seen. In contrast, a profound effect of COMT genetic differences was observed, in that a greater gain/loss difference was seen for the boost trials in the ValVal group. To reiterate, the phasic-tonic hypothesis advanced with respect to the differential effects of Met and Val alleles of the COMT polymorphism (Bilder et al., 2004) proposes that low prefrontal tonic levels of DA (associated to the Val allele) would lead an amplification of the phasic dopamine response in the NAcc.

Critically, our conclusions are based on the significant interaction between condition (gain vs. loss) and COMT (MetMet vs. ValVal) in the NAcc and ACC reflecting mostly a decrease in activity to the loss trials for ValVal participants (see Figure 2d and 4a/b). Thus, it is crucial to our interpretation and the predictions of the phasic-tonic DA regulation model, whether this smaller response to losses in the ValVal group reflects diminished presynaptic input from the midbrain dopaminergic neurons. In a recent study, Tom et al. (2007) showed that the activation in the ventral striatum decreased as the size of a potential loss increased. Thus, the degree of suppression of the BOLD

response to losses appears to be related to the impact of the loss. This also is consistent with primate electrophysiological recordings showing decreased midbrain dopamine neural firing for negative events (Mirenowicz and Schultz, 1996). As the ventral striatum is one of the target regions of dopaminergic midbrain neurons, less dopaminergic input to the ventral striatum is expected after losses. This reduction of input to the NAcc could lead to a reduced or even negative BOLD signal.

The present results complement a recent paper investigating the effects of COMT and dopamine transporter (DAT) polymorphisms on reward anticipation (Yacubian et al., 2007). In this study the ventral striatum showed activation that scaled as a function of both, reward probability and magnitude. MetMet participants showed larger responses in the ventral striatum and the prefrontal cortex compared to ValVal carriers, i.e. an effect that is seemingly opposite to the one found in the current study. The pattern of results in the Yacubian et al. (2007) study was considerably more complicated, however. Overall, an increase in striatal activity was seen when anticipation of high probability large rewards was compared to low probability small rewards. When genotypes for both genes were examined in isolation, no effect was seen on the slope of this striatal activation increase. However, when MetMet homozygous participants were considered that were also carrying the 9R variant of DAT an increase of striatal activity was seen from low probability small to high probability large rewards, while ValVal / 9R participants showed an opposite tendency. Interestingly, MetMet participants also carrying the 10R variant showed higher striatal activity for low probability small rewards than high probability large rewards, while, again, carriers of the ValVal / 10R combination showed an opposite effect. It is important to point out that Yacubian et al. (2007) studied reward *anticipation*, whereas the present study focused on the *delivery* of unexpectedly high reward outcomes and participants were not able to predict when

boost trials would appear. The differences between both studies might thus be related to differences in the neural mechanisms involved in anticipation and processing of reward outcomes. For example, reward anticipation has been shown to rely more on tonic dopaminergic activity (Fiorillo et al., 2003), whereas the processing of unexpected rewards is thought to be related to phasic dopaminergic activity (Schultz, 2002). As MetMet participants are thought to have higher tonic but blunted phasic dopaminergic response, this could explain their smaller response in the current study but greater response in the Yacubian et al. (2007) study.

The greater ACC activation for boost gains in the ValVal group (Fig. 2e) is consistent with previous observations showing that this region is modulated by the valence of performance feedback (larger for positive than negative, Nieuwenhuis et al., 2005). This region has also been found to be activated in several reward studies (Elliott et al., 1998; Knutson et al., 2000; Delgado et al., 2003; Rogers et al., 2004; Taylor et al., 2006) and a number of recent investigations highlighted the interactions of the ACC and the ventral striatum (Lee et al., 2007; Walton et al., 2007; Rushworth and Behrens, 2008). The larger differential activation observed in the ValVal group in conjunction with the greater effect in this group for the NAcc suggests that the reinforcement learning system functions at a higher gain in this group.

The more pronounced activation in the right inferior parietal lobe for the ValVal group could be related to an increased salience of positive vs. negative outcomes in this group in boost trials, as this region has been shown to reflect allocation of attention resources (Corbetta et al., 2000). Also, the posterior parietal, as well as the cingulate cortex, have been associated to the desirability of an action in oculomotor tasks (Platt and Glimcher,

1999; Glimcher, 2003; Dorris and Glimcher, 2004; McCoy and Platt, 2005; Sugrue et al., 2004; Sugrue et al., 2005).

2.4.2. DRD4 effects in the insular cortex and rostral ACC

Two regions showed increased activity in the DRD4/CC homozygous participants relative to the TT group as a function of reward magnitude: the rostral ACC and the anterior insular cortex. Magnitude related activations in the insular cortex have been previously reported (Elliott et al., 2000; Knutson et al., 2000; Breiter et al., 2001; Delgado et al., 2003). The magnitude effect in the rostral ACC may be related to the role of this area in emotional processing (Devinsky et al., 1995; Bush et al., 2000). Interestingly, lesions in rats in the ACC impair the choice of a high-cost/high-reward option, without affecting the choice of a less-demanding and less-rewarding option (Walton et al., 2003).

The modulation of magnitude-related activity by the DRD4 polymorphism in both regions suggests a role of the D4 receptor in the assessment of the magnitude or impact of outcomes. This may go hand-in-hand with the reported associations between this polymorphism and novelty seeking (Okuyama et al., 2000; Ronai et al., 2001; Schinka et al., 2002; Golimbet et al., 2007). This interpretation should be regarded tentative at this point due to the lack of knowledge about the transcriptional effects of this polymorphism (Ogawa et al., 1990; Kereszturi et al., 2006). The importance of genetic differences of D2-type receptors, to which the D4 receptor belongs, has been underscored by previous functional investigations, however. For example, Fan et al. (2003) studied the insertion/deletion of a guanosine residue at the upstream position -1217 of the DRD4 gene and found greater conflict-related brain activity in the ACC in participants carrying the insertion variant of the polymorphism. Focusing on the

presence/absence of the A1 allele on the dopamine D2 receptor gene, Cohen et al. (2005) showed that this polymorphism predicted a significant amount of inter-subject variability in the magnitudes of reward-related, but not anticipation-related, activations. Moreover, Klein et al. (2007) demonstrated that presence of the A1-allele, known to lead to a reduced receptor density, is associated to a reduced BOLD response to negative feedback in the medial prefrontal cortex.

2.5. Conclusions

In the present study we demonstrate a double dissociation with regard to the impact of two dopaminergic polymorphisms on the processing of rewards: The COMT Val(108/158)Met polymorphism modulated valence related responses in the ventral striatum and the ACC for unexpectedly large gains/losses, whereas the C/T polymorphism at position -521 of the dopamine receptor D4 gene was associated to differential activity as a function of reward magnitude.

Chapter 3[♣]

3. Functional connectivity approach:

Functional brain connectivity of reward processing in humans

3.1. Introduction

Bribing someone with cash or, alternatively, threatening him with a high penalty powerfully influences behaviour, as we try to adapt our actions in order to obtain the rewards and avoid punishments. Expectations of both punishment and reward also have an impact on future decisions, since we try to increase the probability of the occurrence of positive reinforcement and to minimize the recurrence of adverse events (Daw et al., 2006).

The delineation of the neural circuits subserving the processing of rewards and punishments and their translation into action is therefore of great importance, but controversial findings have been reported. On the one hand, there is ample evidence indicating that monetary gains and losses activate a similar fronto-subcortical network but to a differential degree (Gottfried et al., 2003; van Veen et al., 2004; Nieuwenhuis et al., 2005; Dreher, 2007; Marco-Pallares et al., 2007; Tom et al., 2007). On the other

---

[♣] Camara et al. **Functional brain connectivity of reward processing in humans.** (In preparation).

hand, recent studies suggest that reward and punishment outcomes may be processed by different neural circuits (Frank et al., 2004; Yacubian et al., 2006; Wrase et al., 2007). For example, modelling work of Frank et al. (Frank et al., 2004) distinguishes between two excitatory/inhibitory pathways in the basal ganglia, which show differential modulation during positive and negative reinforcement processing. Dopamine release is typically evoked by positive outcomes, and in turn increases the activity in the excitatory pathway and suppresses the activity in the in the inhibitory connection. In contrast, negative events are associated with dips in dopamine levels, and thus show opposite effects. Drawing on neuroimaging results, Yacubian et al. (Yacubian et al., 2006) distinguish two systems involved in predictions made concerning either possible gains or losses: By this account the ventral striatum generates predictions based on possible gains and compares these to actual outcomes, whereas the amygdala is involved in the prediction of possible losses, again comparing these to actual outcomes. Furthermore, Wrase et al. (Wrase et al., 2007) showed that different neural systems adjust motor behaviour in response to differences in reward and punishment outcomes.

Although there is a large body of neuroimaging literature concerning the regions involved in the processing of reward and punishments, the picture provided is rather static. In the present communication we therefore investigate the functional connectivity patterns between different cortical and subcortical regions in response to monetary gains and losses. Indeed, a complete understanding of reward processing requires not only to identify the activated brain regions, but also to distinguish how these regions flexibly interact in response to different outcomes. Previous results addressing other cognitive processes have shown that analyses of functional connectivity are not redundant when compared with standard analyses of brain

activation changes (Gazzaley et al., 2004; Rissman et al., 2004; Buchsbaum et al., 2005; Ranganath, Heller, Cohen, Brozinsky, and Rissman, 2005; Fiebach and Schubotz, 2006). In particular, different functional connectivity patterns may reveal different brain networks that in turn might mediate various aspects of behaviour. For instance, Cohen et al. (Cohen, Heller, and Ranganath, 2005) demonstrated an increase of the estimated functional connectivity between the anterior cingulate (ACC) and the nucleus accumbens (NAcc), when comparing high-risk vs. low-risk gambling decisions. Cohen et al. (Cohen, Elger, and Weber, 2008) also reported recently that the microstructural properties of white matter tracts connecting the amygdala to the hippocampus, orbitofrontal cortex, and the ventral striatum predicted functional connectivity derived from fMRI time series and participants' behaviour following both positive and negative feedback in a reversal learning task (Cohen et al., 2008).

Which regions might interact in the processing of reward? The ventral striatum has been proposed to be involved in the selection of appropriate responses and the modulation of goal-directed behaviour (Berridge and Robinson, 1998; Kelley and Berridge, 2002). This region has shown increased activation in the presence of positive reward outcomes (monetary gains) when compared to negative outcomes (monetary losses) in several studies (Delgado et al., 2000; Delgado et al., 2003; May et al., 2004; Riba et al., 2008). More importantly, studies by Tom et al. (Tom et al., 2007) have recently shown that activation in the ventral striatum decreased as the size of the potential loss increased. The ventral striatum receives synaptic inputs from the orbitofrontal cortex (OFC), dorsolateral prefrontal cortex, (DLPFC), limbic structures such as hippocampus and amygdala (Groenewegen et al., 1999), and is the target of dense dopaminergic projections originating in the ventral tegmental area (VTA, Voorn et al., 1986). The VTA has been repeatedly associated to learning and motivation

(Schultz, 2007). Taking into account this information, the ventral striatum is a key candidate in the study of functional connectivity in the context of reward processing.

With this aim, healthy volunteers were involved in a simple gambling task adapted from Gehring and Willoughby (2002) and Riba et al. (Riba et al., 2008). In this task unexpected and large monetary gains and losses (henceforth boost trials) occurred infrequently in addition to frequent gain and loss trials of smaller magnitudes. We used the "beta series correlation" method proposed by Rissman et al. (Rissman et al., 2004) to examine event-related changes in whole-brain functional connectivity with the ventral striatum as a seed region and to compare reward and punishment functional connectivity patterns. The beta series bivariate method uses a standard general linear model approach but adapts the model in such a way that separate beta values (general linear model parameter estimates) are obtained in order to modulate activation changes for each component of each individual trial. With this approach, a series of parameter estimates can be extracted from a seed region, correlated across the brain to identify specific networks. If two regions are functionally interacting during a specific event, the fluctuation of BOLD activity of both regions across trials should be correlated. We predict that the role of reward and punishment outcomes might be functionally differentiated by examining patterns of brain connectivity. To our knowledge, no other study has directly compared functional connectivity with reward and punishment outcomes.

3.2. Materials and methods

3.2.1. Participants

Seventeen young adult students [10 women, 21.6 ± 2.6 (SD) mean age] from the University of Barcelona participated in the study. All participants were healthy, right-handed native Spanish speakers with no history of neurological or psychiatric episodes. They all gave written informed consent to a protocol approved by the University of Barcelona ethics committee.

3.2.2. Design

Several important modifications were made to the monetary gambling task designed by Gehring and Willoughby, (2002). In the standard trials (80%) a warning signal was presented ("*"; 500 ms duration) followed by the presentation of two numbers (5 and 25) displayed in white against a black background in the two possible combinations, [5 25] or [25 5]. Participants had to select one of the two numbers by pressing a spatially corresponding button with the left or right index finger. One second after the choice, one of the numbers turned green and the other turned red. If the number selected by the participant changed to red, the participant incurred a loss of the corresponding amount of money in Euro cent. In contrast, if the number turned into green, this indicated a gain.

In addition to the standard trials described above, two additional conditions were created in order to assess brain responses to unexpected rewards and losses. In 10 % of the trials ("boost unexpected trials"), an unexpected large gain or loss occurred. Independently of the chosen item (either 5 or 25) the feedback turned into 125 (125 €

cents) again having either green or red color indicating wins or losses. This change in magnitude occurred equally often for the "5" and "25" trial bets in order to avoid positive or negative biases in choosing "25" items. To control for the fact that boost trials were both, large and unexpected, in an additional 10 % of the trials ("similar unexpected") the chosen number turned to either 7 (instead of 5) or 27 (instead of 25). While these trials were unexpected, the magnitude of the gain or loss was virtually unchanged. Additionally, each run included 12 randomized fixation trials that lasted 20 seconds.

Participants were provided with an initial 10 € sum and were encouraged to win as much as possible. They had performed in a similar event-related potential task (without unexpected trials) several weeks to months earlier and thus were familiar with the task in general. They were informed about the potential occurrence of unexpected trials. The experiment comprised four blocks of 140 trials each. The four possible outcomes for the standard trials ([25 5] [5 25] [5 25] [25 5]; italics = red = loss, bold = green = gain), for the unexpected similar trials ([25 7] [5 27] [7 25] [27 5]), and for the unexpected boost trials ([25 125] [5 125] [125 25] [125 5]) were presented in random order. These combinations were counterbalanced by condition, making the statistically expected outcome zero on each trial in order to avoid confounds of differential probability of gains or losses. At the end of each run, participants were informed about the accumulated amount of money. At the end of the experiment, participants were paid the final amount obtained.

3.2.3. MRI scanning methods

fMRI data was collected using a 3T whole-body MRI scanner (Siemens Magnetom Trio, Erlangen, Germany). Visual images were back-projected onto a screen using an LED-

projector and participants viewed the images through a mirror on the head coil. Magnet compatible response buttons were used. Conventional high-resolution structural images [magnetization-prepared, rapid-acquired gradient echoes (MPRAGE) sequence, 192 slice sagittal, TR = 2500 ms, TE = 4.77 ms, TI = 1100 ms, flip angle = 7°, 1mm thickness (isotropic voxels)] were followed by functional images sensitive to blood oxygenation level-dependent contrast (echo planar T2*-weighted gradient echo sequence, TR=2000 ms, TE=30 ms, flip=80°). Each functional run consisted of 336 sequential whole-brain volumes comprising 32 axial slices aligned to the plane intersecting the anterior and posterior commissures, 3.5 mm in-plane resolution, 4 mm thickness, no gap, positioned to cover all but the most superior region of the brain and the cerebellum.

3.2.4. Image processing

Functional images were analyzed using standard procedures implemented in the Statistical Parameter Mapping software (SPM2, *http://www.fil.ion.ucl.ac.uk/spm)*. First, functional volumes were phase shifted in time with reference to the first slice to minimize purely acquisition-dependent signal-variations across slices. Head-movement artefacts were corrected based on an affine rigid body transformation, where the reference volume was the first image of the first run (e.g., Friston et al., 1996). Functional data was then spatially smoothed with an 8 mm full-width half-maximum (FWHM) isotropic Gaussian Kernel.

For the group-level analyses, realigned functional data was averaged and the mean functional image was normalized to a standard stereotactic space using the EPI derived MNI template (ICBM 152, Montreal Neurological Institute) provided by SPM2. After an

initial 12-parameter affine transformation, an iterative non-linear normalization was applied using discrete cosine basis functions by which brain warps are expanded in SPM2 (Ashburner et al., 1999). Resulting normalization parameters derived for the mean image were applied to the whole functional set. Finally, functional EPI volumes were resampled into 4 mm cubic voxels and then spatially smoothed with an 8 mm full-width half-maximum (FWHM) isotropic Gaussian Kernel to minimize effects of inter-subject anatomical differences. Notice that all statistical analyses, with the exception of the group statistics in the functional connectivity analysis (see below) were performed in native space (i.e., without spatial normalization).

3.2.5. Data analysis

3.2.5.1. Univariate fMRI analysis

The statistical evaluation of our data was based on a least-square estimation using the general linear model by modeling the different conditions with a regressor waveform convolved with a canonical hemodynamic response function (Friston et al., 1998). Thus, an event-related design matrix was created including the conditions of interest: Gain 5, Gain 25, Gain 7/27, Gain 125, Loss 5, Loss 25, Loss 7/27, Loss 125 and fixation. Both native and normalized data was high-pass filtered (to a maximum of 1/90 Hz), and serial autocorrelations were estimated using an autoregressive model (AR(1) model). Resulting estimates were used for non-sphericity correction during the model estimation. Confounding effects in global mean were removed by proportional scaling, and signal-correlated motion effects were minimized by including the estimated movement parameters.

One of the attributes that boosts the impact of reward is the degree of uncertainty that exists in the estimation of the action's value. Indeed, reward information becomes more relevant as the uncertainty of the reward prediction and the magnitude of the outcome increases (Schultz et al., 1997; Fiorillo et al., 2003). Accordingly, in order to focus on those conditions in which the impact of feedback in the reward processing system was largest, the analysis was constrained to the unexpected boost gain and loss trials. To compare these trials, we created two analogous functional contrasts: Gain (125) vs. Fixation and Loss (125) vs. Fixation. Second, brain regions responding selectively to gains and losses were defined by the Gain (125) vs. Loss (125) contrast reflecting the effect of valence in the unexpected boost trials.

3.2.5.2. Region of Interest Analysis (ROI)

A standard approach used for identifying functional networks requires the definition of an *a priori* region of interest, which is then used to determine which voxels throughout the whole-brain are functionally interacting with the selected ROI. Given the strong evidence concerning the main role of the ventral striatum in processing rewards and losses, functional ROIs were selected by applying a statistical threshold of $P < 0.01$ (uncorrected) to the anatomically defined search space. Specifically, the left and right NAcc ROI was functionally defined for each participant in native space by identifying the statistically significant activation cluster in the Gain (125) vs. Loss (125) boost trials contrast.

3.2.5.3. Functional connectivity analysis

Functional connectivity analysis was performed using the method proposed by Rissman et al. (Rissman et al., 2004) using the parameter estimates obtained in the

context of the general linear model. The analysis was based on the hypothesis that if different regions are involved in a network, strongly correlated activity patterns should be observed among them and functional brain connections can thus be inferred.

In particular, each specific trial was modelled as an independent covariate in the study design matrix, which allowed the assessment of a trial-to-trial parameter estimate for each condition. For each participant, the parameter estimates series obtained were sorted by conditions. For the conditions of interest [boost loss and boost gain], the corresponding parameter estimates were averaged across all voxels of the left and right NAcc ROI. Thereafter, individual native space correlation maps were generated for each participant and condition by correlating the seed region with the beta series of each voxel in the whole brain. To allow statistical inferences to be made based on the correlation magnitude, an arc-hyperbolic tangent transform was applied to normalize the correlation coefficients, which were then z-transformed. The z-transformed correlation maps were spatially smoothed with an 8 mm full-width half-maximum (FWHM) isotropic Gaussian Kernel to minimize effects of inter-subject anatomical differences. The resulting condition-specific connectivity maps were then normalized by applying the corresponding normalization parameters, which had been computed earlier. The individual contrast images were entered into a second-level analysis using a one-sample t test using a random effects analysis within the general linear model in order to characterize the networks involved in processing gains and losses. Maps thresholded at $P < 0.00001$, uncorrected for multiple comparisons, were used for further discussion. Thereafter, correlation maps were compared between the gain and loss contrast at the group level applying a paired samples t-test, using a $P < 0.001$ uncorrected for multiple comparison threshold.

Finally, under the assumption that functional interactions between brain regions should reflect differential functional brain activations, we investigated how the differential connectivity profile observed between the gain and loss condition interacted with the functional activation pattern: group-level standard parameter estimates were averaged separately by condition and compared with each other in the statistically significant connectivity cluster. The connectivity cluster applied for testing the expected interaction was defined under the differential connectivity pattern, using a $P < 0.05$ uncorrected for multiple comparison threshold.

3.3. Results

3.3.1. Univariate analysis for gain and loss trials

In the present gambling task, we focus our analysis on the unexpected gain and loss boost trials. Standard functional univariate analysis was performed in order to compare the overall pattern of activity for gains and losses. This analysis revealed a very similar fronto-subcortical-parietal network when monetary gains or losses were incurred (see Table 3.1). To summarize the tabulated results, significant activations were observed in the cingulate cortex, the superior frontal cortex, the inferior parietal lobe, the insular cortex, parahippocampal regions, the thalamus, the caudate nuclei, and the ventral striatum. Indeed, and consistent with previous studies, monetary gains elicited greater activation compared to loss trials. The gain vs. loss contrast [i.e., gain (125) vs. loss (125)] showed bilateral activation in the ventral striatum (NAcc) in all participants (peak activity, MNI coordinates, x, y, z, left hemisphere, -16, 4, -4, $t = 8.81$, $P < 0.002$; right hemisphere, coord. 16, 8, -16, $T = 8.62$, $P < 0.002$; P-value at FWE voxel level corrected). Additionally, no significant differences were found in the inverse contrast

(loss vs. gain trials), even after lowering the threshold to $P < 0.05$ uncorrected. Overall, the analysis shows that positive and negative outcomes evoked very similar brain activity (see Figure 3.1).

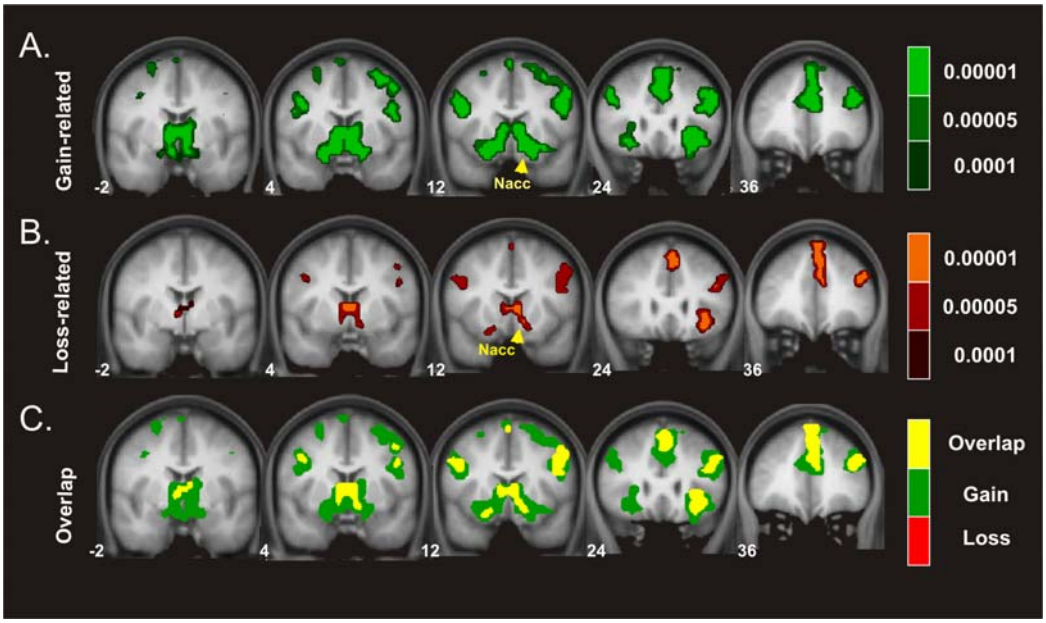

Figure 3.1: Coronal views of group average whole-brain univariate functional analysis superimposed on a group-averaged structural MRI image in standard stereotactic space (*T*-score overlays). Depicted the Gain vs. fixation contrast (A) and the Loss vs. fixation contrast (B) using different statistical thresholds ($p < 0.0001$; $p < 0.0005$; $p < 0.001$). Positive and negative outcome patterns are simultaneously represented in (C): GAIN green; $p < 0.001$, LOSS (red; $p < 0.001$), and conjunction GAIN ∩ LOSS (yellow; $p < 0.001$ and $p < 0.001$).

3.3.2. Functional connectivity analysis

Concerning functional connectivity, we used the ventral striatum (NAcc) identified above as a seed region to contrast gains vs. losses and to determine which brain regions significantly correlated with activity in the ventral striatum. First, functional connectivity was examined separately for gains and losses and then tested for significant differences in connectivity between both conditions. The list of the functional connectivity interactions reported in this paper is presented in Table 3.2.

An extensive network of regions including the hippocampus, insular cortex, and orbitofrontal cortex exhibited activity that correlated significantly with the activity seen in the ventral striatum in gain trials as well as in loss trials (see Figure 3.2).

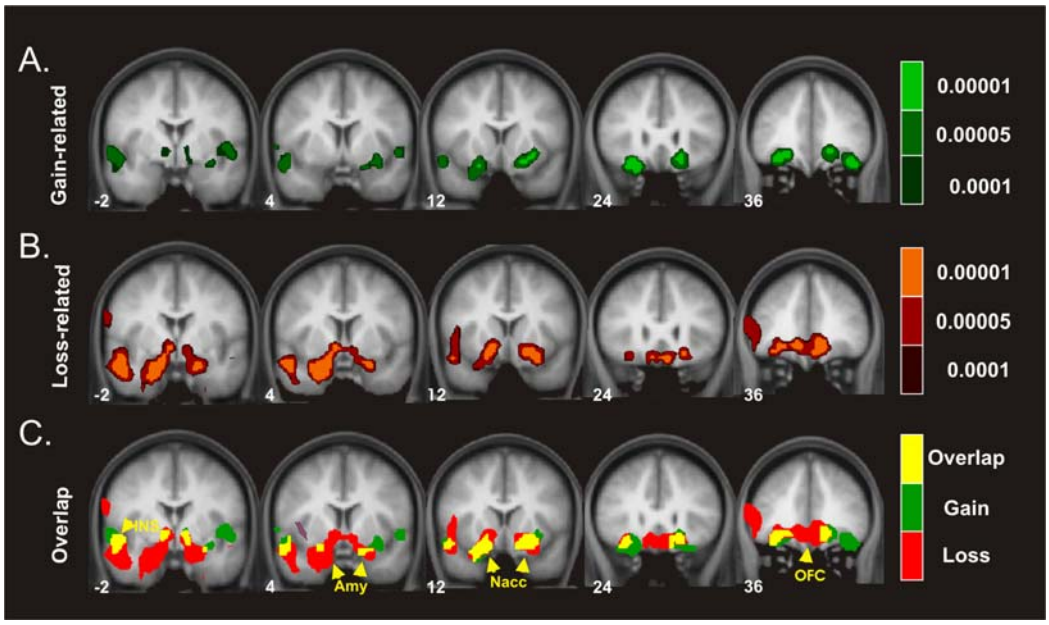

Figure 3.2: Coronal views of the group average whole-brain interregional interactions with the ventral striatum superimposed on a group-averaged structural MRI image in standard stereotactic space (*t*-score overlays). Functional connectivity is examined in the reward (A), and punishment (B) condition using different statistical thresholds ($p < 0.0001$; $p < 0.0005$; $p < 0.001$). Gain and Loss connectivity patterns are simultaneously depicted in (C): GAIN green; $p < 0.001$, LOSS (red; $p < 0.001$), and conjunction GAIN ∩ LOSS (yellow; $P < 0.001$ and $p < 0.001$).

We also investigated which regions showed a significant difference in correlation with the NAcc for gain > loss trials. Whereas this contrast revealed no significant differences in connectivity, we found significant differences in the inverse contrast (i.e. loss > gain) in the medial orbitofrontal cortex (OFC, peak activity, -8, 24, -16).

Finally, in order to investigate the impact of the differential connectivity pattern observed in the functional domain, group-level standard parameter estimates were compared between conditions in the statistically significant connectivity cluster. Indeed, the differential connectivity pattern also revealed a differential functional activation pattern when the gain and loss conditions were directly compared (F (1,16) = 5.3, P < 0.036, cluster size = 44 voxels extent). A clear increase in BOLD signal was observed for gains, whereas a decrease was seen for losses (see Figure 3.3).

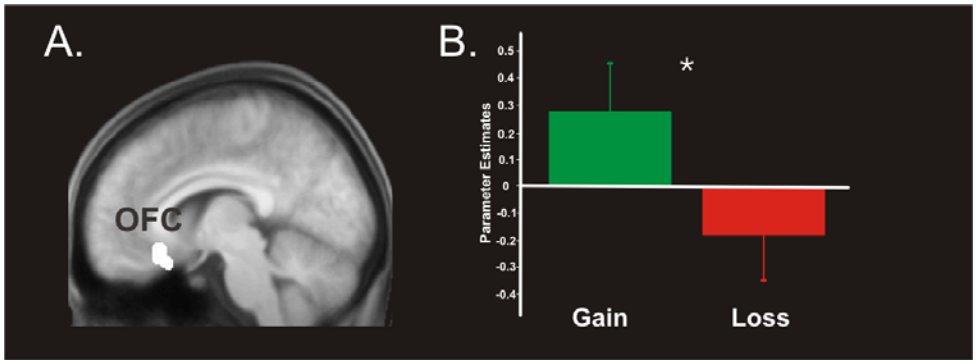

Figure 3.3: Group-level parameters estimates from the univariate analysis are compared between the gain and the loss condition in the OFC cluster identified in the functional connectivity analysis (contrast between gains and losses). The left panel plots the region of interest selected superimposed in the group-averaged structural MRI image in standard stereotactic space (A). The right panel shows a bar graph depicting the beta values (general linear model parameter estimates) for gains and losses (B). Error bars represent standard errors about the mean across subjects.

Table 3.1: Main effects for valence in standard functional analysis

Gain (125) vs. Fix

		Stereotactic coordinates				
Brain region	**~BA**	**X**	**Y**	**Z**	**T peak**	**p value FEW-cor**
R IPL	40	36	-56	48	21.57	0.0001
L IPL	40	-36	-52	52	14.17	0.0001
SMA/ACC		4	24	52	14.58	0.0001
L ventral striatum		-16	12	-12	12.24	0.0001
R ventral striatum		8	4	-8	10.89	0.0001
R Talamus		4	-16	8	10.13	0.0001
L Talamus		-4	-12	8	9.28	0.001
R Caudate		8	8	4	8.44	0.003
R DLPC	46	44	36	28	10.49	0.0001
R INS		36	20	-8	9.76	0.0001
L FSG/pahip	37	-36	-56	-12	11.07	0.0001
		-28	-64	4	10.30	0.0001
Cu	18	-4	-50	-4	12.42	0.0001

Loss (125) vs. Fix

		Stereotactic coordinates				
R IPL	40	32	-56	48	12.65	0.0001
L IPL	40	-36	-52	52	10.27	0.0001
SMA/ACC		0	32	32	6.98	0.0001
R DLPC	46	44	36	24	7.53	0.015
L INS		36	20	-12	7.31	0.021
		4	8	8	6.76	0.015
		12	8	-8	6.12	
R pahip		24	-52	4	8.45	0.003

R FSG	20	36	-64	-12	7.71	0.0001
L FSG/pahip	37	-36	-56	-8	10.12	0.0001
Cu		12	-88	4	7.99	0.007

Notes: MNI coordinates and T value for the peak location in a particular identified anatomical cluster. $p < 0.0001$; 20 voxels spatial extent uncorrected for multiple comparisons. Reported the p-value FWE-corrected *p*-value at voxel-level. BA = approximate Brodman's area; L = Left hemisphere; R = Right hemisphere; IPL= inferior parietal lobe; SMA=supplementary motor area; ACC=anterior cingulate cortex; DLPC= dorso lateral prefrontal cortex; INS=insula; FSG=fusiform gyrus; pahip=parahippocampus; Cu=cunneus;

Table 3.2: Main effects for valence in the interregional interactions with the ventral striatum

A. Gain-related interregional interactions with the ventral striatun

		Stereotactic coordinates				
Brain region	**~BA**	x	y	z	***T* peak**	***p value FEW-cor***
L VLPC	11	-24	28	-12	7.86	0.012
	11	-32	40	-12	7.18	0.034
R VLPC	11	20	32	-8	6.9	0.049
R INS		40	-12	-4	7.70	0.015
R Cerebellum		32	-64	-32	7.32	0.028
R Hippocampus		32	-24	-4	7.29	0.029
R Amy		20	-16	-20	7.19	0.034
L MTG	21	-48	-36	-16	7.16	0.035
R ventral striatum		16	-12	-16	7.04	0.041

B. Loss-related interregional interactions with the ventral striatun

		Stereotactic coordinates				
L MTG	21	-52	-52	0	8.65	0.003
	21	-52	4	-20	7.98	0.010
L Hippocampus		-28	-24	-24	8.52	0.004
		-32	-40	-16	4.86	0.019
R MTG	21	52	-12	-8	8.28	0.006

R ventral striatum		20	16	-8	8.04	0.009
L ventral striatum		-8	4	-4	6.97	0.05
L ACC/OFC	34/10	-12	44	-8	7.85	0.012
R ACC/OFC	34/10	12	40	-8	7.62	0.019
L Amy		-24	4	-24	7.71	0.015
R Amy		28	8	-16	7.02	0.046
R INS		48	-24	0	7.45	0.023
L Cerebellum		-8	-52	-40	7.02	0.047
SN/TA		-12	-20	0	6.99	0.048

C. Loss vs. Gain interregional interactions with the ventral striatun

		Stereotactic coordinates				
Brain region	**~BA**	x	y	z	***T* peak**	***p* value**
Medial OFC	11	-8	24	-16	3.12	0.003

Notes: MNI coordinates and T value for the peak location in a particular identified anatomical cluster. $p < 0.0001$; 20 voxels spatial extent uncorrected for multiple comparisons. Reported the p-value FWE-corrected *p*-value at voxel-level. In the Loss vs Gain contrast $p < 0.001$ uncorrected for multiple comparisons. BA = approximate Brodman's area; L = Left hemisphere; R = Right hemisphere; VLPC=Ventral Lateral Prefrontal Cortex; MTG=medial temporal gyrus; INS=Insular cortex; ACC=Anterior cingulate cortex; Amy= amygdala; SN/TA= substantia nigra/ventral tegmental area.

3.4. Discussion

Applying a recently developed functional connectivity procedure (Rissman et al., 2004) in an event-related fMRI experiment addressing the neural processing of monetary rewards and losses, we examined the extent to which the interregional interactions maintained by the ventral striatum (NAcc) can be used to characterize and, possibly, dissociate the processing of gains and losses. Standard univariate fMRI analysis revealed a very similar neural network to be active for gains and losses processing,

except for the larger activation observed in the ventral striatum in gain trials. This pattern agrees with previous fMRI studies that underscored the fundamental role of this neural network in the processing, encoding, updating, and maintenance of rewards and punishments (Delgado et al., 2000; Breiter et al., 2001; Knutson et al., 2001; Delgado et al., 2003; Knutson et al., 2003; McClure et al., 2004; Yacubian et al., 2006; Tom et al., 2007; Riba et al., 2008).

The functional connectivity analysis using the ventral striatum as a seed region revealed a topographically distinct subcortical-limbic-anterior prefrontal circuit when compared to the previous standard fMRI analysis. Again similar response patterns were seen for gain and loss trials but the correlation between ventral striatum and the OFC was stronger in loss trials than in gain trials. This indicates a differential functional connectivity between both regions during the processing of gains and losses. In a more general way, the different neural network patterns observed between the standard analysis and the connectivity analysis stress the importance of studying functional connectivity as a complementary tool, as it has been successfully demonstrated in previous studies (Rissman et al., 2004; Gazzaley et al., 2004; Buchsbaum et al., 2005; Ranganath et al., 2005; Fiebach and Schubotz, 2006).

3.4.1. Functional connectivity analysis of gains and losses

Connectivity analysis using the ventral striatum activation as a seed region revealed that the mesolimbic pathway, including the orbitofrontal cortex, the insular cortex, the amygdala, and the hippocampus, exhibited activity that correlated with the activity observed in the ventral striatum in the processing of gains and losses. In light of known functional and neuroanatomical data, we will consider the possible role of each of these

regions in the processing of feedback associated with positive and negative outcomes in the following paragraphs.

3.4.1.1. The insular cortex

The functional role of the insular cortex in the processing homeostatic information, in the conscious perception of interoceptive states and emotional information has been well established (Damasio et al., 2000; Craig, 2003; Preuschoff, Quartz, and Bossaerts, 2008). The role of this region in drug craving has also been supported by several imaging studies (Wang et al., 1999; Garavan et al., 2000; Sell et al., 2000; Contreras et al., 2007). Anatomically, the insular cortex has bidirectional connections with many structures implicated in reward and decision making, including the orbitofrontal cortex, the ACC, the NAcc and the amygdala (Reynolds and Zahm, 2005). The anterior insula has also been related to reward-related uncertainty (Ernst et al., 2002; Sell et al., 2000; Paulus, Rogalsky, Simmons, Feinstein, and Stein, 2003; Hsu, Bhatt, Adolphs, Tranel, and Camerer, 2005; Reynolds and Zahm, 2005; Contreras et al., 2007; Preuschoff et al., 2008) and risk aversion (Kuhnen and Knutson, 2005; Preuschoff et al., 2008). In fact, in order to determine the correct value of an uncertain outcome, it is necessary to evaluate the risk, which is then used to estimate the expectancy of a possible reward (Preuschoff and Bossaerts, 2007). In agreement with this view, our results suggest that interregional functional connectivity between the insula and the ventral striatum appears equally strong during the processing of gains and losses. This result is partially in disagreement with the idea that the insula is primarily involved in the processing of negative events (Phillips et al., 1998; Morris et al., 1999). Because of its extensive interconnectivity, the insular cortex might be crucial for integrating emotion-related and interoceptive information and to feed this information forward to

the orbitofrontal and anterior cingulate cortex, thus influencing decision making, as well as directly affecting other reward-related limbic regions like the amygdala and NAcc.

3.4.1.2. Amygdala and Hippocampus

The amygdala projects to a wide range of brain areas, among them the hippocampus (Braak, Braak, Yilmazer, and Bohl, 1996), the ventral striatum, (McDonald, 1998; Alheid, 2003) and the substantia nigra/ventral tegmental area (McDonald, 1998), which might exert reciprocal influences in reward and affect processing (Baxter and Murray, 2001). Traditionally, the amygdala has been associated with the processing of aversive states (Baxter and Murray, 2001; Yacubian et al., 2006). However, several studies have also proposed a central role for this structure in processing both aversive and pleasant emotions (Salinas and White, 1998; Hamann, Ely, Grafton, and Kilts, 1999; Phan, Wager, Taylor, and Liberzon, 2004; Phelps and LeDoux, 2005).

The present results did not show significant differences in the connectivity patterns associated with positive and negative feedback (i.e. gains and losses) between the amygdala or the hippocampus and the NAcc. The involvement of both structures in reward-related processing has been previously reported (Salinas and White, 1998). Interestingly, the interregional connectivity encountered between the NAcc and the hippoccampus converges with existing evidence about the involvement of this region in reward processing, which probably reflects the integration of contextual aspects related to reward processing (Moore and Price, 1999; Wittmann et al., 2005; Adcock, Thangavel, Whitfield-Gabrieli, Knutson, and Gabrieli, 2006). In agreement with this idea, the activation of the substantia nigra/ventral tegmental area, and hippocampus

have also been associated with facilitation of memory formation (Schott et al., 2004; Schott et al., 2006; Wittmann, Schiltz, Boehler, and Duzel, 2008).

3.4.1.3. The role of the medial OFC in reward processing

The medial OFC was differentially involved in the processing of loss compared to gain outcomes. Its role in the processing of rewards and punishment has been extensively documented (Rolls, 1996; Rolls, 2000). O'Doherty et al. (O'Doherty, Kringelbach, Rolls, Hornak, and Andrews, 2001) reported an increase in the activity of the medial OFC as a function of the magnitude of the reward or loss incurred. They showed a graded increase in the activation of this region in relation to reward, but also a decrease relative to baseline when a punishment was delivered, a pattern similar to the one documented in Figure 3.3 for the present study. The degree of the deactivation observed in the OFC for loss trials might reflect diminished presynaptic input from NAcc neurons. This idea is supported by reports that NAcc activity is suppressed after reward outcomes (Breiter et al., 2001; May et al., 2004) and when anticipated rewards are not obtained (Delgado et al., 2000; Breiter et al., 2001; Knutson et al., 2001; O'Doherty et al., 2002; Knutson et al., 2003). Moreover, Yacubian et al. (Yacubian et al., 2006) found higher deactivation in the NAcc during loss trials when the loss condition was less likely to occur and in Tom et al. (Tom et al., 2007) activation in both the ventral striatum and the medial OFC decreased as the size of the potential loss increased. This suggests that the BOLD decrease in the NAcc and the medial OFC responses is related to the impact of the loss outcome. The present study adds the important finding of a stronger functional connectivity observed in losses compared to gains between the OFC and the NAcc.

In contrast to results seen in the functional connectivity analysis, we did not observe significant differences in the univariate analysis in the OFC for gain and loss trials. This was not true when the ROI analysis was inspected, since a significant differential activity pattern was observed (larger activation in gains). An open question is to what degree functional connectivity information can be dissociated into functional activation. One possibility is that the OFC might exhibit an overall decrease in activity when the outcome is reached although selected populations of interconnected OFC neurons remain active during outcome delivery. The BOLD signal reflects the processing of the local cortical circuitry, which results from widespread neural activity, and therefore might not be able to discern activations of selected subpopulations. In contrast, the sensitivity of the beta correlation analysis might be sensitive enough to detect trial-to-trial fluctuations in the BOLD signal (Gazzaley et al., 2004).

3.5. Conclusions

Monetary gains and losses activated a similar frontal-striatal-limbic network when large monetary outcomes were delivered. Gains and losses were functionally differentiated in the medial orbitofrontal cortex for which greater functional connectivity was shown in loss trials. Overall, the present results suggest that a very similar neural network might be involved in the processing of both gains and losses. Moreover, it is necessary to highlight that even though the proposed method attempts to untangle positive and negative feedback processing, the analysis presented here is inherently correlational and thereby no strong statements can be made about the directions of influence of one region on another. Thus, while coactivity highlights the fact that different regions are related, the nature of this relationship is not considered.

Chapter 4[♣]

4. Anatomical univariate MRI approach:

Age-related water diffusion changes in human brain:

a voxel-based approach

4.1. Introduction

Normal brain development is a complex and dynamic process exhibiting a high degree of variability across the lifespan. Existing age-related magnetic resonance imaging (MRI) volumetric studies have revealed an increase in sulcal volume and an enlargement of the lateral ventricles, accompanied by a shrinkage in brain tissue volume (Uylings and de Brabander, 2002) occurring predominantly in the prefrontal and parietal lobes (Resnick, Pham, Kraut, Zonderman, and Davatzikos, 2003b). However, these studies have focused mainly on macrostructural changes and, consequently, they are limited in resolution. In contrast, neuropathological studies have reported age-related deterioration in the micro-structure of white matter,

---

[♣] Camara, E., Bodammer, N., Rodríguez-Fornells, A., Tempelmann, K. (2007). **Age-related water diffusivity changes: a voxel-based approach.** Neuroimage, 34: 1588-99.

including demyelination or axonal loss in the cerebral cortex (Aboitiz and Montiel, 2003; Marner, Nyengaard, Tang, and Pakkenberg, 2003).

Diffusion tensor imaging (DTI) has proved itself to be a suitable method for monitoring micro-structural changes, neural architecture (Beaulieu, 2002) and possibly plasticity-related processes (Tovar-Moll et al., 2007). As such it is a promising tool for the quantitative estimation of brain organization and brain development (Moseley, 2002).

At the microscopic level, brain parenchymal structures have distinct boundaries, including axon membranes and myelin sheaths, which constrain the diffusional propagation of water molecules and force the latter in certain preferential directions. Thus, the water diffusion averaged over the individual voxels, as expressed by the apparent diffusion coefficient (ADC), is reduced in accordance with the local occurrence of these membranes. According to the present anisotropy of cellular structure, this reduction in diffusion due to membrane hindrance is also angular-dependent (Beaulieu, 2002). The degree of diffusion anisotropy can be specified using one of the anisotropy indices, e.g. the relative anisotropy index (RA) (Pierpaoli and Basser, 1996), which is calculated from the directionally dependent signal decay due to diffusion. As the diffusion properties ADC and RA are directly related to the micro-structure of the medium studied, they can be used to characterize tissue and to detect possible histological changes due to physiological and pathological states. Both ADC and RA measures have been shown to reliably detect local white matter changes in normal aging (Nusbaum, Tang, Buchsbaum, Wei, and Atlas, 2001). Thus, the number of applications that DTI can offer in the study of aging and neurodegenerative disorders (Kubicki et al., 2002) has soared over the past several years. Most of the DTI aging

studies have focused on region-of-interest (ROI) (Sullivan and Pfefferbaum, 2003; Abe et al., 2002; Gideon, Thomsen, and Henriksen, 1994) or histogram analysis (Gideon, Thomsen, and Henriksen, 1994; Chen, Li, and Hindmarsh, 2001; Chun, Filippi, Zimmerman, and Ulug, 2000; Engelter, Provenzale, Petrella, DeLong, and MacFall, 2000; Abe et al., 2002c; Sullivan and Pfefferbaum, 2003). However, these methods only permit the description of diffusion properties at the regional or global level, respectively, i.e., beyond the method-inherent averaging of micro-structural information over each voxel. Using ROI-based analysis, the spatial resolution provided by DTI is not exploited. In particular, region-of-interest analysis has several limitations, as for example, it is restricted to just the few regions chosen for analysis by a priori hypotheses. In this sense, the results obtained might be affected by the criteria chosen to define the ROIs because possible bias might be introduced due to manual or semi-automated definitions of the ROIs (Virta et al., 1999). The additional averaging over to some extent arbitrarily outlined regions also reduces spatial resolution. Therefore, ROI analysis might not be sensitive enough to detect some biologically meaningful differences which could be otherwise detected at the voxel level (Virta et al., 1999). Finally, subvolumes of the ROI might be inherently influenced by partial volume effects associated with tissue loss, gliosis or by compaction. These morphological changes might influence the detection of white matter differences after averaging. Given these concerns, the benefits of voxel-based analysis become apparent as an attractive method to investigate local age-related white matter changes in the whole brain. Voxel-based analysis has previously been applied to DTI data in aging studies in a preliminary study using a small sample of healthy volunteers (Nusbaum et al., 2001) and in a study comparing young and old age groups (Head et al., 2004). Recently, it has been used as an exploratory tool for the whole brain by Salat et al. (Salat et al., 2005).

The main challenge facing voxel-based diffusion parameter analysis involves meeting the requirement for an optimal matching of the brains being compared. Thus, high demands are placed on the normalization procedure. By contrast, in the methodology related to voxel-based morphometry the objective is different, since in this case a slightly imperfect normalization is not only tolerable, it is even desired in order to keep anatomical differences on a mesoscopic scale (Ashburner and Friston, 2001). Standard normalization procedures, as provided, for example, by SPM, lead to a sufficient match between different brains at a macroscopic scale and remove global differences in anatomy. However, if the intention is to examine tissue properties at a voxel level, identical brain coordinates have to be compared across the whole study population, discarding even mesoscopic structural differences.

Unfortunately, this goal is almost impossible to achieve. First, brain structures, in particular the sulcal-gyral pattern, show considerable diversity across different brains, which makes the finding of a perfect match even by non-linear 3-D transformations unfeasible. Furthermore, a high degree of exactness of the normalization procedure requires high-dimensional parameter spaces in which the brain warps can be expanded and optimised. Thus, more degrees of freedom incur more potential local minima, leading to possibly erroneous results in the registration of the brain images (Ashburner et al., 2001). However, in the case of a moderate number of warping parameters, even large-scale anatomical differences, such as different ventricular volumes, might not be fully compensated by normalization. Additionally, neighbouring tissue might be forced to follow highly contrasted edges due to the application of non-perfectly adjusted brain warps. Consequently, the named sources of anatomical mismatch might have a considerable impact on inter-subject comparisons. Hence, analyses using voxel-size resolution require optimised normalization protocols, including the creation of a

suitable internal-study brain template (Good et al., 2001), in order to minimize inter-subject anatomical variations as well as possible. A standard normalization procedure might not solve potential problems owing to the systematic effects caused by brain atrophy, which correlates with age (Good et al., 2001). In this sense, Salat et al. (Salat et al., 2005) considered their voxel-based diffusion anisotropy maps of the whole brain as only exploratory measures, compared to ROI analysis. However, it is our belief that these maps do constitute a good starting point for a detailed analysis as long as additional checks are applied. The aim of the present study is to examine possible age-related white matter changes in healthy subjects based on ADC and RA whole brain data. For this purpose, a voxel-based linear regression analysis was performed using an optimised normalization protocol in order to facilitate the characterization of micro-structural differences at a voxel level. However, special care needs to be taken when interpreting the results obtained with ADC data, which might potentially be affected at the tissue/CSF interfaces, because in these regions morphological changes related to age seem to be relatively large and the normalization procedure might not properly match the brain structures. In the case of RA images, considerable morphology-related effects might be derived from potential displacements of fibres that are not properly fitted by the normalization procedure. In this vein, comparisons with age-related MR volumetric studies (Good et al., 2001) can be helpful in order to roughly identify regions prone to morphological changes with age.

Therefore, it is essential to control any potential problems arising from the normalization procedure, especially in a study involving a large age range, where these systematic differences in brain structure may generate significant effects. For this reason, the combination of ROI analysis, which is not subject to normalization constraints, and voxel-based analysis could play an important role in validating the

data. Therefore, additional ROI analysis was performed in three anatomically defined brain structures (genu and splenium of the corpus callosum and the putamen) in order to confirm our voxel-based findings at the regional level and to compare them with ROI analysis results published elsewhere.

An alternative method for detecting possible influences of non-perfect normalization in cross-sectional studies involves the introduction of tools designed to detect these artefacts. Here, we propose a mask procedure applicable to ADC images in order to distinguish morphologic involvement from real white matter changes.

4.2. Materials and Methods

4.2.1. Participants

Fifty-four healthy volunteers underwent DTI brain examinations, 22 women and 32 men (mean age 37.3 ± 17.0, range 19-71 years). Written informed consent according to the approval of the Local Ethical Committee was obtained from all participants before MR examinations.

4.2.2. MRI scanning methods

DTI was performed on a GE Signa Horizon LX 1.5 T neuro-optimised MR tomograph (General Electric Medical Systems, Milwaukee, WI, USA) employing a diffusion tensor spin echo EPI sequence. Diffusion weighting was conducted using the standard PGSE method. Images were measured using 3 mm thick slices, no gap, TR = 10 s, TE = 70 ms,

128 × 128 acquisition matrix, interpolated by zeropadding to 256 × 256, FOV 28 cm, 39 axial slices. Four averages were acquired per slice and diffusion gradient direction.

In order to obtain diffusion tensors, diffusion was measured along 12 non-collinear directions, chosen according to the DTI acquisition scheme proposed by Papadakis et al. (Papadakis, Xing, Huang, Hall, and Carpenter, 1999), and the values specified by Skare et al. (Skare, Hedehus, Moseley, and Li, 2000) using a single b-value of 1000 s/mm^2. For each gradient direction, inverted diffusion gradient polarity was measured as well, again collecting four averages each. Hence, a total of 24 diffusion-weighted measurements were performed. They were divided into four blocks, each one preceded by a non-diffusion-weighted acquisition.

4.2.3. Image processing

4.2.3.1. Analysis of diffusion-weighted data

First, raw diffusion-weighted data were corrected for eddy-current-induced distortions, taking advantage of the symmetrical deformations caused by opposite diffusion gradient directions (Bodammer, Kaufmann, Kanowski, and Tempelmann, 2004). Secondly, head motion correction was performed based on the non-diffusion-weighted images. The first non-diffusion-weighted image of each block was realigned with the first – likewise non-diffusion-weighted – image of the first series using the realignment algorithm provided by the Automated Image Registration (AIR) package (Woods, Grafton, Holmes, Cherry, and Mazziotta, 1998). Then the determined transformation parameters were applied to the remaining diffusion-weighted images of the respective block.

In order to extract diffusion tensor elements from an overdetermined set of diffusion-weighted images, singular value decomposition was used. Diffusion tensors were diagonalized extracting the eigenvectors and eigenvalues. Based on the eigenvalues, the ADC and RA diffusion parameters were calculated on a voxel-by-voxel basis.

4.2.3.2. Optimized normalization protocol

Normalization of all ADC and RA data sets to the same anatomical space was performed also based on the non-diffusion-weighted image volumes using a three-step processing scheme (Figure 4.1). These image processing steps were carried out with SPM2 (Wellcome Department of Cognitive Neurology, Institute of Neurology, UK). Special effort was made to create an optimised study brain template offering study-inherent contrast and distortions, according to the applied sequence parameters and additionally including the averaged anatomical characteristics of all study participants. The detailed steps of the normalization procedure were as follows:

(1) First, the non-diffusion-weighted images ($b \approx 0$ s/mm^2) were normalized using the EPI-derived MNI template (ICBM 152, Montreal Neurological Institute) provided by SPM. After an initial affine transformation, an iterative non-linear normalization was applied using a lower threshold of 25 mm for the spatial periods of the discrete cosine basis functions by which brain warps are expanded in SPM (Ashburner et al., 1999). From the resulting normalized data sets a first preliminary study template was created by averaging.

(2) In a second run, the non-diffusion-weighted image volumes of all subjects were normalized again – but now using the study template that was created before in step (1). A second and final study template, which defines the anatomical space of the present study, was generated by averaging these newly normalized images after the extraction of only brain parenchyma. The extraction of brain tissue was performed by a three-class brain segmentation, i.e. segmentation of grey matter, white matter, and CSF/non-brain-tissue, retaining only voxels where the probability of belonging to GM or WM as assessed by SPM2 exceeded 0.8. The threshold was selected based on preliminary tests which showed that a lower threshold resulted less effective in removing non-brain voxels, whereas a higher threshold did not retain all brain parenchyma voxels.

(3) In a third step, based on the optimized protocol first introduced by Good et al. (Good et al., 2001), individual native-space brain parenchyma maps were extracted from the measured non-diffusion-weighted images and normalized to the final extracted-brain template. Parameters of the previous non-linear transformation were reapplied to the ADC and RA maps without Jacobian modulation of the signal intensities, generating the unmasked ADC and RA maps set. Afterwards, normalized non-diffusion-weighted images were segmented. By merging of the GM and WM segments normalized binary brain mask images were created and applied to the ADC and RA maps. That is, a second set of masked ADC and RA images were obtained where only brain parenchyma was included. Moreover, a standard deviation (SD) map was computed from the binary mask images of the study participants.

4.2.3.3. Voxel-based analysis

Linear regression analysis was carried out for both sets of images (masked and non-masked images) using SPM99. Voxel-wise t-tests were performed to detect voxels where the slope of ADC or RA data against age as fitted by linear regression was significantly different from zero.

In order to estimate the extent of the interfacial areas between CSF and brain parenchyma, the voxel-wise standard deviations of all participants' binary mask images were calculated. The resulting standard deviation image varied between zero (the respective voxel corresponded to the same category for all subjects, i.e. either brain or non-brain) and 0.5 (for 50% of subjects the voxel corresponded to brain tissue, for another 50% to CSF or non-brain tissue). Thus, the standard deviation image presented its highest values in those voxels for which the probability over all the examined subjects to constitute the CSF/brain border was relatively high. Consequently, the standard deviation image allowed us to map potential CSF/parenchyma interfaces. Hence, we were able to use these maps to identify regions with noticeable normalization mismatch.

In sum, two versions of the normalized ADC and RA maps were created, in order to be further used in statistical analysis: (i) one version in which they are reduced to the brain-parenchymal volume and (ii) the original parameter maps containing also non-brain tissue and CSF. Finally, all individually normalized ADC and RA data sets were smoothed by convolving them with isotropic 8 mm and 4 mm FWHM (full width at half maximum) Gaussian kernels. We report only the 4 mm FWHM Gaussian kernel result because it preserved the same regional patterns as shown with the 8mm kernel size, but with better spatial resolution.

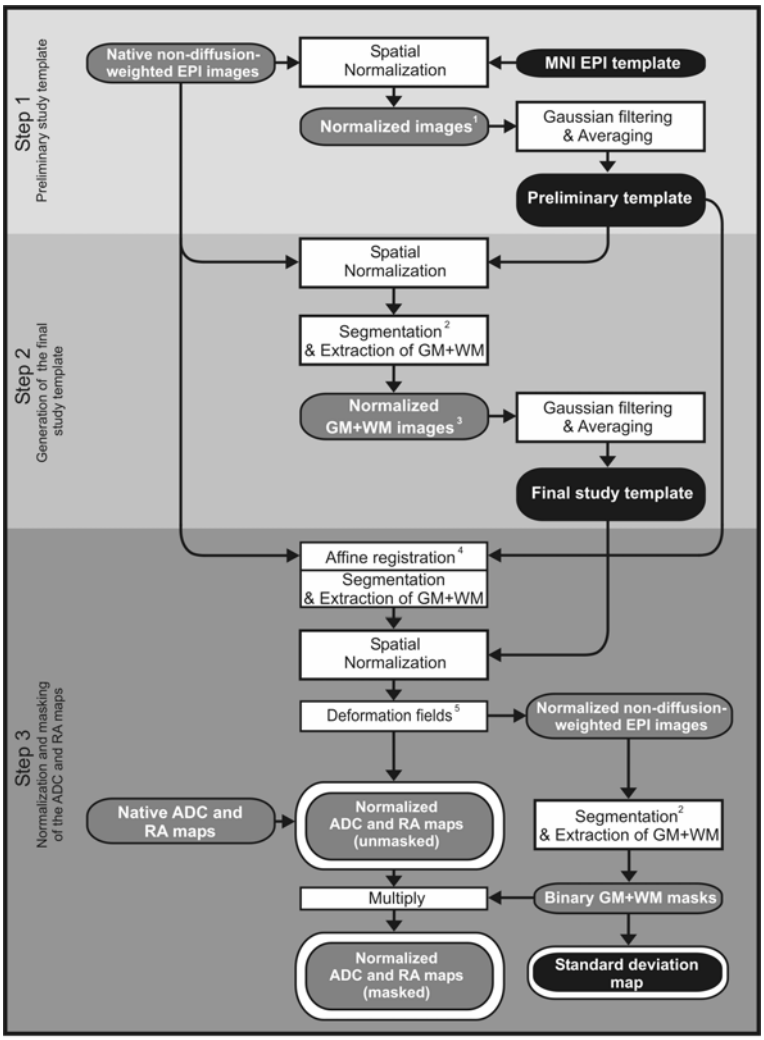

1) non-diffusion-weighted EPI images spatially normalized to the MNI EPI template
2) the segmentation was performed without previous affine registration
3) non-diffusion-weighted images containing only brain tissue spatially normalized to the preliminary study template
4) affine registration was performed in order to allow the usage of anatomical GM/WM a priori probability maps; registration parameters were not further used for normalization
5) deformation field consists of affine and non-linear normalization transform, applied without intensity modulation

Figure 4.1: Flowchart describing the three-step normalization procedure used in this study. In steps 1 and 2 the study template is optimized. In step 3 the normalization itself is performed, normalization transforms are applied to the ADC and RA maps, and a map showing the SD of the normalized binary brain mask images over all study participants is calculated. ADC, RA maps and the SD map are highlighted by a white margin as these are the images which are further processed in statistical analysis or used as an indication for non-perfect normalization. Black-filled round-edged boxes represent images which only comprise one volume for the whole study, whereas grey boxes indicate series of individual image sets.

On the other hand, such brain boundary regions, where the normalization results were not optimal, should show considerable differences in the ADC-versus-age linear regression results dependent on whether binary brain masks were applied or not. This is due to the diffusion in CSF regions being reflected by high ADC values, when no masking is applied, whereas the application of binary masks converts these values to zero. Therefore, ADC correlation maps should be inverted in regions close to CSF/parenchyma borders if the correlations do not reflect real white matter changes but rather inaccurate normalization. This interrelation was used to estimate whether significant regression results might have been caused by morphological or micro-structural causes. For the labelling of the white matter fibre tracts the DTI brain atlas by Wakana et al. (Wakana, Jiang, Nagae-Poetscher, van Zijl, and Mori, 2004) was used.

4.2.3.3. Region-of-interest analysis

Four regions-of-interest (ROI), namely the genu and splenium of the corpus callosum and both putamina, were marked out in each participant's brain using the semi-automated procedure provided by MRIcro (Rorden C; University of South Carolina, Columbia, USA; *http://www.sph.sc.edu/comd/rorden/mricro.html*). These particular regions were chosen for this type of analysis because of their important role in diffusion tensor imaging and aging studies (Head et al., 2004; Moseley, 2002), (notably for the corpus callosum), their high statistical effect size as observed in the voxel-based analysis (in the putamen), and their vicinity to the ventricles, which means they are especially prone to imperfect correction in the normalization process. The outlines of these regions were identified in the RA maps, where they are easily isolated and differentiated. In order to minimize possible partial volume effects arising at the

borders of the selected brain sub-structures the outermost layer of each marked region was reduced.

In the case of the corpus callosum, the segmentation of the genu and splenium ROIs was performed on non-normalized sagittally resliced RA images from 1 cm left to 1 cm right of the midsagittal plane. The genu was defined as the anterior 25% of the corpus callosum, while the splenium was the posterior 25%. Mean ADC and RA values were determined for each participant separately.

The putamen ROIs were seen on 4-5 axial slices. They were delimited by the surrounding internal and external capsule fibre tracts on the RA images in native space. The globus pallidus was excluded as much as possible, selecting only the less intensive voxels that presented a putamen shape. Mean ROI ADC and RA values were extracted and correlated with age. Additionally, for the putamina, the combined mean of left and right putamen voxels was calculated. Significance was determined by using a standard one-tailed *t*-test analysis and Pearson's correlation was used to determine the correlation coefficients.

4.3. Results

4.3.1. Voxel-based analysis

Without the application of brain masks, voxel-based linear regression analysis showed regional decreases in relative anisotropy (RA) in midfrontal white matter regions, the corpus callosum, predominantly in the genu, and the anterior-posterior regions of the

corona radiata. The medial cerebral peduncle and bilateral hippocampal complex also showed a significant decline in RA (see Figure 4.2 and Table 4.1).

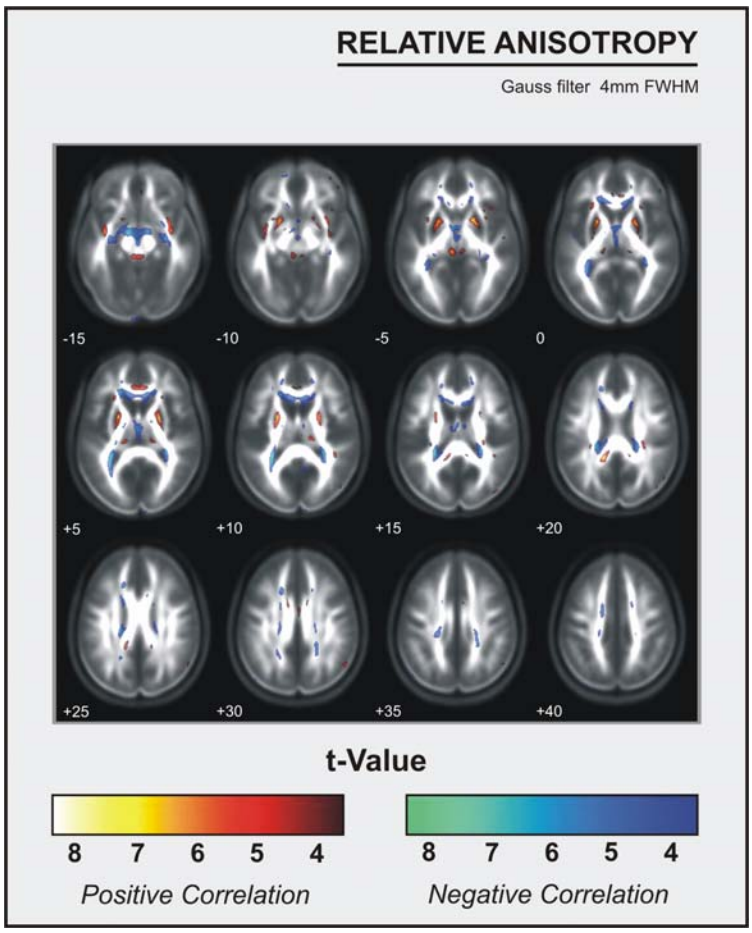

Figure 4.2: Normalized and averaged axial RA maps with relative-anisotropy-index-related t-score overlays. Figures show positive (red) and negative (blue) correlations.

In contrast, positive correlations with age were found for regions surrounding the external part of the corpus callosum, bilateral inferior fronto-occipital fasciculus and the medial lemniscus. Surprisingly, a statistically significant increase in RA was also seen in putamina bilaterally.

Without the application of brain masks, voxel-based linear regression analysis showed positive significant correlations between the ADC and age in the midfrontal white matter regions and the corpus callosum. Notable increases were observed in periventricular regions, surrounding cerebral peduncle, bilaterally in insular regions, and in the periphery of the brain, mostly focused in frontal and parietal lobes. Regions with significant ADC declines with age were identified in the internal capsule bilaterally, surrounding the exterior part of corpus callosum and in the pontine cistern (see Figure 4.3a and Table 4.2).

With brain masking, linear regression analysis found significant correlations in the same regions (see Figure 4.3b and Table 4.2). However, the sign of the correlation of ADC values with age was reversed in insular regions (bilateral), right inferior frontal plane, and in the periventricular area. In other regions where the ADC was correlated with age, the sign of the correlation coefficients was kept constant when brain masking was applied. Examples are the negative correlation in the genu and the posterior limb of the internal capsule as well as the pontine cistern. Positive correlations in both masked and unmasked ADC maps were found in the genu of the corpus callosum.

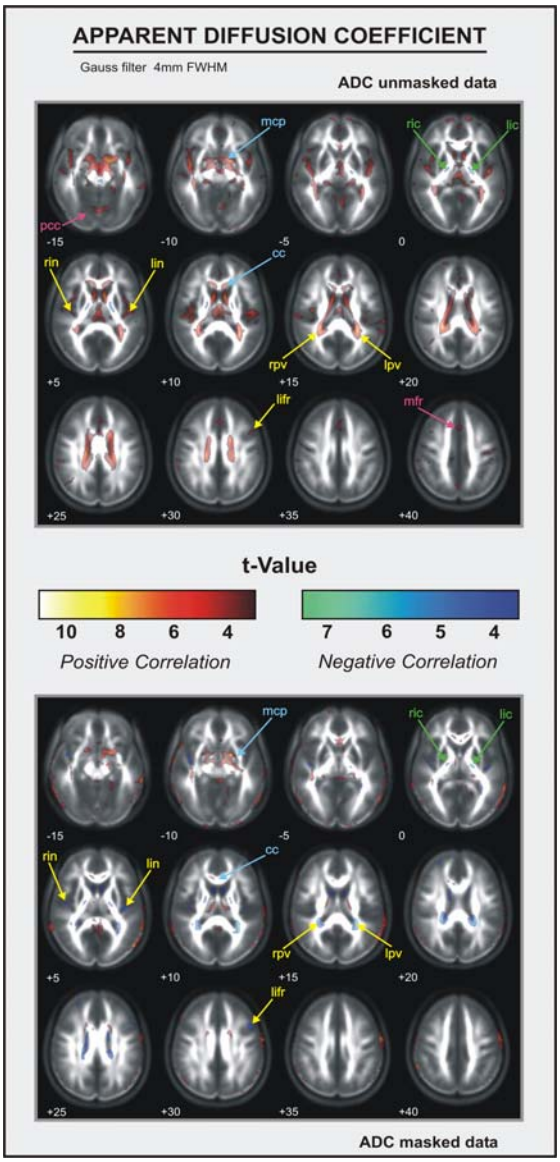

Figure 4.3: Normalized and averaged axial RA maps with apparent-diffusion-coefficient-related t-score overlays using unmasked data (a) in contrast to masked data (b). Figures show positive (red) and negative (blue) correlations. The main regions are labelled as posterior cerebellar cistern (pcc), pointine cistern (pc), middle cerebral peduncle (mcp), right internal capsule (ric), left internal capsule (lic), right insula region (rin), left insula region (lin), corpus callosum (cc), right periventricular region (rpv), left periventricular region (lpv), right inferior frontal region (rifr), left inferior frontal region (lifr), middle frontal region (mfr). Arrow colours represent positive correlation for unmasked data and negative for masked data (yellow), positive correlation only for unmasked data (purple), positive correlation for masked and unmasked data (blue), and negative correlation for masked and unmasked data (green).

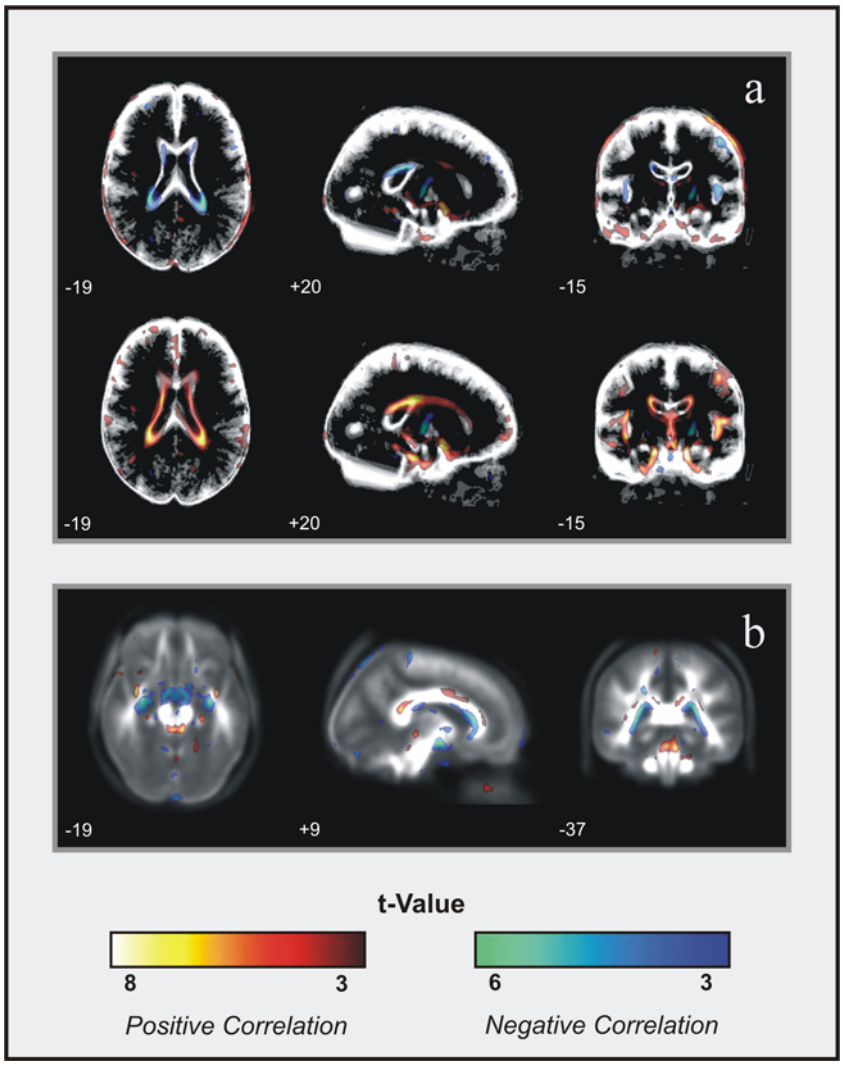

Figure 4.4: Overlays on tri-planar standard deviation maps. Inverted patterns obtained using masked vs. non-masked analysis in ADC maps (a); fibre shifting in RA maps (b). Figures show positive (red) and negative (blue) correlations.

4.3.2. Region-of-interest analysis

4.3.2.1. Corpus callosum

A significant negative correlation between RA and age was obtained in the anterior part of the corpus callosum, indicating a linear decrease of RA with age (r = -0.4, p < 0.002). There was no significant correlation between age and ADC (r = 0.15) in this

region, although a positive tendency was observed. Nor were there significant effects on ADC (r = -0.08) or RA (r = -0.2) in the posterior corpus callosum (see Figure 4.5).

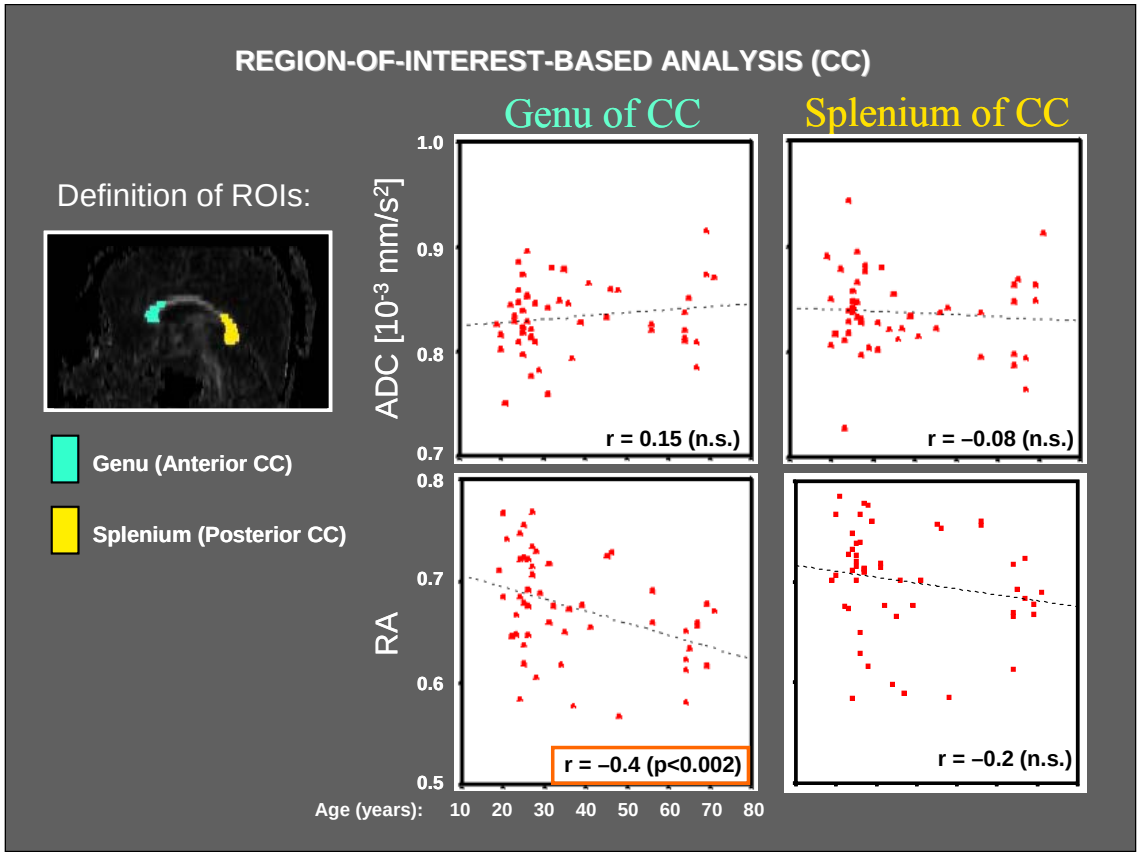

Figure 4.5: ROI-based analysis (corpus callosum); scatterplots of both RA-vs-age (a) and ADC-vs-age (b).

4.2.3.2. Putamen

RA showed a significant increase in the putamina with age (r = 0.58, p < 0.001; see Figure 4.6a), both in each putamen and in the total mean value. No significant correlation was obtained in the putamina between age and ADC (r = -0.018), (see Figure 4.6b).

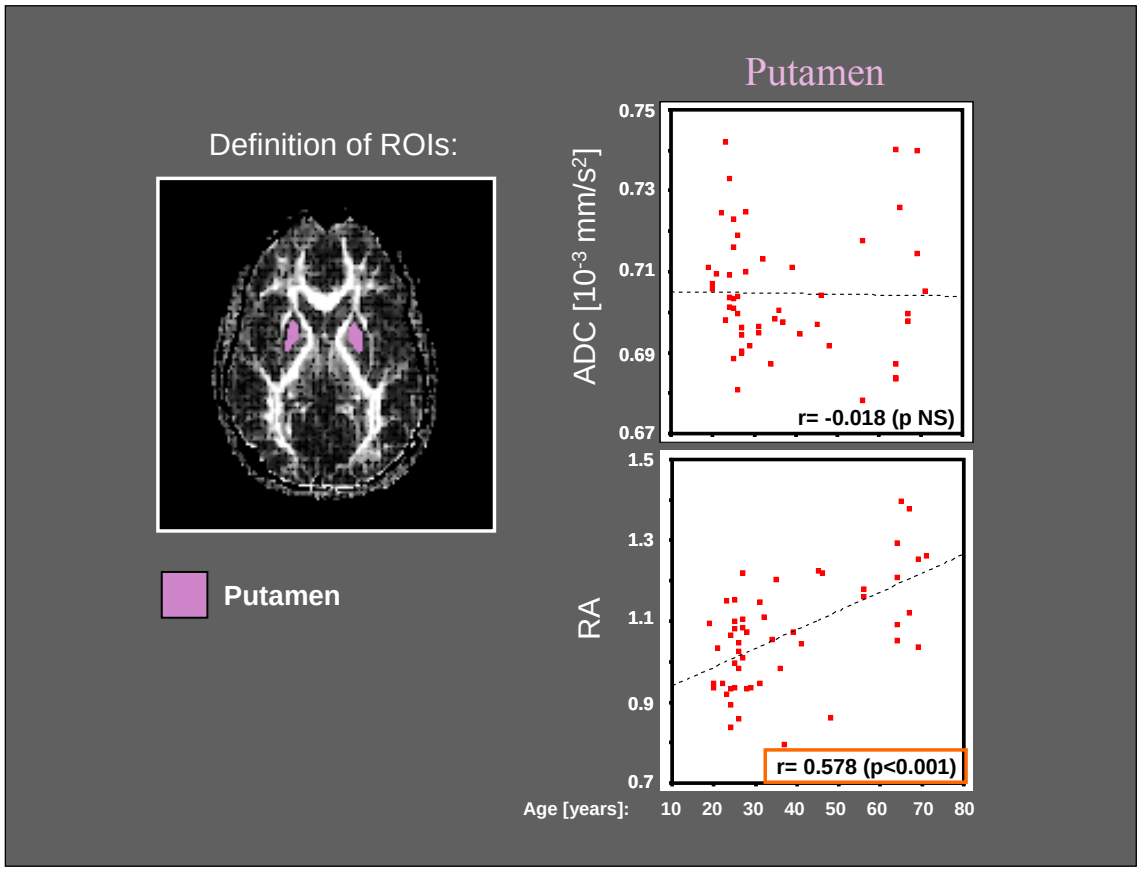

Figure 4.6: ROI-based analysis (putamina); scatterplots of both RA-vs-age (a) and ADC-vs-age (b).

Table 4.1: Locations and significance levels (*t*-value of the peak and corrected *p*-value for the cluster) of the main clusters with significant correlation between RA and age
Relative Anisotropy

		MNI coordinates					
		x	**y**	**z**	**t peak**	**Cluster p**	**Masked or unmasked**
POSITIVE CORRELATION							
Hemisphere	Structure						
L	Putamen	-25	-1	6	7.58	<0.0001	UM
R	Putamen	22	2	3	7.49	<0.0001	UM
R	Border to genu of corpus callosum	14	-46	20	7.29	<0.0001	UM
R+L	Border to medial lemniscus	5	-29	-6	6.60	<0.0001	UM
R	Uncinate fasciculus	38	-6	-14	6.30	<0.0001	UM
L	Uncinate fasciculus	-37	-3	-16	6.07	<0.0001	UM
L	Posterior thalamus	-14	-24	9	5.79	<0.0001	UM
R+L	Anterior border to splenium of corpus callosum	-4	35	5	5.67	<0.0001	UM
NEGATIVE CORRELATION							
R	Border to tapetum	27	-41	12	7.90	<0.0001	UM
R	Internal capsule	11	-7	13	7.22	<0.0001	UM
L	Border to tapetum	-29	-38	12	6.45	<0.0001	UM
L	Anterior corpus callosum	-18	31	-2	6.23	<0.0001	UM
R	Anterior region of corona radiata	16	30	21	5.67	<0.0001	UM
L	Anterior hippocampus	-32	-14	-15	5.61	<0.0001	UM
R	Fasciculus occipito-frontalis	17	23	27	5.38	<0.0001	UM

Table 4.2: Locations and significance levels *(T*-value of the peak and corrected *P*-value for the cluster) of the main clusters with significant correlation between ADC and age.

Apparent Diffusion Coefficient

		MNI coordinates					
		x	**y**	**z**	**t peak**	**Cluster p**	**Masked or unmasked**
POSITIVE CORRELATION FOR UNMASKED DATA AND NEGATIVE FOR MASKED DATA							
Hemisphere	Structure						
R	Insula/Sylvian fissure	49	-16	8	8.87	<0.0001	UM
		39	-19	2	5.30	<0.0001	M
R	Border to lateral ventricle	8	7	8	8.18	<0.0001	UM
		6	11	2	5.30	<0.001	M
L	Border to lateral ventricle	-10	5	12	7.44	<0.0001	UM
		-15	6	23	4.95	<0.001	M
L	Border to splenium of corpus callosum	-21	-22	27	7.92	<0.0001	UM
		-26	-36	20	6.05	<0.0001	M
L	Insula/Sylvian fissure	-41	-14	14	7.47	<0.0001	UM
		-43	-11	-8	5.07	<0.001	M
R	Inferior frontal region	44	-17	48	7.28	<0.0001	UM
		45	-16	50	6.08	<0.002	M
POSITIVE CORRELATION ONLY FOR UNMASKED DATA							
L	Posterior cerebellar cistern, surrounding tent cerebellum	-9	-81	-22	6.32	<0.0001	UM
R+L	Midfrontal regions	-1	22	38	6.16	<0.0001	UM
NEGATIVE CORRELATION FOR MASKED AND UNMASKED DATA							
R	Internal capsule	19	-14	-1	6.78	<0.0001	UM

		19	-14	0	6.32	<0.002	M
L	Internal capsule	-19	-10	0	5.44	<0.005	UM
		-19	-10	1	4.86	<0.03	M
POSITIVE CORRELATION FOR MASKED AND UNMASKED DATA							
R	Border to middle cerebral peduncle	16	3	-12	9.06	<0.0001	UM
		18	4	-11	8.73	<0.0001	M
R	Anterior corpus callosum	17	5	28	7.53	<0.0001	UM
		18	8	27	5.94	<0.0001	M

4.4. Discussion

Voxel-based analysis of tissue-water diffusion – akin to voxel-based morphometry – is a fully automated whole brain imaging data processing technique allowing for the identification of specific local differences in brain tissue properties on a voxel-by-voxel basis. In the present study, several brain areas were associated with aging on the base of tissue-water diffusion data, not only regionally as previously shown by studies focusing on ROI-based analysis, but also with voxel-size resolution. The voxel-based approach for the statistical analysis of diffusion parameter data allows whole-brain searches for significant effects without any need for a priori regionally selective hypotheses. However, our results show that the interpretation of each significant region has to be undertaken very carefully because the voxel-based statistical analysis in diffusivity studies may yield a mixture of different effects, particularly in the presence of atrophy.

With voxel-wise linear regression analysis several regions showed significant correlations with age, reflecting histological changes accumulated over the lifespan.

However, not all of them necessarily mirror real changes inside white matter regions. In periventricular regions, for example, the significant age-related changes in both ADC and RA values may well be due to the ventricular enlargement that occurs with aging. The impossibility of fitting all the ventricles perfectly by the normalization procedure suggests that, even after normalization, the ventricles of the younger volunteers remain smaller than those of their elder counterparts. If we accept this assumption, an increase in ADC would be due to the comparison of CSF voxels in the older participants with parenchyma in the younger ones, thereby reflecting both an increase in ADC and a decrease in RA values, as our results report. When a particular voxel near the ventricular regions is inspected, it tends to correspond to CSF in the case of the older participants and to parenchyma in the case of the younger ones. This clearly shows that a significant correlation in itself is not sufficient to infer that, in a particular region, age-correlated micro-structural changes are prominent. In fact, the CSF-brain interfaces and the outer boundaries of fibre tracts may be susceptible to morphologic involvement. Therefore, a further assessment is needed in order to ensure that the pattern observed is not due to morphological alterations arising from problems in the normalization procedure.

Although these findings seem to indicate morphological origins, a similar pattern might result from coherence loss in white matter tracts or variations in other histological properties. Specifically, diffusivity and anisotropy may be affected by tissue characteristics such as the average tissue water content, the degree of myelination, the density of neuronal fibres or glial cells (Virta et al., 1999). In addition, the partial volume effects of white-matter and non-white-matter components may contribute to the diffusion parameters determined and, consequently, to the results reported in the statistical analysis (Head et al., 2004).

Given that the statistical inference may be affected by a wide range of possible causes, a method is needed in order to discriminate between them, i.e., a tool which can distinguish between micro-structural and global age-related changes. With this aim in mind, a mask procedure was applied to the ADC images in the present study.

Using this mask procedure, inverted correlation patterns were obtained at periventricular borders, bilateral insular regions, the pontine cistern and right inferior frontal plane, indicating that these regions do not exhibit actual white matter changes, but rather morphological alterations with age. These regions coincided with those reported in a previous morphometric analysis which found age-related macrostructural changes (Good et al., 2001). Interestingly, our candidate regions for predominant morphological influence indicated by the mask procedure are in agreement with the results of Good et al. (2001). They reported a positive correlation with age in the Sylvian fissures and a negative correlation in the pontine cistern, corresponding to the sign-inverted correlations that our ADC regression analysis detected when comparing masked and unmasked results (see Figure 4.3 and 4.4a).

Unfortunately, we cannot expect these inverted correlation patterns in the RA images. As masked and non-masked RA values both tend to yield low values in CSF and at CSF-brain interfaces, the masking procedure here is of little use. Nevertheless, if the regions present an inversion of the ADC correlation maps, it is very likely that significant correlations found in RA maps with age in these regions are also involved in morphological alterations and are not due to real white matter changes. In addition, RA might reflect the effects of fibre displacement that has not been properly fitted by the

normalization procedure. In this case, the results might be affected by the mixing of fibre tracts with grey matter regions. Indeed, the patterns found in the areas surrounding both the pyramidal tracts and the corpus callosum support this idea. A positive significant correlation of RA with age was observed in the external part of the fibre, suggesting that in the elderly group the pyramidal tracts and the corpus callosum were displaced outwards by the enlargement of the ventricles. Confirmation of this idea was provided by a negative correlation in the internal part of the fibres. The pyramidal tracts and the corpus callosum appear to occupy a more internal location in the youngest subjects. Thus, although in the case of RA images the mask procedure does not allow us to disentangle the influence of normalization, the inverted correlations obtained with age at each side of the fibre tract could provide the key for detecting morphological fibre displacements misaligned in the normalization process (see Figure 4b).

While for many regions the correlation of ADC and/or RA must be attributed to morphological changes of the brain, there are still several candidate regions for true white-matter changes associated with aging. For example, in agreement with previous reports (Nusbaum, Tang, Buchsbaum, Wei, and Atlas, 2001c; O'Sullivan et al., 2001; Abe et al., 2002; Sullivan and Pfefferbaum, 2003), our voxel-based analysis revealed significant age-related increases in the ADC in the genu of the corpus callosum, accompanied by a significant decrease in the corresponding RA values. When ROIs were statistically analysed in native space (without applying a normalization procedure), our results indicated that the anterior fibre tracts are more markedly affected than their posterior counterparts. Recent DTI studies reported very similar results (Head et al., 2004), associating the decrease in anisotropy with axonal loss, demyelination, increased water content, and combinations of these factors.

Researchers have paid particular attention to both hippocampal and frontal regions and their implications in aging, mostly because of the involvement of these regions in episodic memory and executive functions. Regarding the medial temporal lobe structures, our analysis showed a positive correlation between ADC and age in anterior hippocampal regions, and a negative tendency between RA and age. These results may suggest the presence of real age-related physiological changes in this region. As no inverted patterns were obtained when the masked analysis was performed it is very unlikely that these changes were due only to morphological variations. In fact, volumetric studies tend to report a reduction in the volume of the hippocampus with aging (Good et al., 2001). However, not all studies have observed the same pattern of reduction associated with aging (Good et al., 2001). These discrepancies may be due to the methodological differences in the definition of the boundaries of the anterior hippocampal regions (Raz, Rodrigue, Kennedy, and Acker, 2004; Jack, Jr., Theodore, Cook, and McCarthy, 1995).

Concerning the frontal regions, a number of histopathological and neuroimaging studies (Kemper, 1994; Resnick, Pham, Kraut, Zonderman, and Davatzikos, 2003; Salat et al., 2004; Head et al., 2004) indicate the vulnerability of frontal white matter in non-demented aging. These results are in agreement with previous pathological reports that have associated this pattern with neuronal loss causing the expansion of the extracellular space (Meier-Ruge, Ulrich, Bruhlmann, and Meier, 1992), while other studies have described this process as a shrinkage of large neurons (Abe et al., 2002). Considering these studies in relation to the present study, our data show that central frontal areas exhibit highly significant positive correlations between age and ADC values. Moreover, this effect converges with the significant negative correlation obtained between age and RA in the same region. These results are also in agreement

with previous findings (Head et al., 2004; Salat et al., 2005). Therefore, it is very likely that this pattern of correlations is due to actual white-matter changes. The lack of an inverted pattern of correlations when the mask analysis was applied further supports this idea.

However, a word of caution is in order, because frontal areas may also be prone to increased partial volume effects due to their susceptibility to macrostructural volume loss with age (Good et al., 2001); this would have a negative effect on the mask analysis. Furthermore, the high variability in sulcal boundaries between subjects makes it difficult to obtain a perfect fit at the micro-structural level. In principle, we cannot rule out the possibility that actual white-matter changes and morphological variations interact in the pattern of results observed.

In agreement with the significant age-related decline of the fractional anisotropy in the internal capsule reported by Virta et al. (Virta et al., 1999), and Salat et al. (Salat et al., 2005), our results replicated this negative correlation between anisotropy and aging. In addition, in the same region a significant negative correlation in ADC was found in both the masked and the unmasked analysis. It is difficult to determine the biological significance of this negative correlation between ADC and age, as in other parts of the brain the correlations observed between these two variables (which must be attributed to micro-structural changes) tend to be positive. However, our results suggest that actual white matter age-related changes in the internal capsule are responsible for this pattern of correlation.

Finally, we were surprised to find a highly significant increase of the RA values in the putamen. This result is consistent with a recent study of ADC and RA age-related

changes in several brain regions (Bhagat and Beaulieu, 2004), in which the putamen was the only structure that showed a certain increase in anisotropy with age. However, the authors did not propose any pathophysiological explanation for this result. Additionally, in the entire lentiform nucleus, Abe et al. (Abe et al., 2002) observed a slight increase in diffusion anisotropy with age (p = 0.094). To the best of our knowledge, these are the only reports that provide explicit observations of ROI-based measurements of anisotropy in subcortical grey matter regions and its relationship with aging. Previous structural MRI studies revealed a reduction in the volume of the putamen with increasing age (Good et al., 2001). A very early pathological report (Bugiani, Salvarani, Perdelli, Mancardi, and Leonardi, 1978) found a significant negative correlation between age and cell count in the putamen. In a recent morphometric study, Brickman et al. (Brickman et al., 2003) reported a partial pervasion of the putamen by axonal projections. As a hypothetical explanation for the positive correlation observed between RA in the putamen and age, it appears that age-related cell loss might affect isotropic cell structures to a higher degree than pervasive axons leaving a raised partial volume of larger anisotropy. However, this is only speculation and a microphysiological explanation is required.

Thus far, we have emphasized the utility of voxel-based diffusion parameter analysis, in contrast to the ROI analysis. However, the role of smoothing data in terms of spatial resolution requires further discussion. Image volume data are frequently smoothed in statistical MRI data analysis so that they can be approximated to a Gaussian random field, which enhances the sensitivity of the statistical analysis and reduces the inter-subject variance. This latter effect is particularly helpful when a non-optimized normalization process occurs, since the image blurring that is obtained reduces the inter-subject differences. The benefits to be derived from Gaussian kernel filtering on

the voxel-based diffusivity data have been discussed by Jones et al., (Jones, Symms, Cercignani, and Howard, 2005). However, if we adhere to the matched filter theorem, smoothing severely diminishes the resolution of diffusion analysis. Thus, because of the robust statistical effect encountered in our study the data were smoothed with a small Gaussian filter of 4 mm FWHM, which enabled us to analyse the present data at a micro-structurally meaningful level. However, further studies are needed to determine an optimal smoothing kernel value. Additionally, it is important to bear in mind that some regions, even after applying moderate levels of smoothing, might exhibit non-normally distributed residuals and consequently, statistical parametric tests might not be the most adequate ones (Jones et al., 2005). Non-parametric analyses might be required in order to examine this issue more appropriately.

4.5. Conclusions

As noted above, the normalization process has certain limitations when conducting a voxel-based analysis. Given these limitations, great care must be exercised both in obtaining and in interpreting DTI data, in particular when analysing white matter changes and the effects of aging, where different underlying processes may co-occur. Anatomically defined regions-of-interest may be used to corroborate results from voxel-based analysis, allowing white matter to be tested without the influence of the normalization process (Salat et al., 2005).

Furthermore, linear regression analysis may not be the only statistical approach for investigating white matter changes. Non-linear effects over age may also influence the results observed; if so, non-linear methods are needed to delineate the time course.

Despite these disparities in the possible interpretations given to the DTI analysis, it is clear that DTI is still a highly sensitive method for the evaluation of the underlying micro-structure of the fibre tracts. Therefore, as long as researchers are aware of possible artifacts arising from these methodological constraints, voxel-based analysis is a very useful approach for identifying and comparing age-related micro-structural white matter alterations in the whole brain. However, additional tools, such as the masking procedure described here, are needed in order to validate these results. In this direction, Smith et al. (Smith et al., 2006) have recently proposed a straightforward method to appropriately match previously skeletonised fibre structures and to carry out statistics only for those voxels that remain within the fibre skeletons. This method can be expected to be very important in future studies in order to compare white matter fibre tract changes across subjects but it would not detect systematic changes of diffusion properties in regions like the putamen.

Finally, it is necessary to point out that although the proposed method attempts to disentangle actual changes in diffusivity from changes that are due to underlying morphological age-dependent differences, it does not reveal how age-related diffusivity changes can be affected by other tissue characteristics such as differences in average tissue water content, the degree of myelination and the density of neuronal fibres or glial cells.

Chapter 5♣

5. Combined fMRI/DTI approach:

Structural white matter brain differences predict functional hemodynamic responses in a reward processing task

5.1. Introduction

The relationship between the function of the brain and its structure is still a fundamental open question. Structure–function relationships exist at many spatial scales and across different levels of brain organization that range from synapses to neural populations. At a fine spatial scale for example, changes in synaptic number (Anderson et al., 1996), dendritic volume (Green et al., 1983), mitochondrial and vascular density (Anderson et al., 1996; Black et al., 1991), and glial volume (Sirevaag et al., 1991) have been associated with motor skill learning. At a larger scale, it has been reported that functionally segregated cortical regions are sustained by specific intra-cortical and cortico-cortical anatomical connections (Passingham et al., 2002). Unfortunately, an accurate description of these interactions is still not possible to achieve because of the complexity of the brain. However, certain aspects of the

---

♣ Camara et al. **Structural white matter brain differences predict functional hemodynamic responses in a reward processing task** (In preparation).

relationship between structure and brain function can be investigated combining functional (fMRI) and diffusional (DTI) information. This type of research should be able to highlight the existing relationship between brain micro-structure (e.g., white-matter interconnectivity and the integrity of the corresponding white-matter bundles) and the individual differences observed in the BOLD response in specific cognitive tasks.

With this aim, we conducted a functional MRI/ DTI study in which a large sample of 35 subjects performed a reward-processing task. We predicted that individual white matter differences (using Fractional Anisotropy, FA) might be associated to individual differences observed in BOLD responses.

5.2. Materials and methods

5.2.1. Participants

Thirty-five young adult students [10 women, 21.8 ± 2.2] from the University of Barcelona participated in the study. All participants were healthy, right-handed native Spanish speakers and with no history of neurological or psychiatric episodes. They all gave written informed consent to a protocol approved by the University of Barcelona ethics committee.

5.2.2. Functional Design

Several important modifications were made to the monetary gambling task designed by (Gehring et al., 2002). Each trial began with a warning signal ("*"; 500 ms duration)

followed by the presentation of two numbers (5 and 25) displayed in white against a black background in the two possible combinations, [5 25] or [25 5]. Participants had to select one of the two numbers by pressing a response button with the left or right index finger. One second after the choice, one of the numbers turned green while the other turned red. If the number selected by the participant changed to red, the participant incurred a loss of the corresponding amount of money in Euro cent. In contrast, if the number turned into green, this indicated a gain.

In addition to the standard trials described above (80%), two additional conditions were created to assess brain responses to unexpected rewards and losses. In 10 % of the trials ("boost unexpected trials"), an unexpected large gain or loss occurred: In these trials the number "125" appeared in either red or green signaling the loss or gain of the corresponding sum in Euro cent. This change in magnitude occurred equally often for "5" and "25" trial bets in order to avoid positive or negative biases in choosing "25" items. To control for the fact that boost trials were both, large and unexpected, in an additional 10 % of the trials ("similar unexpected") the chosen number turned to either 7 (instead of 5) or 27 (instead of 25). While these trials were unexpected, the magnitude of the gain or loss was virtually unchanged. Additionally, each run included 12 randomized fixation trials that lasted 20 seconds.

Participants were provided with an initial 10 € sum and were encouraged to win as much as possible. Participants had performed a similar event-related potential task (without unexpected trials) several weeks to months earlier and thus were familiar with the task in general. They were informed about the potential occurrence of unexpected trials. The experiment comprised four blocks, each one comprising 140 trials. The four

possible outcomes for the standard trials ([*25* **5**] [*5* **25**] [**5** *25*] [**25** *5*]; italics = red = loss, bold = green = gain), for the unexpected similar trials ([*25* **7**] [*5* **27**] [**7** *25*] [**27** *5*]), and for the unexpected boost trials ([*25* **125**] [*5* **125**] [**125** *25*] [**125** *5*]) were presented in random order. These combinations were counterbalanced by condition, making the statistically expected outcome zero on each trial in order to avoid confounds of differential probability of gains or losses. At the end of each run, participants were informed about the accumulated amount of money. At the end of the experiment, participants were paid the final amount obtained.

5.2.3. MRI scanning methods

All scans were performed on using a 3T whole-body MRI scanner (Siemens Magnetom Trio, Erlangen, Germany) employing an eight channel phased array head coil. Each subject underwent the following scans.

5.2.3.1. fMRI acquisition

fMRI data was collected while visual images were back-projected onto a screen using an LED-projector and participants viewed the images through a mirror on the head coil. Magnet-compatible response buttons were used. Conventional high resolution structural images [magnetization-prepared, rapid-acquired gradient echoes (MPRAGE) sequence, 192 slice sagittal, TR = 2500 ms, TE = 4.77 ms, TI = 1100 ms, flip angle = 7°, 1mm thickness (isotropic voxels)] were followed by functional images sensitive to blood oxygenation level-dependent contrast (echo planar T2*-weighted gradient echo sequence, TR=2000 ms, TE=30 ms, flip=80°). Each functional run consisted of 336 sequential whole-brain volumes comprising 32 axial slices aligned to the plane intersecting the anterior and posterior commissures, 3.5 mm in-plane resolution, 4 mm

thickness, no gap, positioned to cover all but the most superior region of the brain and the cerebellum.

5.2.3.2. DTI-MRI acquisition

Diffusion weighting was conducted using the standard TRSE (twise refocused spin echo) sequence. Images were measured using 2 mm thick slices, no gap, TR = 8200ms, TE = 85 ms, 128 × 128 acquisition matrix, FOV 256mm x 256mm, 64 axial slices. In order to obtain diffusion tensors, diffusion was measured along 12 non-collinear directions, chosen according to the standard Siemens DTI acquisition scheme using a single b-value of 1000 s/mm^2. Two signal averages and three runs were acquired per slice and diffusion gradient direction. Each run preceded by a non-diffusion-weighted acquisition.

5.2.4. Image processing

5.2.4.1. Functional Preprocessing

Functional images were analyzed using standard procedures implemented in the Statistical Parameter Mapping software (SPM2, *http://www.fil.ion.ucl.ac.uk/spm*). The preprocessing included slice-timing, realignment, normalization and smoothing. First, functional volumes were phase shifted in time with reference to the first slice to minimize purely acquisition-dependent signal-variations across slices. Head-movement artifacts were corrected based on an affine rigid body transformation, where the reference volume was the first image of the first run (e.g., Friston et al. (1996)). Functional data was then averaged and the mean functional image was normalized to a standard stereotactic space using the EPI derived MNI template (ICBM 152, Montreal

Neurological Institute) provided by SPM2. After an initial 12-parameter affine transformation, an iterative non-linear normalization was applied using discrete cosine basis functions by which brain warps are expanded in SPM2 (Ashburner et al., 1999). Resulting normalization parameters derived for the mean image were applied to the whole functional set. Finally, functional EPI volumes were resampled into 4 mm cubic voxels and then spatially smoothed with an 8 mm full-width half-maximum (FWHM) isotropic Gaussian Kernel to minimize effects of inter-subject anatomical differences.

5.2.4. Data analysis

5.2.4.1. Functional Data analysis

The statistical evaluation was based on a least-square estimation using the general linear model by modeling the different conditions with a regressor waveform convolved with a canonical hemodynamic response function (Friston et al., 1998). Thus, an event-related design matrix was created including the conditions of interest: Gain 5, Gain 25, Gain 7/27, Gain 125, Loss 5, Loss 25, Loss 7/27, Loss 125 and fixation.

The data was high-pass filtered (to a maximum of 1/90 Hz), and serial autocorrelations were estimated using an autoregressive model (AR(1) model). Resulting estimates were used for non-sphericity correction during the model estimation. Confounding effects in global mean were removed by proportional scaling, and signal-correlated motion effects were minimized by including the estimated movement parameters. The individual contrast images were entered into a second-level analysis using a one-sample *t* test employing a random effects analysis within the general linear model.

5.2.4.2. Main contrast of interest

One of the attributes that boost the impact of reward is the degree of uncertainty that exist in the estimation of the action's value. Indeed, reward information becomes more relevant as the uncertainty of the reward prediction increases (Fiorillo et al., 2003). Specifically, as the reward becomes increasingly predictable, it's ability to elicit activity to the reward itself decline. Accordingly, in order to enhance reward-related activity, the analysis was constrained to the boost trials in which the unexpectancy and thereby the corresponding reward outcome activity was maxima. Thus, brain regions responding selectively to gains and losses were defined by the Gain (125) vs. Loss (125) contrast reflecting the effect of valence in the unexpected boost trials.

The contrast was investigated in the entire sample (35 subjects) and was thresholded at $p < 0.05$, corrected for multiple comparisons (Ashburner and Friston, 1999; Worsley and Friston, 1995). The maxima of suprathreshold regions were localized by rendering them onto the mean volunteers' normalized T1 structural images on the MNI reference brain. Maxima and all coordinates are reported in MNI coordinates, as used by SPM and labeled in line with the Talairach atlas. Main effects of Valence were encountered using this multiple comparison correction approach.

5.2.4.3. Diffusion analysis: Fractional Anisotropy images

At the microscopic level, brain parenchymal structures have delimiter boundaries, including axon membranes and myelin sheaths, which constrain the diffusional propagation of water molecules in certain preferential directions. Thus, the water diffusion averaged over the individual voxels is reduced in accordance with the local occurrence of these membranes. According to the present anisotropy of cellular

structure, this reduction in diffusion due to membrane hindrance is also angular-dependent (Beaulieu, 2002). In particular, the degree of diffusion anisotropy can be specified using one of the anisotropy indices, e.g. the fractional anisotropy index, which is calculated from the directionally dependent signal decay due to diffusion (Pierpaoli et al., 1996). Indeed, FA approximates the degree to which water diffuses preferentially in one direction. FA index was calculated in each voxel at the whole-brain level, FA varies between 0, non preferential direction diffusion, and 1, in the case diffusion is constrained to only one direction.

5.2.4.4. Analysis of diffusion-weighted data

DTI data were movement corrected and eddy current-induced distortions were removed before to the estimation of the diffusion tensors. The first non-diffusion-weighted image of each block was realigned with the first image of the first series. Then the determined transformation parameters were applied to the remaining diffusion-weighted images of the respective block. Then, all the images were averaged across the 3 runs. In order to assessed FA values, using SPM2 diffusion toolbox (*http://www.fil.ion.ucl.ac.uk/spm/*), diffusion tensor elements were extracted from an overdetermined set of diffusion-weighted images. Afterward, diffusion tensors were diagonalized and thereby the eigenvectors and eigenvalues were obtained. Based on the eigenvalues, FA diffusion index was calculated on a voxel-wise basis. One subject was discarded due to movement artifacts.

5.2.4.5. Optimized normalization diffusion MRI protocol

Normalization of the FA data was performed based on the FA anisotropy images applying the same process reported at Camara et al. (Camara, Bodammer, Rodriguez-

Fornells, and Tempelmann, 2007) by using SPM2 package (Wellcome Department of Cognitive Neurology, Institute of Neurology, UK) without Jacobian modulation of the signal intensities. Special effort was made to create an optimized study brain template offering study-inherent contrast and distortions, according to the applied sequence parameters and including the averaged anatomical characteristics of all studied participants. Briefly, first, FA images were normalized using the EPI-derived MNI template (ICBM 152, Montreal Neurological Institute) provided by SPM. From the resulting normalized data sets a first preliminary study template was created by averaging. Then, FA images were normalized again using the previously created study template. Thus, a second and final study template was created by averaging these newly normalized images after the extraction of only brain parenchyma. The extraction of brain tissue was performed by a three-class brain segmentation. Afterwards, individual native-space brain parenchyma maps were extracted from the initial FA images and normalized to the final extracted-brain template. Finally, all individually normalized FA images were smoothed by convolving them with isotropic 8 mm FWHM (full width at half maximum) Gaussian kernels.

5.2.4.5. Voxel-based analysis

Voxel-wise t-tests were performed to detect those voxels in which the slope of FA data against memory-related measures were significantly different from zero. With this aim, previously normalized FA images were independently regressed on the difference of the beta values derived from the Gain and Loss unexpected boost conditions by applying a simple regression SPM2 model. Locations and significance levels from the correlation analysis were restricted to significant thresholds, 0.001, and 0.01 (60 voxels spatial extent) with a $p \leq 0.05$ corrected at cluster level were reported. The maxima of

suprathreshold regions were labelled by using the white matter fibre tracts from the DTI brain atlas by Wakana et al. (Wakana et al., 2004). Maxima and all coordinates are reported in MNI coordinates.

5.2.4.6. Region-of-interest analysis

Additionally, a region of interest analysis was performed in order to confirm voxel-based findings. Therefore, from the main significant cluster FA value was averaged across the whole region of interest, and correlated with the difference of the beta values derived from the Gain and Loss unexpected boost conditions. Significance was determined by using a standard two-tailed t-test analysis and Pearson's correlation was used to determine the correlation coefficients.

5.3. Results and Discussion

Our main contrast of interest was the gain versus loss comparison. In order to enhance reward responses, analyses were focused on this contrast in the unexpected boost trials, as reward information becomes more relevant as the uncertainty of the reward prediction increases (Fiorillo et al., 2003). This contrast showed an increased response in the left ventral striatum (NAcc) after unexpected large gains of money when compared to unexpected large losses (peak coordinates: -8, 4, -8 mm; $t = 6.68$, $p < 0.05$ FWE-corrected at whole-brain level; 20 voxels spatial extent) in the fMRI analyses. This result was in line with several fMRI studies providing convergent evidence about the crucial role of the NAcc in reward processing (Yacubian et al., 2006; Knutson et al., 2001; Knutson et al., 2003; Delgado, Nystrom, Fissell, Noll, and Fiez, 2000a; Delgado et al., 2003). In contrast, we did not find any area largely activated for loss against gain trials, neither in standard nor in boost, which suggests that the same brain network

seems to be involved in processing positive and negative outcomes, although with a differential amount of activation (Tom et al., 2007; Dreher, 2007).

Additionally, FA maps quantifying the degree of water diffusion anisotropy were created from the diffusion images in order to characterize micro-structural properties. Then, we performed a voxel-based whole-brain correlation analysis using an optimised normalization protocol (Camara et al., 2007) to relate individual brain FA measures to the difference of the beta values derived from the main peak of the previous Gain and Loss unexpected boost conditions. A negative correlation was found when regressing the functional pattern and the corresponding FA values at the whole brain ($p < 0.00001$), (peak coordinates: 22, 11, -12; $r = 0.65$, $t = 5.86$, $p < 0.05$ corrected at cluster level; 60 voxels spatial extent) showing the coupling between functional and structural measures. Specifically, FA values at the right uncinate / inferior fronto-occipital fasciculus correlated with the hemodynamic response at the ventral striatum region acquired during the functional reward-processing task (Figure 5.1). This result was observed bilaterally and probably, this pattern might reflect the interconnectivity between orbito-frontal and ventral striatal regions (Ungerleider, Gaffan, and Pelak, 1989).

In this regard, frontotemporal regions mediated by the uncinate fasciculus have been described to encode the processing of the prediction error for monetary rewards (Ramnani, Elliott, Athwal, and Passingham, 2004). Accordingly, in a recent study, Tom et al. (Tom et al., 2007) showed that the activation in the ventral striatum decreased as the size of the potential loss increased, which directly points out to the idea that the amount of suppression observed in the BOLD responses is directly related to the impact of the loss outcome. More concretely, Tom et al. suggested that a single system

mediated by the ventral striatum and the prefrontal cortex might encode individual differences in the differential amount of activation observed between gain and loss outcomes.

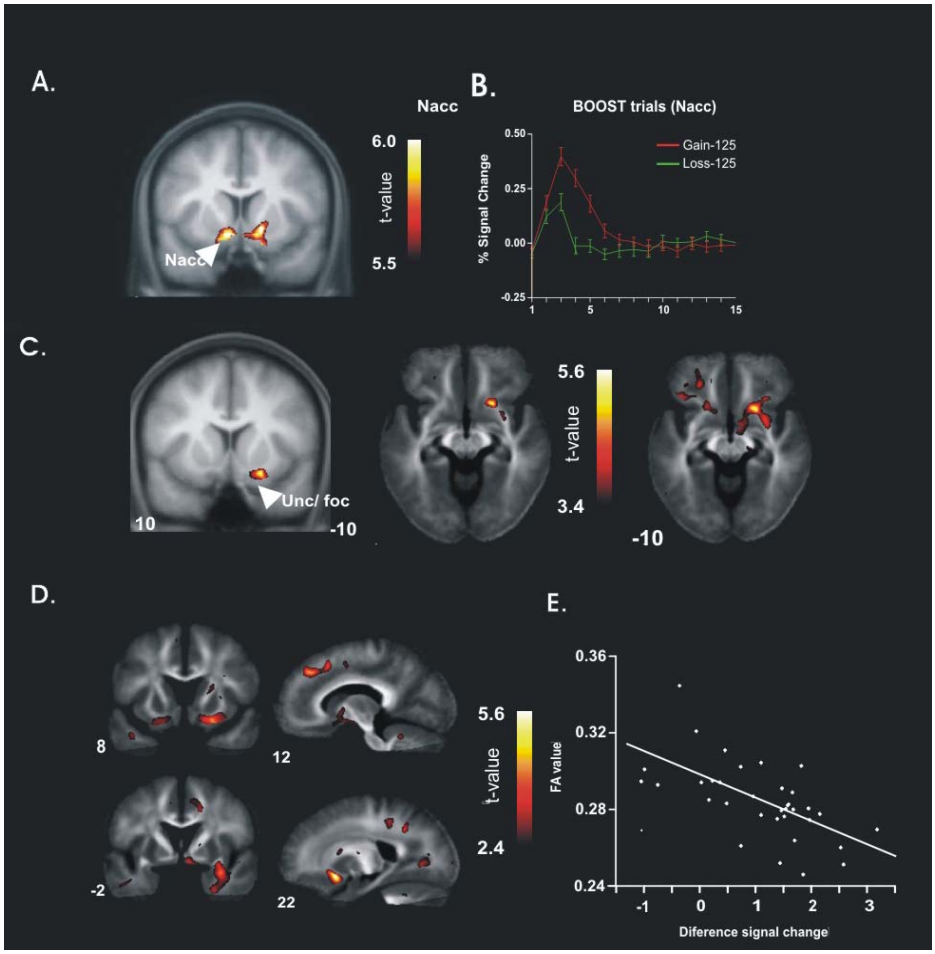

Figure 5.1: A. DTI-fMRI coupling pattern: Depicted the negative correlation obtained after regressing the difference of the beta values derived from the Gain and Loss unexpected boost conditions (panel B) and the corresponding FA values at the whole brain ($P < 0.001$), (peak 22, 11, -12). *t*-scores are overlaid on a coronal view from the group-averaged FA image in MNI standard stereotactic space. B. Additional tri-planar views of the DTI-fMRI correlation are shown with a less conservative significant threshold ($p > 0.01$) for the sake of visualization of the underlying white matter tracts in the region of interest. *t*-scores are overlaid on the mean group FA image. The most important result is that FA values at the right uncinate (unc) / inferior fronto-occipital fasciculus (ifo) correlated with the hemodynamic response at the ventral striatum region acquired during the functional reward processing task. C. Scatter plot showing each individual beta value for the fMRI contrast (gain vs. loss) and the corresponding FA value averaged across for the whole region of interest at the unccinate / ifo cluster ($r = 0.613$, $p < 0.00001$).

5.4. Conclusions

Overall, by studying reward processing we have observed neurophysiological coupling between functional and structural magnetic resonance properties in humans. Specifically, we evidenced that micro-structural white matter brain differences correlated strongly with functional hemodynamic responses in a reward-processing task. However, considering the present results, it is difficult to determine the physiological mechanisms underlying such fMRI-DTI coupling. The causality of the observed relationship remains unclear, thus it is not possible to claim whether functional properties are modulated structurally or instead structure is functionally constrained. Further studies are required in order to clarify the physiological mechanisms underlying such pattern. These findings clearly suggest new prospects for the integration of individual micro-structural and functional properties in brain function and its dynamics.

Chapter 6♣

6. Anatomical connectivity approach:

False memories are related to micro-structure of brain white matter

6.1. Introduction

Memory distortions are common and therefore are not only of practical concern but also may allow further insight into the cognitive and neural architecture of the human memory system (Brainerd and Reyna, 2002; Schacter, Verfaellie, and Pradere, 1996) Unsurprisingly, false memories (FM) can be elicited easily in the laboratory (Roediger and McDermott, 1995). For example, in the Deese-Roediger-McDermott (DRM) paradigm, lists of semantically related words are presented during encoding (e.g., seat – sofa – stool – table etc.) with one prototypical exemplar of the category ("lure" word: chair) missing. Interestingly, the lure word is often produced in free recall or recognition tests. True memory (TM) recognition has been shown to rely on accurate, context-rich and vivid retrieval of an event (i.e., *recollection*), whereas FM recognition appears to reflect the feeling of knowing something without specific contextual details and the semantic gist of the list (Brainerd et al., 2002). Recollection and familiarity- or gist-based retrieval are qualitatively different processes subserved by different neural

---

♣ Fuentemilla L., Camara E., Kramer U., Cunillera T., Marco-Pallares J., C. Tempelmann, Münte T. F., Rodriguez-Fornells A. False memories are related to micro-structureof brain white matter (submitted).

structures (Sauvage, Fortin, Owens, Yonelinas, and Eichenbaum, 2008) and recently it has been shown that TM and FM retrieval in the DRM paradigm are mediated by different neural mechanisms (Kim and Cabeza, 2007). Specifically, highly confident TM recognitions have been shown to be supported by the medial temporal lobe, a structure that has been related to recollection, whereas highly confident FM recognition engaged frontoparietal regions, which are thought to mediate familiarity-based memory retrieval (Kim and Cabeza, 2007).

The tendency to produce FM shows marked interindividual behavioural differences (Blair, Lenton, and Hastie, 2002; Gerrie and Garry, 2007; Watson, Bunting, Poole, and Conway, 2005) and is also associated with brain activation differences across the life-span(Dennis, Kim, and Cabeza, 2008; Paz-Alonso, Ghetti, Donohue, Goodman, and Bunge, 2008). In children age-related increases in TM were associated with changes in the medial temporal lobe (MTL) activation profile, whereas increases in FM were related with activation changes in ventrolateral prefrontal cortex (Paz-Alonso, Ghetti, Donohue, Goodman, and Bunge, 2008). In older adults, on the other hand TM recognition led to weaker activity in the hippocampus compared to young controls, whereas FM was associated with increased activity in the left middle temporal gyrus, a region involved in semantic processing and semantic gist (Dennis, Kim, and Cabeza, 2008).

In the present investigation we asked, whether individual differences in TM/FM retrieval may be related to differences in the organization of white matter connections (defined as per fractional anisotropy (FA) values derived from diffusion tensor magnetic resonance images) of the critical brain regions: Whereas the information

processed in the MTL thought to lead to TM, is predominantly sent through the inferior longitudinal fascicle (ILF), the frontoparietal network related to FM is connected by the superior longitudinal fascicle (SLF). FA ranges from 0 to 1 with larger values indicating that diffusion occurs predominantly along one direction as is the case for highly organized and directed white matter tracts (Le Bihan, 2003). To the extent to which the functioning of brain areas critical for FM and TM retrieval is dependent on the organization of their connecting fiber tracts we predicted that (i) better TM retrieval should be positively correlated to FA in the ILF supporting the functions of medial temporal lobe structures, whereas (ii) a greater susceptibility to FM recognition should be related to FA in the SLF.

To examine this hypothesis we tested 48 young native speakers of Spanish in a version of the DRM paradigm and subsequently obtained diffusion tensor images using a 3 Tesla MR scanner. A voxel-based whole-brain level linear regression analysis was performed to relate FA to indices of TM and FM recall and recognition.

6.2. Materials and methods

6.2.1. Participants

Forty-eight healthy, right-handed students [32 women, mean age 21.2 ± 2.8 (SD)] from the University of Barcelona gave written informed consent to a protocol approved by the University of Barcelona ethics committee prior to participation.

6.2.2. Design

The memory paradigm comprised four lists of semantically related words presented in a quite room via loudspeakers at a rate of 1 every 2 seconds. Critically, each list contained 14 semantic related Spanish words associated of one lure word that was *not* presented. The lists were taken from the original DRM study (Roediger et al., 1995). After each list, participants wrote down as many words as they could remember on an unmarked sheet of paper (recall test). After twenty minutes, as an additional test of memory, studied words, lure words and new words were presented and the participants had to make an old / new decision (recognition test). The recognition list comprised the first and eighth words of each of the study lists (*studied* words), the four words semantically associated to each list (*lures*) and four words neither presented during the study phase nor semantically related to any of the studied words (*new* words). In order to avoid possible biases when comparing lure words with other neural words (Gallo and Roediger, 2002), new words tested where lures in other lists in the original DRM experiment (Roediger et al., 1995) which were not studied in the present experiment.

In the case of "old" decisions, participants were instructed to make a Remember-Know judgement in order to have a subjective about the recognition judgement (Tulving, 1985). Subjects were instructed to mark "Remember", if they had a conscious and vivid recollection of the words from the study list, as for example, if they remembered what they were thinking about at the time the word was presented", the order in which the word was presented" (neighbour words of the study list), or the physical characteristics associated to the presentation of the word. A "Know" judgement was encouraged in the case they were sure that the word was presented, but they could not recollect its actual occurrence or any related details. The experimenter ensured, before beginning the

recognition test that participants understood correctly the instructions addressing the distinction between remember-know judgements.

Table 6.1: Study lists.

Studied words		
Hilo	Agrio	Colina
Alfiler	Azúcar	Valle
Ojo	Amargo	Escalar
Costura	Bueno	Cima
Afilado	Sabor	Cumbre
Punto	Dientes	Pico
Pinchazo	Amable	Llanura
Dedal	Miel	Glaciar
Pajar	Chocolate	Cabra
Espina	Bombón*	Bicicleta
Lastimarse	Pastel	Escalador
Inyección	Tarta	Cordillera
Jeringa	Golosina	Escarpado
Tela	Cariñoso*	Esquiar
Non-studied words (possible lures)		
Aguja	Dulce	Montaña

Percentage of recalled words was computed dividing the number of recalled items by the total amount of words in each list (14 words). The percentage of lures recalled was calculated in relation of the total amount of possible lures (4 possible lures). In the recognition phase, the percentage of recognized words was computed in relation of the total amount of studied words introduced in the list (8 words). The percentage of recognized lure words was computed based on the 4 lure words introduced in the list.

Percentage of recognized unrelated words was computed also in relation to the 4 unrelated words introduced in the list.

6.2.3. MRI scanning methods

6.2.3.1. DTI-MRI acquisition

DTI data were collected using a 3T whole-body MRI scanner (Siemens Magnetom Trio, Erlangen, Germany) employing an eight channel phased array head coil with parallel imaging (GRAPPA) and an acceleration factor of 2. Diffusion weighting was conducted using the standard TRSE (twise refocused spin echo) sequence. Images were measured using 2 mm thick slices, no gap, TR = 8200ms, TE = 85 ms, 128 × 128 acquisition matrix, FOV 256mm x 256mm, 64 axial slices. In order to obtain diffusion tensors, diffusion was measured along 12 non-collinear directions, chosen according to the standard Siemens DTI acquisition scheme using a single b-value of 1000 s/mm^2. Two signal averages and three runs were acquired per slice and diffusion gradient direction. Each run preceded by a non-diffusion-weighted acquisition.

6.2.4. Image processing

6.2.4.1. Pre-processing of diffusion-weighted data

DTI data were movement corrected and Eddy current-induced distorsion was removed prior to the estimation of the diffusion tensors. The first non-diffusion-weighted image of each block was realigned with the first image of the first series. Then, the determined transformation parameters were applied to the remaining diffusion-weighted images of the respective block. Subsequently, all images were averaged across the 3 runs. In order to assessed FA values, using the SPM2 diffusion toolbox

(http://www.fil.ion.ucl.ac.uk/spm/), diffusion tensor elements were extracted from an over-determined set of diffusion-weighted images. Diffusion tensors were diagonalized and thereby the eigenvectors and eigenvalues were obtained. Based on the eigenvalues, FA was calculated on a voxel-wise basis. Normalization of the FA data was performed based on the FA anisotropy images without Jacobian modulation of the signal intensities as reported previously (Camara et al., 2007).

Briefly, FA images were first normalized using the EPI-derived MNI template (ICBM 152, Montreal Neurological Institute) provided by SPM2. From the resulting normalized data sets a first preliminary study template was created by averaging. Then, FA images were normalized again using the previously created study template. Thus, a second and final study template was created by averaging these newly normalized images after the extraction of only brain parenchyma. The extraction of brain tissue was performed by a three-class brain segmentation. Afterwards, individual native-space brain parenchyma maps were extracted from the initial FA images and normalized to the final extracted-brain template. Finally, all individually normalized FA images were smoothed by convolving them with isotropic 8 mm FWHM (full width at half maximum) Gaussian kernels.

6.2.5. Data analysis

Voxel-wise analysis was performed to detect those voxels in which FA correlated with memory-related measures. With this aim, previously normalized FA images were independently regressed on the proportion of true and false memory recall and recognition scores by applying a simple regression model in SPM2. The analysis was constrained to those voxels with FA > 0.15 in each single participant. This cut-off

allowed to reliably isolating white matter from the rest of the brain(Jones et al., 1999). Locations and significance levels from the correlation analysis were restricted to three different uncorrected significant thresholds: $p < 0.05$, $p < 0.01$, and $p < 0.005$ (all of them with 60 voxels spatial extent). The use of this gradual threshold allows the visualization of the underlying white-matter path. However, only regions significant at cluster level (uncorrected $p < 0.01$, n = 60 voxels) were reported in Table 6.1 and discussed in the text. The maximum of suprathreshold regions was labeled using a white matter fibre DTI brain atlas (Wakana et al., 2004). Maxima and coordinates are reported in MNI space.

6.2.5.1. Region-of-interest analysis

Additionally, a region of interest analysis was performed in order to confirm voxel-based findings. Therefore, from the main peak activity, FA values were extracted and correlated with memory-related measures. Pearson's correlation was used to determine the correlation coefficients (see Results in figure 6.2)

6.3. Results

6.3.1. Behavioral data

A robust FM effect was obtained: Lure words were falsely recalled 46% ± 26 of the time, whereas studied words (TM) were recalled in 74% ± 9 of the cases (TM vs. FM recall, $t(47) = 6.53$; $p < 0.001$). FM and TM recall were not correlated ($r = 0.08$; Pearson correlation coefficient) which is in line with the view that FM and TM are at least partially mediated by distinct retrieval processes (Brainerd et al., 2002b; Schacter et al., 1996b).

Similarly, the recognition test was associated with a high degree of FM (75% ± 27 false recognition of lure words) in the presence of almost perfect recognition of the studied words (94 % ± 9) (TM vs. FM recognition difference, t (47) = 4.61; p < 0.001). False old decisions to unrelated new words were rare (2% ± 7) (FM vs. unrelated new words, t (47) = 17.17; p < 0.001). For studied words, in 78% ± 20% of the cases participants opted for a Remember judgment, thus, they were able to consciously recollect a distinct and vivid memory experience. More important, a large percentage of the lure words that were considered old words were judged to be Remembered (58% ± 36) (TM vs. FM Remember, t (47)= 4.43; p < 0.001). This was not the case for unrelated new words (~ 0 %). The large percentage of remembered experiences for FM demonstrated the power of the DRM paradigm in inducing memory illusions. Most importantly, these results also demonstrated the qualitative difference between this type of errors and normal false alarms: FM are normally accompanied by the subjective experience of having experienced an event that never occurred.

6.3.2. Diffusion tensor imaging analysis

Distinct patterns of correlation were obtained between FA and FM and FA and TM for both, recall and recognition tests (Table 6.2). Significant positive correlations between recall (respectively recognition) TM and FA were found bilaterally in regions coinciding with the ILF near medial temporal regions including hippocampus and parahippocampal structures which play a crucial role for recollection in animals (Sauvage, Fortin, Owens, Yonelinas, and Eichenbaum, 2008) and humans (Dennis, Kim, and Cabeza, 2008; Kim and Cabeza, 2007). This fascicle extends from the ventral and lateral temporal regions to the posterior parahippocampal gyrus and has been

associated to memory processes, as well as object and face processing (Schmahmann et al., 2007).

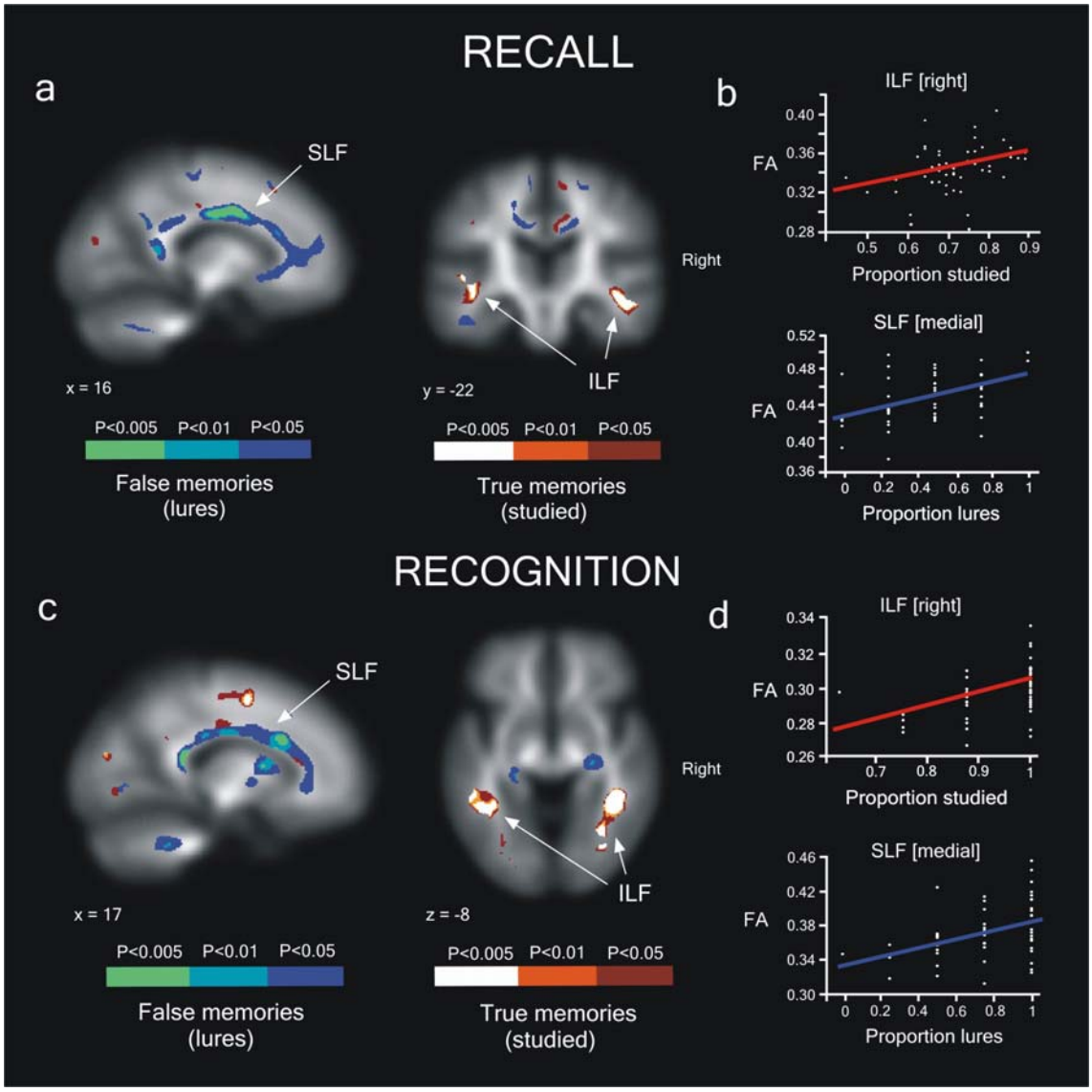

Figure 6.1: Individual differences in true and false memory (TM/FM) free recall and recognition scores associated to white matter changes (Fractional Anisotropy, FA). (a) Significant white matter clusters that correlated with TM and FM recall overlaid on the FA mean image from all participants (p < 0.005, n = 60 voxels spatial extent). The same results are shown with a more liberal statistical threshold to visualize the white-matter pathway (p < 0.01; p < 0.05; n = 60 voxels). (b) Depicted the mean FA value for each participant at two selected regions of interest for TM (right ILF, peak coordinates 46 -25 -13) and FM (right SLF, peak 17 -1 34). (c) Significant white matter clusters that correlated with the proportion of TM and FM recognition scores overlaid on the FA mean from all participants (p < 0.005; see also for white-matter tract visualization reduced statistical threshold images, p < 0.05; p < 0.01). (d) Mean FA value for each participant at two selected regions of interest for TM recognition (right ILF, peak coordinates 40 -46 -6) and FM recognition (right SFL, peak coordinates, 21 15 22). Red and blue lines represent regression lines for TM and FM recognition respectively.

Recall (respectively recognition) FM on the other hand was correlated with FA in several parts of the SLF (Figure 6.1a/c, Table 6.2). The SLF is the principal connection between frontal and postrolandic parietal and temporal (superior and medial) association regions (Schmahmann et al., 2007; Catani, Jones, and ffytche, 2005; Makris et al., 2005), lateral to the cingulum bundle. It thus connects several gray-matter areas implicated in familiarity-based memory retrieval processes (Yonelinas, Otten, Shaw, and Rugg, 2005). Whereas recall FM yielded positive correlations for several parts of the SLF as well as for the ILF, correlations were restricted to the SLF for recognition FM.

A further regression analysis was performed between memory scores and mean FA values extracted from the activation clusters found in the whole brain analysis at $p < 0.005$. Each cluster associated to either FM or TM recall (response recognition) scores showed significant positive correlation (all $p < 0.01$), whereas no significant correlation resulted when clusters associated to TM where correlated with FM scores and vice versa (all $p > 0.1$; see Figure 6.2), thus further supporting the notion that FM and TM are supported by dissociable brain systems including their respective fiber tracts. Representative regression analyses for TM and FM scores are shown in figures 6.1b and 6.1d.

Table 6.2: White matter changes associated to TM and FM recall and recognition. All peak values reported were significant at cluster level ($P < 0.01$, uncorrected; n = 60 voxels spatial extent). Correlation coefficients (r) were calculated with the voxels configuring each cluster ($P < 0.005$). For slope measure FA/*s*, *s* refers to the regressed memory scores. Peak coordinates of each cluster are reported in MNI coordinates.

Cluster	Side	Cluster size (mm^3)	*r*	Slope (FA/*s*)	*t* value	Peak coordinate		
						x	y	z
True Memories								
Recall								
ILF	R	1486	0.39	0.08	3.75	46	-25	-13
	L	631	0.39	0.11	4.22	-44	-25	0
IFO/ILF	L	983	0.44	0.12	3.98	-33	-76	-4
Recognition								
ILF	R	5953	0.46	0.07	4.75	40	-46	-6
	L	3818	0.35	0.06	4.86	-37	-52	-3
False Memories								
Recall								
SLF Anterior	R	829	0.43	0.07	3.91	9	21	15
SLF Medial	R	918	0.42	0.04	3.50	17	-1	34
SLF Posterior	L	1500	0.45	0.05	3.65	-18	-34	33
IFO/ILF	R	1569	0.33	0.03	3.93	45	-54	-8
Recognition								
SLF Medial	R	1052	0.41	0.05	3.16	21	15	22

Notes: SLF = Superior longitudinal fascicle; ILF = inferior longitudinal fascicle; IFO = inferior fronto-occipital fascicle.

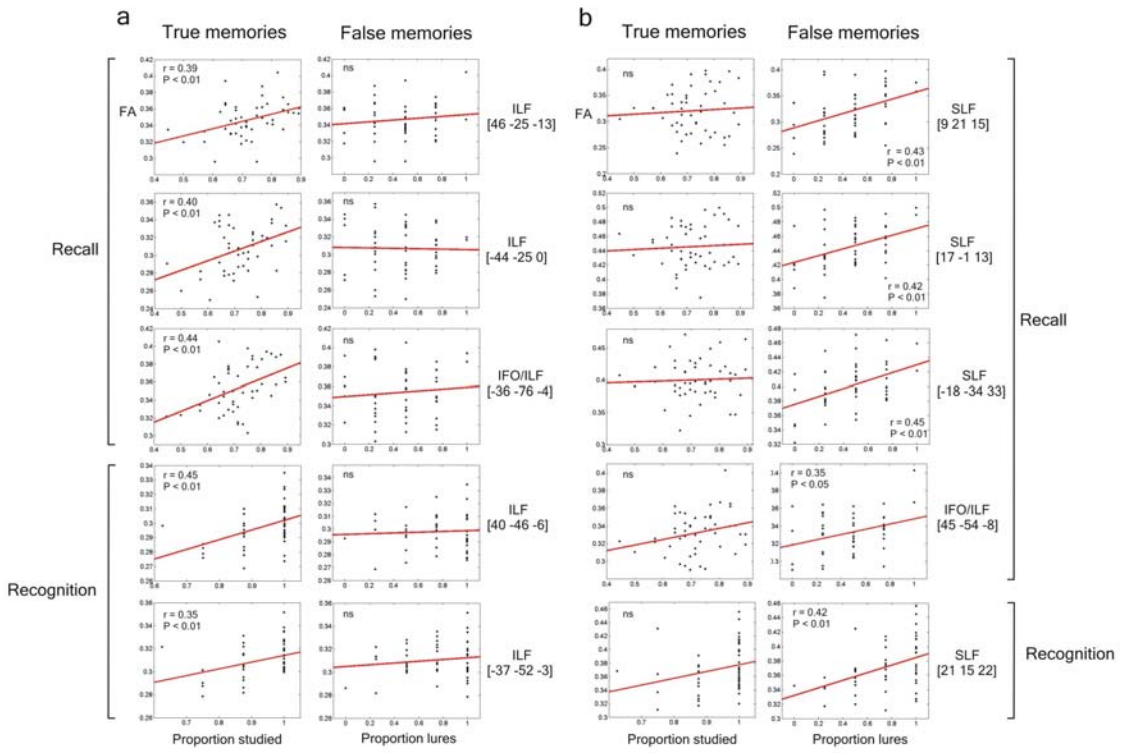

Figure 6.2: Results from the regions of interest analysis. Correlations between FA and TM or FM recall and recognition scores for the peak locations of the regions described in Table 6.1. While most of the peak locations corresponding to the ILF correlated with TM recall and recognition scores, no correlation was observed with FM scores. The reverse pattern was observed for SLF regions.

6.4. Discussion

To summarize, we have demonstrated, within a population of unselected healthy young adults, a significant variation of TM and FM and that this variation is associated with differences in the micro-structural properties of two dissociable fiber tracts. FA has been shown to reflect axonal micro-structure (e.g., axon size, extent of myelination) (Basser and Jones, 2002; Chepuri et al., 2002), which determines the quality of axonal transmission (Waxman and Bennett, 1972). Greater FA in the ILF, connecting MTL structures, is related to higher TM scores. This result dovetails nicely with functional imaging results of greater MTL activity for TM (Dennis, Kim, and Cabeza, 2008; Kim

and Cabeza, 2007). Greater FA in the SLF, connecting frontal and parietal structures, is related to increased susceptibility to FM, which again coincides with fMRI findings of greater activation in frontoparietal regions for FM decisions (Kim and Cabeza, 2007).

The present results are also in agreement with previous neuropsychological findings, which indicate that medial temporal patients show reduced true and false recognition, while frontal patients show increased false recognition (LaVoie, Willoughby, and Faulkner, 2006; Verfaellie, Rapcsak, Keane, and Alexander, 2004; Schacter, Curran, Galluccio, Milberg, and Bates, 1996; Parkin, Bindschaedler, Harsent, and Metzler, 1996).

The involvement of prefrontal structures in memory illusions is further corroborated by the memory deficit known as confabulation which is associated to ventromedial prefrontal cortex lesions. These patients are characterized by displacing or misremembering the time and location of they own memories, resulting in bizarre stories and the lack of awareness about the improbability of the events recalled. A similar pattern of increased false recognition due to impaired monitoring has been encountered in Korsakoff amnesic patients, which show also concurrent frontal damage (Schacter, Verfaellie, Anes, and Racine, 1998). Age-related decay in the prefrontal cortex might also be related to the increased susceptibility encountered in older adults (Norman and Schacter, 1997).

The association encountered between the SLF and FM in the present study, as well as previous neuroimaging and neuropsychological studies (Slotnick and Schacter, 2004; Schacter, Verfaellie, and Anes, 1997; Schacter et al., 1996; Kim and Cabeza, 2007) suggest a critical role of the prefrontal cortex in strategic monitoring and error-checking process in post-retrieval phases. In this regard, FM may be due to a

breakdown of the monitoring system, which is in charge of differentiating highly associated lure words (due to spread activation from studied words or thematic-gist activation, (Brainerd and Reyna, 2002a) from the encoded studied words (Roediger, III, Watson, McDermott, and Gallo, 2001; Balota and Spieler, 1999). This action-monitoring framework proposes a series of cognitive control processes (e.g., searching, monitoring, verification and organization) in charge of editing the output from medial temporal lobe structures.

This processes should be able to avoid memory illusions and to dampen the strong feeling of familiarity associated to lure words. However, it is important to bear in mind that considering this post-retrieval monitoring account, one might have expected increased activation in the frontoparietal network and better white-matter integrity related to a decrease on FM. However, the functional and structural results reported until now show the opposite relationship: increase activity in the frontoparietal system elicits higher confidence FM elicitation (Kim et al., 2007) as well as susceptibility to FM might be related to quality of the neural transmission in the SLF pathway (better white-matter integrity in the SLF). Thus, these results cannot be accounted by the action-monitoring account.

In agreement with the fuzzy trace theory (Brainerd et al., 2002), we propose that the MTL and frontoparietal networks constitute two independent and parallel retrieval mechanisms which rely on different type of stored memory representations: (i) the MTL system – item-specific episodic information and (ii) the frontoparietal network – semantic gist information. According to this proposal, incoming stimuli are encoded into two qualitative different types of memory traces: a *verbatim* (or item-specific details, e.g. perceptual attributes, position in the list, etc.) and a *gist-trace*, which

represents episodic conceptual information (e.g., thematic similarity or conceptual overlap between the words presented in the list). This theory predicts that at the test phase, TM recognition might be based on item-specific episodic information (subjective experience of recollection), while FM might rely on semantic gist information (general meaning of the studied list) (subjective experience of familiarity). Thus, the increased processing efficiency of both networks and brain white-matter integrity of the underlying pathways might make more veridical and trustful the information retrieved either through the MTL-ILF system, which would elicit a TM, or through the frontoparietal-SLF network, which will end-up in a FM. The negative functional coupling reported between both systems (Kim et al., 2007) might prevent that the decisions are based exclusively on the information accrued though the frontoparietal network or familiarity based information and allows cross-talk between both retrieval systems. For example, retrieval through the MTL system (verbatim information) could inhibit FM retrieval neutralizing meaning or gist familiarity retrieval and preventing FM.

At the same time, one could strategically decide not to accept any memory retrieval experience which it is not directly eliciting a detailed and vivid experience (recollection), thus aborting gist-based retrieval positive experiences and preventing false recall. However even this cognitive strategy will fail in those cases in which false memories induce clear vivid episodes ("phantom recollection"). Notice that in the present study app. 60% of the FM experiences were considered as "remember" items, thus participants reported having a conscious and vivid recollection of these lure words. These experiences tend to occur when thematic or gist-information retrieved is very strong as it is the case in the studied list of the DRM paradigm. In this regard, stable individual differences in the susceptibility to create FM should arise due to the long-

term effects of differentially weighting and relying on the information conveyed by both retrieval routes. In these particular cases, strong gist or thematic trace recollection will overshadow verbatim or item-specific traces inducing to accept false memory retrieval experiences as true.

As a caveat of the present study, we think that further additional empirical studies might be needed in order to disentangle the meaning of this positive correlation. As stated before, larger FA values could be initially interpreted as the extent of tract myelination and density of the axonal fibers comprising axonal bundles. In support of this idea, several evidences suggest that neural impulse activity may actually increase myelination (Bengtsson et al., 2005; Demerens et al., 1996) through the release of cytokine trophic factors that support oligodendrocytes (Fields, 2005; Ishibashi et al., 2006; Demerens et al., 1996b; Bengtsson et al., 2005). However other factors might also contribute to increasing FA (e.g., microscopic deficits of axonal structures, decreases in axonal diameter, branching of axonal bundles or intravoxel fiber crossing) (Beaulieu, 2002).

6.5. Conclusions

To describe the relation between brain structure and function is a fundamental task of neuroscience. Prior work has mainly focused on cortical structures (Draganski et al., 2004) but recently white matter micro-structure in circumscribed brain regions as reflected by FA has been shown to predict behaviour or functional brain activations in decision making (Boorman, O'Shea, Sebastian, Rushworth, and Johansen-Berg, 2007; Tuch et al., 2005a), language (Gold, Powell, Xuan, Jiang, and Hardy, 2007), and memory (Putnam, Wig, Grafton, Kelley, and Gazzaniga, 2008) tasks. At this point the

direction of such relations remains unclear. Innate differences in white-matter structure might explain differences in FM and TM retrieval processes in the current study.

Alternatively, variations in experience or cognitive style might induce neural plasticity of white-matter tracts. FA values reflect axonal size and myelinization which may be susceptible to experience-dependent changes (Juraska and Kopcik, 1988; Demerens et al., 1996) and, indeed, changes in FA induced by long-term musical training have been observed recently (Bengtsson et al., 2005).

The present study evidenced the relevance of studying the neural network interconnectivity in memory research and highlighted the implication of white-matter structural differences as a fundamental key to understand individual variations in cognitive functions.

Chapter 7

7. General Discussion and conclusions:

New approaches to study brain functioning using MRI

The relationship between brain function and structure is a fundamental question in cognitive neuroscience. However, this question has remained elusive due to the lack of a robust method for investigating non-invasively micro-structure differences in the working brain. Recently, the introduction of diffusion tensor imaging (DTI) combined with advanced functional MRI techniques opens a suitable method in order to interrelate brain circuitry and function (Rykhlevskaia et al., 2008).

Different ways of combining structural and functional MRI have been described (see Table 7.1). Traditional functional brain imaging studies analyze each brain region separately by applying univariate statistical approaches, and then structural images are superimposed only for anatomical localization purposes (Table 7.1a). Advancements in imaging methods and analytical techniques permit relating brain function and structure by estimating the fiber path that connects functionally active brain regions (Table 7.1c). In turn, a multivariate analysis permits exploring and investigating interregional structural and functional relationships (Table 7.1b-7.1d). Indeed, the simplest approach consist of identifying the functional network, typically in terms of covariance analysis, and structural images are then overlaid as reference (7.1b). New approaches also integrate anatomical connectivity information by capturing the

underlying structural connectivity pattern from which should emerge the functional activations (7.1d).

Table 7.1: Different ways for combining structural and functional brain imaging data (Adapted from (Rykhlevskaia et al., 2008).

		Functional imaging	
		Regional approach Each region is analyzed independently by using univariate analysis	Interregional approach Regions are combined (analysis of covariances)
Structural Imaging	Each region is analyzed independently (anatomy is used only as reference)	a. Traditional functional brain imaging studies	b. Functional connectivity studies seeded on the basis of anatomical information
	Regions are combined (analysis of white matter tracts)	c. Structural connectivity analysis paired with univariate functional analysis.	d. Analysis of functional connectivity informed by structural connectivity.

In this dissertation, functional and structural MRI information is combined by applying different neuroimaging analysis approaches in order to increase our understanding in the organization and dynamics of the brain circuits that engage neural functions and human behavior. With this proposal in mind, in Experiment 1 and Experiment 2 regional (Table 7.1.a) and interregional (Table 7.1.b) functional patterns in reward processing were investigated. Anatomical information was then integrated in Experiment 4 after correlating functional and microstructural information in the same reward-related task. By studying and combining functional MRI and micro-structural DTI information these three experiments provided a new insight into the relationship between brain structure and function in the reward system.

Moreover, the characterization of individual differences in brain architecture might be crucial in order to understand the way functional brain states arise from their underlying structural substrates. In Experiments 3 and 5 the focused was on the study

of anatomical connectivity and its interactions with biological (aging) and performance variables (memory task). In the Table 7.2 the different approaches and interrelation between all the experiments presented are summarized.

Table 7.2: Summary of the main contents of this dissertation. The same gambling task has been used in Experiments 1, 2 and 4. In Experiment 1 regionally specific effects are investigated using a classical univariate approach. Experiment 2 investigates interregional functional connections, while Experiment 4 incorporates anatomical information. Experiments 3 and 5 study anatomical connectivity and its interactions with biological (aging) and performance variables (memory task).

	Technique			**Variable**		**Aim of study**	
	DTI	**fMRI**	**Approach**	**Performance**	**Biological**	**Topic**	**Object**
Exp 1		X	*Regional*		X	Rw/Exf	*Genetic Differenes*
Exp 2		X	*Interregional*			Rw/Exf	*Functional Connectivity*
Exp 3	X		*Regional*		X	Aging (BP)	*Microstructural Changes*
Exp 4	X	X	*Interregional*			Rw/Exf (BP)	*Functional-Structural coupling*
Exp 5	X		*Regional*	X		Mem/Exf (BP)	*ID in WM correlate with performance*

Note: DTI= Diffusion tensor imaging; fMRI= functional Magnetic resonance imaging; Exp= Experiment; Rw= Reward processing; Exf=Executive functions; BP=Brain Plasticity; Mem= Memory; ID=Individual Differences; WM=White matter.

7.1 Combining structural and functional MRI in reward processing

The same reward-related gambling task was used in Experiments 1, 2 and 4 to evaluate gain and loss feedback processing by using different approaches. In Experiment 1 a classical univariate analysis was applied. Monetary gains and losses activated a similar fronto-striatal-limbic network, in which main activation peaks were observed bilaterally in the ventral striatum. In particular, monetary gains systematically elicited greater activation than monetary losses, a finding that is in accordance with previous

studies (Nieuwenhuis et al., 2005). In Experiment 2 interregional functional connections were investigated using the same task. Interestingly, functional connectivity analysis using the ventral striatum as a seed region showed a distinct mesolimbic network when compared to the previous classical univariate analysis (Experiment 1). Similar responses in both Gain and Loss conditions were observed, however, stronger correlations were found in negative outcomes between the ventral striatum and the medial OFC when compared to positive reinforcements.

The fact that different functional patterns were obtained with both analyses suggests that the brain activations observed in the classical approach might reflect different cognitive mechanisms were engaged when processing reward-related information, and stresses the importance of studying functional connectivity as a complementary tool to the standard fMRI analysis (Rissman et al., 2004; Ranganath et al., 2005; Gazzaley et al., 2004; Fiebach and Schubotz, 2006; Buchsbaum et al., 2005). Thus, setting the functional connectivity seed in the ventral striatum might isolate only one of the distinct neural networks involved in reward processing. In relation to this, O' Doherty et al. (O' Doherty and Bossaerts, 2008) recently argued that decision-making encodes at least four different neural networks related to (i) the representation of expected future rewards, (ii) the variance in the expected reward, (iii) the learning, updating and (iv) actions derived from these representations.

It is usually assumed that neurons with common functional properties are locally grouped and present similar functional patterns. In standard fMRI analysis it is possible to distinguish the contributions of large-scale neurocognitive networks that subserve a specific psychological state or cognitive process (Mesulam, 1990). Besides, using functional connectivity local functional activation patterns can be identified that

respond similar to other distal regions and that might be anatomically connected through projection thalamocortical, cortico-cortical or cortico-subcortical (Innocenti and Price, 2005). It is important to highlight that anatomical connections constrain the flow of information between distal regions and the influence that one region can exert over others. In this regard, very interesting results have been recently obtained applying fiber-tracking reconstructions, which allow the detection of the most likely anatomical pathway connecting brain regions (Schonberg et al., 2006; Powell et al., 2006; Kim and Kim, 2005). For example, Toosy et al. (2004), after individually tracking the path that connected the visual regions activated by a photic stimulation paradigm, found that the mean fractional anisotropy of the estimated tracts significantly correlated with the functional activation induced in the visual cortex.

In Experiment 4 we directly evaluated the hypothesis that individual BOLD responses in the ventral striatum might be constrained by its extrinsic anatomical connections. Individual whole-brain FA measures were correlated with the differential BOLD response in the ventral striatum derived from the Gain minus Loss contrast in the gambling task. A negative significant correlation was found in the uncinate-inferior fronto-occipital fasciculus between both meaures. It has been suggested that the uncinate fasciculus reflects the interconnectivity between orbito-frontal and ventral striatal regions (Ungerleider, Gaffan, and Pelak, 1989). Accordingly, this neurophysiological coupling is consistent with the differential connectivity pattern obtained between the ventral striatum and the OFC when the Gain and Loss conditions were compared in Experiment 2. The strong correlation observed might also suggest that differences in functional interconnections are constrained by the strength of its anatomical connections.

Up to now, not many studies have reported a direct correspondence between micro-structure and brain function (Rykhlevskaia et al., 2008; see for example Cohen et al., 2008). An interesting further approach would be to estimate the tract that connects the ventral striatum with the medial OFC region. A detailed quantification of this tract might give more information about the nature of the mechanism that gives rise to this relationship observed between structure and functional response.

7.2 Individual differences in functional and anatomical connectivity

Understanding the relationship between biological variations that leads to individual differences in functional and structural circuits may also help to disentangle the nature of the underlying coupling. Individual differences in performance and its correlations with the activation of brain regions have long been used in order to infer the role of a specific region in a cognitive process. However, it is important to consider that other factors might also be affecting the individual differences observed in BOLD responses. For example, recent reports reveal that individual differences in BOLD response might also be explained based on genetic factors, particularly dopaminergic genes (Yacubian et al., 2007). In Experiment 1, we observed regional BOLD changes in several reward-related regions associated with COMT and DRD4 dopaminergic genes.

In a similar vein, changes in brain structure have been largely associated with individual differences observed in cognitive processes, mental or neurological disorders and developmental and aging processes. In this vein, in Experiment 3, it was observed that DTI can be sensitive to capture white matter changes across the lifespan. Indeed, a voxel-based analysis, which correlates the relative anisotropy and the apparent

diffusion coefficients with age, was performed by applying an optimised normalization protocol. Linear regression analysis revealed negative significant correlations with age in the corpus callosum, prefrontal regions, the internal capsule, the hippocampal complex, and the putamen. Nevertheless, not only should the developmental reorganization of neural pathways that depends on a single type of morphological modulation be considered, but also a combination of both developmental individual process as well as experience-related events.

Another aspect that might influence individual differences in white-matter changes across life is the role of life-experiences which should directly shape brain plasticity. Indeed, the neural plasticity associated with learning and development is being increasingly studied using functional neuroimaging approaches (see for a review, Poldrack, 2000). Classical morphometry voxel-based analyses have shown functional-related regionally structural correlates in the adult human brain with intensive trained cognitive skills or learning (Draganski et al., 2004; Gaser and Schlaug, 2003; Maguire et al., 2006). However, few reports until now have correlated microstructural-related parameters with cognitive or behavioural performance measures. For example, using an oddball task, Madden et al. (Madden et al., 2004) encountered a correlation between fractional anisotropy and behavioural reaction times in the anterior limb of the internal capsule for older healthy adults, whereas the fractional anisotropy in the splenium was a predictor of the reaction time for younger adult volunteers. Tuch et al. (Tuch et al., 2005a) found on a similar visual self-paced choice reaction-time task correlations between fractional anisotropy and reaction times in the thalamus and some of its porojection pathways. Recently, Gold et al. (Gold et al., 2007) also reported that fractional anisotropy correlated with the speed of lexical decision in both left parietal and frontal white matter regions.

More importantly, Bengtsson et al. (Bengtsson et al., 2005) compared white matter measures in professional pianists to age-matched controls. Professional pianists presented larger anisotropy in the posterior limb of the internal capsule compared to controls. A positive correlation was found between anisotropy and number of hours that they had practiced the instrument as a child, adolescent and adult, but in different fibre tracts, depending on the age that piano practice occurred. This result indicates that white matter changes were predicted in terms of the number of hours that each subject had spent in acquiring the skill rather than performance being predetermined by a limitation on white matter development.

The previous studies showed that at least some of the individual differences observed in performance might be predicted at a micro-structural level. In Experiment 5, it was observed that microstructural properties of different white matter tracts quantified by fractional anisotropy were correlated with true and false memory retrieval. The former was correlated to diffusion anisotropy in the inferior longitudinal fascicle, the major connective pathway of the medial temporal lobe, while a greater proneness to retrieve false items was related to the superior longitudinal fascicle connecting fronto-parietal structures. This last piece of information provides evidence for the relevance of studying anatomical interconnectivity and highlights the implication of white-matter structural differences as a fundamental key to understand individual variations in cognitive functions.

7.3 Brain dynamics and organization

A large body of literature and the results herein presented highlight that the relationship and interaction between brain function and structure is very complex, and brain dynamics and organization are altered on the basis of innate and developmental individual differences as well as experience-related changes. Considering only the present results, however, it is difficult to determine the physiological nature of the existing interrelation between brain function and structure.

Some evidence support that neural impulse activity may actually increase myelination and alter white matter structure through the release of specific trophic factors that promote oligodendrocyte genesis (Demerens et al., 1996; Fields, 2005; Ishibashi et al., 2006). Indeed, oligodendrocyte plasticity and myelin recovery are not simply a developmental process; they are modifiable structures that can influence axon connectivity which is critical for information processing. Many reports suggest that myelin may modulate the degree of anisotropy in a given tract; however, diffusion indexes reflect mainly indirect markers of white matter properties, such as axon diameter or axonal membranes that hinder water diffusion perpendicular to the long axis of the fibers (Beaulieau et al., 2002).

These studies showing that the induced neural activity elicits long-lasting alterations in white matter structure open a clear physiological link between brain function and structure. Nevertheless, further studies are needed in order to clarify the physiological mechanisms for the observed correlation pattern. Importantly, the causality and the nature of the coupling observed remain unsolved.

7.4. Future directions

Current views in cognitive neuroscience stress the importance of studying interconnectivity patterns and support the idea that most cognitive functions are widely distributed in the brain via interconnected distal segregated regions (Rykhlevskaia et al., 2008). Accordingly, traditional neuroimaging studies have shifted the focus on regionally univariate analysis to connectivity approaches.

In this regard, multivariate analyses have evidenced the remarkably useful description of brain processing in terms of functional patterns by taking advantage of the functional information across the whole-brain instead of constraining the functional analysis of the time course of individual voxels. Many improvements have been made in recent years to describe and localize functional patterns (for a review see Rogers et al., 2007).

Some of the more advanced analysis techniques, such as dynamic causal modelling, model the brain as a dynamic system that is subject to inputs and produces outputs in terms of parameters that represent the coupling between brain states. Thus, experimental conditions modulate neuronal responses in specific anatomical regions, but they also change effective connectivity by influencing the interactions between regions (Friston et al., 2003). From a new perspective, pattern recognition methods, including support vector machine or linear discriminant analyses among others, promise to decode and predict brain function in terms of distributed activity patterns (Polyn et al., 2005; Grill-Spector et al., 2006; Haynes and Rees, 2006). These classification-based techniques train classifiers to capture the functional pattern that distinguishes each experimental condition, typically from a subset of the experimental trials in predefined regions. Then, according to the similarity of the activation patterns

obtained in the initial training and the remaining data set, the reliability of the classification method is evaluated. In contrast to standard functional analyses, in which data is averaged and sorted between conditions and main effects are obtained at the group level, the use of pattern recognition methods permits the prediction and generalization of specific functional patterns in a trial-by-trial based within individuals.

However, until recently, most of the connectivity approaches are especially suited to study patterns of functional long-scale connectivity, but they do not tackle the fine-grained details of functional and anatomical connectivity (Bressler and Tognoli, 2006). In this vein, fMRI faces the challenge of detecting smaller functional units in specific brain regions, typically enhancing spatial specificity by increasing magnetic field strength. Thus, the use of high (3.0-4.0T) or ultra-high (7.0-8.0T) magnetic fields accompanied with optimized pulse sequences and technical strategies such as parallel imaging (Lütcke et al., 2006), are likely to play an important role in the future, since they should enhance the spatiotemporal resolution in brain functional and structural localization. For example, high resolution functional MRI can improve the quality of brain mapping because of its sensitivity to detect the activation of smaller regions (e.g., < 1 mm^3). As a smaller voxel size is explored the BOLD response should be captured with more precision. In particular, when the voxel size decreases, the average signal in the voxel remains constant, but the average noise decreases and therefore the BOLD response is measured with enhanced signal detection. Conversely, this is not true at neural population levels, because functional MRI is limited by the intrinsic physical and biological properties of the hemodynamic-based signal. The density of the vessels from which the BOLD signal is measured, is less than 3% of a voxel volume, while dense population of neurons, synapses and glia occupy most of the intervascular space (Logothetis, 2008). Accordingly, the point-spread function of the BOLD signal in

relation to the distance between neural specialized clusters constrains the localization of the evoked neural response (Logothetis, 2008; Grill-Spector, 2008).

In contrast, white-matter micro-structural MRI or diffusion imaging apparently does not have these limitations (there are specific problems in terms of eddy currents and sensitivity to motion, see Le Bihan et al., 2006a) and will provide a powerful tool for progressively adding more information that could be used to inform about brain function and mapping neural histoarchitecture in vivo. Accordingly, diffusion tensor imaging is already providing surprising correlations between behaviour or electrophysiological correlates and micro-structure, which represents a direct link between structure and brain function (Thakkar et al., 2008; Westlye et al., 2008).

New insights in molecular diffusion of water are tentatively looking at brain activity through the intrinsic water physical properties during brain activation (Le Bihan et al., 2006). In particular, it has been reported that water diffusion slightly slows down several seconds before the BOLD response is detected. It has been interpreted as an expansion of cortical cell membranes swelling during brain activation. This proposal reflects a very interesting approach to capture the neural activation mechanisms underlying brain processing (for a review see Le Bihan et al., 2007).

However, the progress of diffusion tensor imaging has resulted largely from the rapid development of new analysis tools combined with improvements in coil design and pulse sequences that permits a detailed knowledge of the large-scale high-resolution structural network supporting higher-level brain functions (Hagmann et al., 2007). In particular, fiber-tracking algorithms allow the tractography of brain circuitry in vivo, providing visualizations that were not possible to obtain with any other non-invasive

method. However, methodological problems still exist regarding derived-fiber tracking pathways and the biological nature of the signal detected. In particular, the main limitation of fiber-tracking arises from the fact that confounding multiple fiber directions within a single voxel might create false positive connections and therefore misestimate the resulting fiber pathways. To overcome these limitations probabilistic fiber tractography and Q-ball imaging have been recently introduced (Dyrby et al., 2007; Tuch et al., 2005b). The goal of probabilistic tractography algorithms is to create probabilistic maps of fiber connectivity between brain regions that can be used to trace fiber pathways into gray matter (Behrens et al., 2003; Parker et al., 2003). These voxel-based connectivity maps may reflect, besides the integrity and coherence of white matter tracts, some additional information, such as tract geometry (Ciccarelli et al., 2006). Q-ball imaging, in turn, is a high-angular resolution diffusion imaging that allows accurately the reconstruction of the orientation of the underlying fiber neural population after modelling it based on a spherical harmonic representation. A further decomposition of the diffusion orientation distribution profile succeeds in separating fiber bundles and crossing regions. In sum, we believe that one of the main goals of neuroimaging in the coming years might be the study of brain dynamics inferred from structural architecture.

Nevertheless, considering the known limitations of tractography, post-morten studies combined with invasive neuron tract tracing techniques will be necessary in the future in order to validate the anatomical accuracy of fiber-tracking reconstructions. Post-morten imaging permits using stronger magnetic fields and long scanning times as well as stronger magnetic fields. It significantly enhances both spatial resolution and signal to noise ration. In addition, motion artifacts are discarded (Dyrby et al., 2007).

The relationship between brain function and structure is also going to be a crucial issue in the future. More and more, MRI neuroimaging studies combine fMRI data with diffusion information, interrelating brain dynamics and organization. Indeed, the method of seeding fiber tracking algorithms in functionally active brain regions is currently the launch point for directly interrelating brain function and structure (Staempfli et al., 2008). However, due to low anisotropy in functional activated regions (gray matter), fiber-tracking has to be improved in the gray to white matter transition region in order to more reliably converge from functional MRI to diffusion information. This could be reached by improving both spatial resolution and diffusion sensitivity during data acquisition (Staempfli et al., 2008). From another perspective, in the same way that we proposed in this dissertation, functional and micro-structural information might be directly combined by correlating the functional activation from a seed region with DTI data. This kind of analysis pretends to explore the large-scale connections that emerge from a particular region. Further studies might explore whether functional and structural links might be better predicted in terms of regionally specific structural properties (anatomical connectivity) instead of long distal anatomical connections (Passingham et al., 2002). Thus, we would expect that a direct local microstructural comparison might better adjust the resolution of the functional/structural coupling compared to the long distance associations.

It is important to bear in mind that any functional or DTI approach is self-serving. Up to here, the potential advantages of using functional and DTI information in order to tackle brain processing has been stressed, but a full understanding of brain dynamics and organization will require the combination of theories on the brain's functional organization and several neuroimaging methods as well as development of technical approaches that facilitates the integration and accurate registration of information

from different modalities. Casanova et al. (Casanova et al., 2007), for instance, have developed a biological parametric mapping toolbox that facilitates the integration of information from other modalities by using a voxel-based multiple regression approach. Thus, the combination of different neuroimaging data (such as lesion studies, electrical measurements of brain activity, transcranial magnetic stimulation, optical imaging, developmental brain-behaviour relationships or modelling data, among others), will probably be the best strategy for tracing brain architecture and dynamics. For example, since combined hybrid PET/MRI devices are now available, other important developments will likely result from combining PET and MRI measurements in the same session. Such devices will allow researchers to investigate task-related molecular (e.g., receptor availability/binding) and blood flow changes simultaneously, thus providing an important link to the nature of the existing relationship between brain function and architecture.

7.5. General conclusions

Overall, two complementary fundamental principles of functional organization, functional integration and functional specialization, appear to be inherent to the human brain. By employing microstructural (DTI) and hemodynamic (fMRI) techniques both functional and structural information and their interactions with biological and performance variables by applying different neuroimaging analysis approaches have been explored. The strategies reviewed in this dissertation have enabled the demonstration of potential uses of micro-structural and functional information to infer functional and structural connectivity. We highlighted that functional segregation and functional integration cannot be studied independently. As

brain regions do not work in isolation, both regionally activation and its corresponding interrelations have to be considered.

Finally, it should be emphasized that multimodal approaches are crucial in order to assess an accurate understanding of brain function and dynamics, in particular the integration of anatomical, functional and possible interactions with biological and performance variables might be crucial for further investigations. This dissertation clearly suggests new prospects for the integration of individual micro-structural and functional properties in brain function and its dynamics. A combined fMRI/DTI approach is important in order to understand the underlying functional brain architecture.

Thus, the discussion began by investigating the functional neural correlates by assuming that they are an indirect measure of brain functioning in relation to cognition. From there, it has been suggested that an anatomical substrate should sustain the nature of the functional activity pattern. However, the micro-structural correlates encountered as functional associations would also reveal the structure of individual variations in cognitive functions. The causality of the coupling observed therefore remains unsolved and poses the question of the direction of the relationship between functional correlates and micro-structure.

Is structure then functionally constrained or on the contrary are functional properties modulated structurally?

At this stage brain function and structure becomes ambiguous.

References

Abe, O., Aoki, S., Hayashi, N., Yamada, H., Kunimatsu, A., Mori, H. et al. (2002). Normal aging in the central nervous system: quantitative MR diffusion-tensor analysis. *Neurobiol.Aging, 23,* 433-441.

Abler, B., Erk, S., Herwig, U., and Walter, H. (2007). Anticipation of aversive stimuli activates extended amygdala in unipolar depression. *J.Psychiatr.Res., 41,* 511-522.

Aboitiz, F. and Montiel, J. (2003). One hundred million years of interhemispheric communication: the history of the corpus callosum. *Braz.J.Med.Biol.Res., 36,* 409-420.

Adcock, R. A., Thangavel, A., Whitfield-Gabrieli, S., Knutson, B., and Gabrieli, J. D. (2006). Reward-motivated learning: mesolimbic activation precedes memory formation. *Neuron, 50,* 507-517.

Aertsen, A., Vaadia, E., Abeles, M., Ahissar, E., Bergman, H., Karmon, B. et al. (1991). Neural interactions in the frontal cortex of a behaving monkey: signs of dependence on stimulus context and behavioral state. *J.Hirnforsch., 32,* 735-743.

Aguirre, G. K., Zarahn, E., and D'Esposito, M. (1998). The variability of human, BOLD hemodynamic responses. *Neuroimage., 8,* 360-369.

Akil, M., Kolachana, B. S., Rothmond, D. A., Hyde, T. M., Weinberger, D. R., and Kleinman, J. E. (2003). Catechol-O-methyltransferase genotype and dopamine regulation in the human brain. *J.Neurosci., 23,* 2008-2013.

Alheid, G. F. (2003). Extended amygdala and basal forebrain. *Ann.N.Y.Acad.Sci., 985,* 185-205.

Amunts, K., Schleicher, A., and Zilles, K. (2007). Cytoarchitecture of the cerebral cortex--more than localization. *Neuroimage., 37,* 1061-1065.

Anderson, B. J., Alcantara, A. A., and Greenough, W. T. (1996). Motor-skill learning: changes in synaptic organization of the rat cerebellar cortex. *Neurobiol.Learn.Mem., 66,* 221-229.

Anderson, S. W., Barrash, J., Bechara, A., and Tranel, D. (2006). Impairments of emotion and real-world complex behavior following childhood- or adult-onset damage to ventromedial prefrontal cortex. *J.Int.Neuropsychol.Soc., 12,* 224-235.

Apicella, P., Ljungberg, T., Scarnati, E., and Schultz, W. (1991). Responses to reward in monkey dorsal and ventral striatum. *Exp.Brain Res., 85,* 491-500.

Ariano, M. A., Wang, J., Noblett, K. L., Larson, E. R., and Sibley, D. R. (1997). Cellular distribution of the rat D4 dopamine receptor protein in the CNS using anti-receptor antisera. *Brain Res., 752,* 26-34.

Ashburner, J. and Friston, K. (1997). Multimodal image coregistration and partitioning--a unified framework. *Neuroimage., 6,* 209-217.

Ashburner, J. and Friston, K. J. (1999). Nonlinear spatial normalization using basis functions. *Hum.Brain Mapp., 7,* 254-266.

Ashburner, J. and Friston, K. J. (2001). Why voxel-based morphometry should be used. *Neuroimage., 14,* 1238-1243.

Au Duong, M. V., Audoin, B., Boulanouar, K., Ibarrola, D., Malikova, I., Confort-Gouny, S. et al. (2005). Altered functional connectivity related to white matter changes inside the working memory network at the very early stage of MS. *J.Cereb.Blood Flow Metab, 25,* 1245-1253.

Balota, D. A. and Spieler, D. H. (1999). Word frequency, repetition, and lexicality effects in word recognition tasks: beyond measures of central tendency. *J.Exp.Psychol.Gen., 128,* 32-55.

Bandettini, P. A. and Cox, R. W. (2000). Event-related fMRI contrast when using constant interstimulus interval: theory and experiment. *Magn Reson.Med., 43,* 540-548.

Basser, P. J. and Jones, D. K. (2002). Diffusion-tensor MRI: theory, experimental design and data analysis - a technical review. *NMR Biomed., 15,* 456-467.

Baxter, M. G. and Murray, E. A. (2001). Effects of hippocampal lesions on delayed nonmatching-to-sample in monkeys: a reply to Zola and Squire (2001). *Hippocampus, 11,* 201-203.

Bayer, H. M. and Glimcher, P. W. (2005). Midbrain dopamine neurons encode a quantitative reward prediction error signal. *Neuron, 47,* 129-141.

Beaulieu, C. (2002). The basis of anisotropic water diffusion in the nervous system - a technical review. *NMR Biomed., 15,* 435-455.

Bechara, A., Dolan, S., Denburg, N., Hindes, A., Anderson, S. W., and Nathan, P. E. (2001). Decision-making deficits, linked to a dysfunctional ventromedial prefrontal cortex, revealed in alcohol and stimulant abusers. *Neuropsychologia, 39,* 376-389.

Behrens, T. E., Johansen-Berg, H., Woolrich, M. W., Smith, S. M., Wheeler-Kingshott, C. A., Boulby, P. A. et al. (2003). Non-invasive mapping of connections between human thalamus and cortex using diffusion imaging. *Nat.Neurosci., 6,* 750-757.

Bengtsson, S. L., Nagy, Z., Skare, S., Forsman, L., Forssberg, H., and Ullen, F. (2005). Extensive piano practicing has regionally specific effects on white matter development. *Nat.Neurosci., 8,* 1148-1150.

Bennett, M. R., Farnell, L., and Gibson, W. G. (2008). Origins of the BOLD changes due to synaptic activity at astrocytes abutting arteriolar smooth muscle. *J.Theor.Biol., 252,* 123-130.

Berridge, K. C. and Robinson, T. E. (1998). What is the role of dopamine in reward: hedonic impact, reward learning, or incentive salience? *Brain Res.Brain Res.Rev., 28,* 309-369.

Bertolino, A., Rubino, V., Sambataro, F., Blasi, G., Latorre, V., Fazio, L. et al. (2006). Prefrontal-hippocampal coupling during memory processing is modulated by COMT val158met genotype. *Biol.Psychiatry, 60,* 1250-1258.

Bhagat, Y. A. and Beaulieu, C. (2004). Diffusion anisotropy in subcortical white matter and cortical gray matter: changes with aging and the role of CSF-suppression. *J.Magn Reson.Imaging, 20,* 216-227.

Bilder, R. M., Volavka, J., Lachman, H. M., and Grace, A. A. (2004). The catechol-O-methyltransferase polymorphism: relations to the tonic-phasic dopamine hypothesis and neuropsychiatric phenotypes. *Neuropsychopharmacology, 29,* 1943-1961.

Biswal, B., Hudetz, A. G., Yetkin, F. Z., Haughton, V. M., and Hyde, J. S. (1997). Hypercapnia reversibly suppresses low-frequency fluctuations in the human motor cortex during rest using echo-planar MRI. *J.Cereb.Blood Flow Metab, 17,* 301-308.

Biswal, B., Yetkin, F. Z., Haughton, V. M., and Hyde, J. S. (1995). Functional connectivity in the motor cortex of resting human brain using echo-planar MRI. *Magn Reson.Med., 34,* 537-541.

Black, J. E., Zelazny, A. M., and Greenough, W. T. (1991). Capillary and mitochondrial support of neural plasticity in adult rat visual cortex. *Exp.Neurol., 111,* 204-209.

Blair, I. V., Lenton, A. P., and Hastie, R. (2002). The reliability of the DRM paradigm as a measure of individual differences in false memories. *Psychon.Bull.Rev., 9,* 590-596.

Bodammer, N., Kaufmann, J., Kanowski, M., and Tempelmann, C. (2004). Eddy current correction in diffusion-weighted imaging using pairs of images acquired with opposite diffusion gradient polarity. *Magn Reson.Med., 51,* 188-193.

Bonfield, J. K., Smith, K., and Staden, R. (1995). A new DNA sequence assembly program. *Nucleic Acids Res., 23,* 4992-4999.

Boorman, E. D., O'Shea, J., Sebastian, C., Rushworth, M. F., and Johansen-Berg, H. (2007). Individual differences in white-matter micro-structure reflect variation in functional connectivity during choice. *Curr.Biol., 17,* 1426-1431.

Braak, H., Braak, E., Yilmazer, D., and Bohl, J. (1996). Functional anatomy of human hippocampal formation and related structures. *J.Child Neurol., 11,* 265-275.

Brainerd, C. J. and Reyna, V. F. (2002b). Fuzzy-trace theory and false memory. *Curr.Dir.Psychol.Sci., 11,* 164-169.

Brainerd, C. J. and Reyna, V. F. (2002a). Recollection rejection: how children edit their false memories. Dev.Psychol., 38, 156-172.

Bressler, S. L. and Tognoli, E. (2006). Operational principles of neurocognitive networks. Int.J.Psychophysiol., 60, 139-148.

Breiter, H. C., Aharon, I., Kahneman, D., Dale, A., and Shizgal, P. (2001). Functional imaging of neural responses to expectancy and experience of monetary gains and losses. *Neuron, 30,* 619-639.

Brickman, A. M., Buchsbaum, M. S., Shihabuddin, L., Hazlett, E. A., Borod, J. C., and Mohs, R. C. (2003). Striatal size, glucose metabolic rate, and verbal learning in normal aging. *Brain Res.Cogn Brain Res., 17,* 106-116.

Brodmann, K. (1914) Physiologie des Gehirns. In: Neue Deutsche Chirurgie (Bruns P, ed), 85-426. Stuttgart: Enke.

Brodmann, K. (1909) Vergleichende Lokalisationslehre der Grosshirnrinde in Ihren Prinzipen Dargestellt auf Grund des Zellenbaues. Leipzig, Germany: Barth.

Brown, V. J. and Bowman, E. M. (1995). Discriminative cues indicating reward magnitude continue to determine reaction time of rats following lesions of the nucleus accumbens. *Eur.J.Neurosci., 7,* 2479-2485.

Buchsbaum, B., Pickell, B., Love, T., Hatrak, M., Bellugi, U., and Hickok, G. (2005). Neural substrates for verbal working memory in deaf signers: fMRI study and lesion case report. *Brain Lang, 95,* 265-272.

Buckner, R. L., Bandettini, P. A., O'Craven, K. M., Savoy, R. L., Petersen, S. E., Raichle, M. E. et al. (1996). Detection of cortical activation during averaged single trials of a cognitive task using functional magnetic resonance imaging. *Proc.Natl.Acad.Sci.U.S.A, 93,* 14878-14883.

Bugga, L., Gadient, R. A., Kwan, K., Stewart, C. L., and Patterson, P. H. (1998). Analysis of neuronal and glial phenotypes in brains of mice deficient in leukemia inhibitory factor. *J.Neurobiol., 36,* 509-524.

Bugiani, O., Salvarani, S., Perdelli, F., Mancardi, G. L., and Leonardi, A. (1978). Nerve cell loss with aging in the putamen. *Eur.Neurol., 17,* 286-291.

Bush, G., Luu, P., and Posner, M. I. (2000). Cognitive and emotional influences in anterior cingulate cortex. *Trends Cogn Sci., 4,* 215-222.

Buxton RB. Introduction to Functional Magnetic Resonance Imaging: Principles and Techniques, Cambridge University Press. 2002.

Buxton, R. B., Wong, E. C., and Frank, L. R. (1998). Dynamics of blood flow and oxygenation changes during brain activation: the balloon model. *Magn Reson.Med., 39,* 855-864.

Camara, E., Marco-Pallares, J., Münte, T.F., Rodriguez-Fornells, A. Neuroimaging analysis II: Magnetic Resonance Imaging.In Millsap, RE. and Maydeu-Olivares, A. Handbook of Quantitative Methods in Psychology. SAGE (in press).

Camara, E., Bodammer, N., Rodriguez-Fornells, A., and Tempelmann, C. (2007). Age-related water diffusion changes in human brain: a voxel-based approach. *Neuroimage., 34,* 1588-1599.

Casanova, R., Srikanth, R., Baer, A., Laurienti, P. J., Burdette, J. H., Hayasaka, S. et al. (2007). Biological parametric mapping: A statistical toolbox for multimodality brain image analysis. *Neuroimage., 34,* 137-143.

Catani, M., Jones, D. K., and ffytche, D. H. (2005). Perisylvian language networks of the human brain. *Ann.Neurol., 57,* 8-16.

Chen, J., Lipska, B. K., Halim, N., Ma, Q. D., Matsumoto, M., Melhem, S. et al. (2004). Functional analysis of genetic variation in catechol-O-methyltransferase (COMT): effects on mRNA, protein, and enzyme activity in postmortem human brain. *Am.J.Hum.Genet., 75,* 807-821.

Chen, J. C., Su, H. J., Huang, L. I., and Hsieh, M. M. (1999). Reductions in binding and functions of D2 dopamine receptors in the rat ventral striatum during amphetamine sensitization. *Life Sci., 64,* 343-354.

Chen, Z. G., Li, T. Q., and Hindmarsh, T. (2001). Diffusion tensor trace mapping in normal adult brain using single-shot EPI technique. A methodological study of the aging brain. *Acta Radiol., 42,* 447-458.

Chepuri, N. B., Yen, Y. F., Burdette, J. H., Li, H., Moody, D. M., and Maldjian, J. A. (2002). Diffusion anisotropy in the corpus callosum. *AJNR Am.J.Neuroradiol., 23,* 803-808.

Chun, T., Filippi, C. G., Zimmerman, R. D., and Ulug, A. M. (2000). Diffusion changes in the aging human brain. *AJNR Am.J.Neuroradiol., 21,* 1078-1083.

Ciccarelli, O., Behrens, T. E., Altmann, D. R., Orrell, R. W., Howard, R. S., Johansen-Berg, H. et al. (2006). Probabilistic diffusion tractography: a potential tool to assess the rate of disease progression in amyotrophic lateral sclerosis. *Brain, 129,* 1859-1871.

Cohen, M. X., Elger, C. E., and Weber, B. (2008). Amygdala tractography predicts functional connectivity and learning during feedback-guided decision-making. *Neuroimage., 39,* 1396-1407.

Cohen, M. X., Heller, A. S., and Ranganath, C. (2005). Functional connectivity with anterior cingulate and orbitofrontal cortices during decision-making. *Brain Res.Cogn Brain Res., 23,* 61-70.

Contreras, M., Ceric, F., and Torrealba, F. (2007). Inactivation of the interoceptive insula disrupts drug craving and malaise induced by lithium. *Science, 318,* 655-658.

Conturo, T. E., Lori, N. F., Cull, T. S., Akbudak, E., Snyder, A. Z., Shimony, J. S. et al. (1999). Tracking neuronal fiber pathways in the living human brain. *Proc.Natl.Acad.Sci.U.S.A, 96,* 10422-10427.

Corbetta, M., Kincade, J. M., Ollinger, J. M., McAvoy, M. P., and Shulman, G. L. (2000). Voluntary orienting is dissociated from target detection in human posterior parietal cortex. *Nat.Neurosci., 3,* 292-297.

Cowan, W. M., Gottlieb, D. I., Hendrickson, A. E., Price, J. L., and Woolsey, T. A. (1972). The autoradiographic demonstration of axonal connections in the central nervous system. *Brain Res., 37,* 21-51.

Craig, A. D. (2003). Interoception: the sense of the physiological condition of the body. *Curr.Opin.Neurobiol., 13,* 500-505.

Critchley, H. D., Mathias, C. J., Josephs, O., O'Doherty, J., Zanini, S., Dewar, B. K. et al. (2003). Human cingulate cortex and autonomic control: converging neuroimaging and clinical evidence. *Brain, 126,* 2139-2152.

Damasio, A. R., Grabowski, T. J., Bechara, A., Damasio, H., Ponto, L. L., Parvizi, J. et al. (2000). Subcortical and cortical brain activity during the feeling of self-generated emotions. *Nat.Neurosci., 3,* 1049-1056.

Daw, N. D., O'Doherty, J. P., Dayan, P., Seymour, B., and Dolan, R. J. (2006). Cortical substrates for exploratory decisions in humans. *Nature, 441,* 876-879.

Dehaene, S., Sergent, C., and Changeux, J. P. (2003). A neuronal network model linking subjective reports and objective physiological data during conscious perception. *Proc.Natl.Acad.Sci.U.S.A, 100,* 8520-8525.

Delgado, M. R., Locke, H. M., Stenger, V. A., and Fiez, J. A. (2003). Dorsal striatum responses to reward and punishment: effects of valence and magnitude manipulations. *Cogn Affect.Behav.Neurosci., 3,* 27-38.

Delgado, M. R., Nystrom, L. E., Fissell, C., Noll, D. C., and Fiez, J. A. (2000). Tracking the hemodynamic responses to reward and punishment in the striatum. *J.Neurophysiol., 84,* 3072-3077.

Demerens, C., Stankoff, B., Logak, M., Anglade, P., Allinquant, B., Couraud, F. et al. (1996). Induction of myelination in the central nervous system by electrical activity. *Proc.Natl.Acad.Sci U.S.A, 93,* 9887-9892.

Dennis, N. A., Kim, H., and Cabeza, R. (2008). Age-related Differences in Brain Activity during True and False Memory Retrieval. *J.Cogn Neurosci.*

Devinsky, O., Morrell, M. J., and Vogt, B. A. (1995). Contributions of anterior cingulate cortex to behaviour. *Brain, 118 (Pt 1),* 279-306.

Dorris, M. C. and Glimcher, P. W. (2004). Activity in posterior parietal cortex is correlated with the relative subjective desirability of action. *Neuron, 44,* 365-378.

Dougherty, R. F., Ben-Shachar, M., Bammer, R., Brewer, A. A., and Wandell, B. A. (2005). Functional organization of human occipital-callosal fiber tracts. *Proc.Natl.Acad.Sci.U.S.A, 102,* 7350-7355.

Draganski, B., Winkler, J., Flugel, D., and May, A. (2004). Selective activation of ectopic grey matter during motor task. *Neuroreport, 15,* 251-253.

Dreher, J. C. (2007). Sensitivity of the brain to loss aversion during risky gambles. *Trends Cogn Sci., 11,* 270-272.

Dyrby, T. B., Sogaard, L. V., Parker, G. J., Alexander, D. C., Lind, N. M., Baare, W. F. et al. (2007). Validation of in vitro probabilistic tractography. *Neuroimage., 37,* 1267-1277.

Egan, M. F., Goldberg, T. E., Kolachana, B. S., Callicott, J. H., Mazzanti, C. M., Straub, R. E. et al. (2001). Effect of COMT Val108/158 Met genotype on frontal lobe function and risk for schizophrenia. *Proc.Natl.Acad.Sci.U.S.A, 98,* 6917-6922.

Elliott, R., Newman, J. L., Longe, O. A., and Deakin, J. F. (2003). Differential response patterns in the striatum and orbitofrontal cortex to financial reward in humans: a parametric functional magnetic resonance imaging study. *J.Neurosci., 23,* 303-307.

Elliott, R., Sahakian, B. J., Michael, A., Paykel, E. S., and Dolan, R. J. (1998). Abnormal neural response to feedback on planning and guessing tasks in patients with unipolar depression. *Psychol.Med., 28,* 559-571.

Engelter, S. T., Provenzale, J. M., Petrella, J. R., DeLong, D. M., and MacFall, J. R. (2000). The effect of aging on the apparent diffusion coefficient of normal-appearing white matter. *AJR Am.J.Roentgenol., 175,* 425-430.

Ernst, M., Bolla, K., Mouratidis, M., Contoreggi, C., Matochik, J. A., Kurian, V. et al. (2002). Decision-making in a risk-taking task: a PET study. *Neuropsychopharmacology, 26,* 682-691.

Fan, J., Fossella, J., Sommer, T., Wu, Y., and Posner, M. I. (2003). Mapping the genetic variation of executive attention onto brain activity. *Proc.Natl.Acad.Sci.U.S.A, 100,* 7406-7411.

Fiebach, C. J. and Schubotz, R. I. (2006). Dynamic anticipatory processing of hierarchical sequential events: a common role for Broca's area and ventral premotor cortex across domains? *Cortex, 42,* 499-502.

Fields, R. D. (2005). Myelination: an overlooked mechanism of synaptic plasticity? *Neuroscientist., 11,* 528-531.

Fiorillo, C. D., Tobler, P. N., and Schultz, W. (2003). Discrete coding of reward probability and uncertainty by dopamine neurons. *Science, 299,* 1898-1902.

Fischl, B., Salat, D. H., Busa, E., Albert, M., Dieterich, M., Haselgrove, C. et al. (2002). Whole brain segmentation: automated labeling of neuroanatomical structures in the human brain. *Neuron, 33,* 341-355.

Fonteijn, H. M., Verstraten, F. A., and Norris, D. G. (2007). Probabilistic inference on Q-ball imaging data. *IEEE Trans.Med.Imaging, 26,* 1515-1524.

Frank, M. J., Moustafa, A. A., Haughey, H. M., Curran, T., and Hutchison, K. E. (2007). Genetic triple dissociation reveals multiple roles for dopamine in reinforcement learning. *Proc.Natl.Acad.Sci.U.S.A, 104,* 16311-16316.

Frank, M. J., Seeberger, L. C., and O'reilly, R. C. (2004). By carrot or by stick: cognitive reinforcement learning in parkinsonism. *Science, 306,* 1940-1943.

Friston, K. J., Buechel, C., Fink, G. R., Morris, J., Rolls, E., and Dolan, R. J. (1997). Psychophysiological and modulatory interactions in neuroimaging. *Neuroimage., 6,* 218-229.

Friston, K. J., Fletcher, P., Josephs, O., Holmes, A., Rugg, M. D., and Turner, R. (1998). Event-related fMRI: characterizing differential responses. *Neuroimage., 7,* 30-40.

Friston, K. J., Frith, C. D., Liddle, P. F., and Frackowiak, R. S. (1993). Functional connectivity: the principal-component analysis of large (PET) data sets. *J.Cereb.Blood Flow Metab, 13,* 5-14.

Friston, K. J., Harrison, L., and Penny, W. (2003). Dynamic causal modelling. *Neuroimage., 19,* 1273-1302.

Friston, K. J., Price, C. J., Fletcher, P., Moore, C., Frackowiak, R. S., and Dolan, R. J. (1996a). The trouble with cognitive subtraction. *Neuroimage., 4,* 97-104.

Friston, K. J., Williams, S., Howard, R., Frackowiak, R. S., and Turner, R. (1996b). Movement-related effects in fMRI time-series. *Magn Reson.Med., 35,* 346-355.

Gallo DA, Roediger HL. Variability among word list in eliciting memory ilusions: Evidence for associative activation and monitoring. Journal of Memory and Language, 47, 469-497.

Garavan, H., Pankiewicz, J., Bloom, A., Cho, J. K., Sperry, L., Ross, T. J. et al. (2000). Cue-induced cocaine craving: neuroanatomical specificity for drug users and drug stimuli. *Am.J.Psychiatry, 157,* 1789-1798.

Gaser, C. and Schlaug, G. (2003). Gray matter differences between musicians and nonmusicians. *Ann.N.Y.Acad.Sci., 999,* 514-517.

Gazzaley, A., Rissman, J., and Desposito, M. (2004). Functional connectivity during working memory maintenance. *Cogn Affect.Behav.Neurosci., 4,* 580-599.

Gehring, W. J. and Willoughby, A. R. (2002). The medial frontal cortex and the rapid processing of monetary gains and losses. *Science, 295,* 2279-2282.

Geijer, T., Jonsson, E., Neiman, J., Persson, M. L., Brene, S., Gyllander, A. et al. (1997). Tyrosine hydroxylase and dopamine D4 receptor allelic distribution in Scandinavian chronic alcoholics. *Alcohol Clin.Exp.Res., 21,* 35-39.

Gerrie, M. P. and Garry, M. (2007). Individual differences in working memory capacity affect false memories for missing aspects of events. *Memory., 15,* 561-571.

Gerstein, G. L. and Perkel, D. H. (1969). Simultaneously recorded trains of action potentials: analysis and functional interpretation. *Science, 164,* 828-830.

Gideon, P., Thomsen, C., and Henriksen, O. (1994). Increased self-diffusion of brain water in normal aging. *J.Magn Reson.Imaging, 4,* 185-188.

Glimcher, P. W. (2003). The neurobiology of visual-saccadic decision making. *Annu.Rev.Neurosci., 26,* 133-179.

Gold, B. T., Powell, D. K., Xuan, L., Jiang, Y., and Hardy, P. A. (2007). Speed of lexical decision correlates with diffusion anisotropy in left parietal and frontal white matter: evidence from diffusion tensor imaging. *Neuropsychologia, 45,* 2439-2446.

Golimbet, V. E., Alfimova, M. V., Gritsenko, I. K., and Ebstein, R. P. (2007). Relationship between dopamine system genes and extraversion and novelty seeking. *Neurosci.Behav.Physiol, 37,* 601-606.

Goncalves, M. S. and Hall, D. A. (2003). Connectivity analysis with structural equation modelling: an example of the effects of voxel selection. *Neuroimage., 20,* 1455-1467.

Good, C. D., Johnsrude, I. S., Ashburner, J., Henson, R. N., Friston, K. J., and Frackowiak, R. S. (2001). A voxel-based morphometric study of ageing in 465 normal adult human brains. *Neuroimage., 14,* 21-36.

Gottfried, J. A., O'Doherty, J., and Dolan, R. J. (2003). Encoding predictive reward value in human amygdala and orbitofrontal cortex. *Science, 301,* 1104-1107.

Grace, A. A. (1991). Phasic versus tonic dopamine release and the modulation of dopamine system responsivity: a hypothesis for the etiology of schizophrenia. *Neuroscience, 41,* 1-24.

Grace, A. A., Floresco, S. B., Goto, Y., and Lodge, D. J. (2007). Regulation of firing of dopaminergic neurons and control of goal-directed behaviors. *Trends Neurosci., 30,* 220-227.

Green, E. J., Greenough, W. T., and Schlumpf, B. E. (1983). Effects of complex or isolated environments on cortical dendrites of middle-aged rats. *Brain Res., 264,* 233-240.

Groenewegen, H. J., Wright, C. I., Beijer, A. V., and Voorn, P. (1999). Convergence and segregation of ventral striatal inputs and outputs. *Ann.N.Y.Acad.Sci., 877,* 49-63.

Grill-Spector, K., Sayres, R., and Ress, D. (2006). High-resolution imaging reveals highly selective nonface clusters in the fusiform face area. *Nat.Neurosci., 9,* 1177-1185.

Gulani, V., Webb, A. G., Duncan, I. D., and Lauterbur, P. C. (2001). Apparent diffusion tensor measurements in myelin-deficient rat spinal cords. *Magn Reson.Med., 45,* 191-195.

Guye, M., Parker, G. J., Symms, M., Boulby, P., Wheeler-Kingshott, C. A., Salek-Haddadi, A. et al. (2003). Combined functional MRI and tractography to demonstrate the connectivity of the human primary motor cortex in vivo. *Neuroimage., 19,* 1349-1360.

Hagmann, P., Kurant, M., Gigandet, X., Thiran, P., Wedeen, V. J., Meuli, R. et al. (2007). Mapping human whole-brain structural networks with diffusion MRI. *PLoS.ONE., 2,* e597.

Hamann, S. B., Ely, T. D., Grafton, S. T., and Kilts, C. D. (1999). Amygdala activity related to enhanced memory for pleasant and aversive stimuli. *Nat.Neurosci., 2,* 289-293.

Hampson, M., Peterson, B. S., Skudlarski, P., Gatenby, J. C., and Gore, J. C. (2002). Detection of functional connectivity using temporal correlations in MR images. *Hum.Brain Mapp., 15,* 247-262.

Hassani, O. K., Cromwell, H. C., and Schultz, W. (2001). Influence of expectation of different rewards on behavior-related neuronal activity in the striatum. *J.Neurophysiol., 85,* 2477-2489.

Haynes, J. D. and Rees, G. (2006). Decoding mental states from brain activity in humans. *Nat.Rev.Neurosci., 7,* 523-534.

He, B. and Lian, J. (2002). High-resolution spatio-temporal functional neuroimaging of brain activity. *Crit Rev.Biomed.Eng, 30,* 283-306.

Head, D., Buckner, R. L., Shimony, J. S., Williams, L. E., Akbudak, E., Conturo, T. E. et al. (2004). Differential vulnerability of anterior white matter in nondemented aging with minimal acceleration in dementia of the Alzheimer type: evidence from diffusion tensor imaging. *Cereb.Cortex, 14,* 410-423.

Heeger, D. J., Huk, A. C., Geisler, W. S., and Albrecht, D. G. (2000). Spikes versus BOLD: what does neuroimaging tell us about neuronal activity? *Nat.Neurosci., 3,* 631-633.

Hikosaka, K. and Watanabe, M. (2000). Delay activity of orbital and lateral prefrontal neurons of the monkey varying with different rewards. *Cereb.Cortex, 10,* 263-271.

Holroyd, C. B. and Coles, M. G. (2002). The neural basis of human error processing: reinforcement learning, dopamine, and the error-related negativity. *Psychol.Rev., 109,* 679-709.

Homae, F., Yahata, N., and Sakai, K. L. (2003). Selective enhancement of functional connectivity in the left prefrontal cortex during sentence processing. *Neuroimage., 20,* 578-586.

Horwitz, B. (2003). The elusive concept of brain connectivity. *Neuroimage., 19,* 466-470.

Horwitz, B. and Braun, A. R. (2004). Brain network interactions in auditory, visual and linguistic processing. *Brain Lang, 89,* 377-384.

Horwitz, B., Rumsey, J. M., and Donohue, B. C. (1998). Functional connectivity of the angular gyrus in normal reading and dyslexia. *Proc.Natl.Acad.Sci.U.S.A, 95,* 8939-8944.

Hsu, M., Bhatt, M., Adolphs, R., Tranel, D., and Camerer, C. F. (2005). Neural systems responding to degrees of uncertainty in human decision-making. *Science, 310,* 1680-1683.

Huettel, S.A., Song, A.W., and McCarthy, G. (2004). Functional Magnetic Resonance Imaging. Sunderland, Massachusetts: Sinauer Associates.

Innocenti, G. M. and Price, D. J. (2005). Exuberance in the development of cortical networks. *Nat.Rev.Neurosci., 6,* 955-965.

Ishibashi, T., Dakin, K. A., Stevens, B., Lee, P. R., Kozlov, S. V., Stewart, C. L. et al. (2006). Astrocytes promote myelination in response to electrical impulses. *Neuron, 49,* 823-832.

Jack, C. R., Jr., Theodore, W. H., Cook, M., and McCarthy, G. (1995). MRI-based hippocampal volumetrics: data acquisition, normal ranges, and optimal protocol. *Magn Reson.Imaging, 13,* 1057-1064.

Jiang, T., He, Y., Zang, Y., and Weng, X. (2004). Modulation of functional connectivity during the resting state and the motor task. *Hum.Brain Mapp., 22,* 63-71.

Johansen-Berg, H., Behrens, T. E., Robson, M. D., Drobnjak, I., Rushworth, M. F., Brady, J. M. et al. (2004). Changes in connectivity profiles define functionally distinct regions in human medial frontal cortex. *Proc.Natl.Acad.Sci.U.S.A, 101,* 13335-13340.

Jones, D. K., Lythgoe, D., Horsfield, M. A., Simmons, A., Williams, S. C., and Markus, H. S. (1999). Characterization of white matter damage in ischemic leukoaraiosis with diffusion tensor MRI. *Stroke, 30,* 393-397.

Jones, D. K., Symms, M. R., Cercignani, M., and Howard, R. J. (2005). The effect of filter size on VBM analyses of DT-MRI data. *Neuroimage., 26,* 546-554.

Juraska, J. M. and Kopcik, J. R. (1988). Sex and environmental influences on the size and ultrastructure of the rat corpus callosum. *Brain Res., 450,* 1-8.

Keizer, K., Kuypers, H. G., Huisman, A. M., and Dann, O. (1983). Diamidino yellow dihydrochloride (DY . 2HCl); a new fluorescent retrograde neuronal tracer, which migrates only very slowly out of the cell. *Exp.Brain Res., 51,* 179-191.

Kelley, A. E. and Berridge, K. C. (2002). The neuroscience of natural rewards: relevance to addictive drugs. *J.Neurosci., 22,* 3306-3311.

Kemper, T. L. (1994). Neuroanatomical and neuropathological changes during aging and dementia. In K.J.e.Albert ML (Ed.), *Clinical neurology of aging* (pp. 3-67). New York: Oxford.

Kereszturi, E., Kiraly, O., Barta, C., Molnar, N., Sasvari-Szekely, M., and Csapo, Z. (2006). No direct effect of the -521 C/T polymorphism in the human dopamine D4 receptor gene promoter on transcriptional activity. *BMC.Mol.Biol., 7,* 18.

Kim, D. S. and Kim, M. (2005). Combining functional and diffusion tensor MRI. *Ann.N.Y.Acad.Sci., 1064,* 1-15.

Kim, H. and Cabeza, R. (2007). Trusting our memories: dissociating the neural correlates of confidence in veridical versus illusory memories. *J.Neurosci, 27,* 12190-12197.

Kirsch, P., Schienle, A., Stark, R., Sammer, G., Blecker, C., Walter, B. et al. (2003). Anticipation of reward in a nonaversive differential conditioning paradigm and the brain reward system: an event-related fMRI study. *Neuroimage., 20,* 1086-1095.

Klein, T. A., Neumann, J., Reuter, M., Hennig, J., von Cramon, D. Y., and Ullsperger, M. (2007). Genetically determined differences in learning from errors. *Science, 318,* 1642-1645.

Knutson, B., Adams, C. M., Fong, G. W., and Hommer, D. (2001). Anticipation of increasing monetary reward selectively recruits nucleus accumbens. *J.Neurosci., 21,* RC159.

Knutson, B., Fong, G. W., Bennett, S. M., Adams, C. M., and Hommer, D. (2003). A region of mesial prefrontal cortex tracks monetarily rewarding outcomes: characterization with rapid event-related fMRI. *Neuroimage., 18,* 263-272.

Knutson, B. and Gibbs, S. E. (2007). Linking nucleus accumbens dopamine and blood oxygenation. *Psychopharmacology (Berl), 191,* 813-822.

Knutson, B., Momenan, R., Rawlings, R. R., Fong, G. W., and Hommer, D. (2001). Negative association of neuroticism with brain volume ratio in healthy humans. *Biol.Psychiatry, 50,* 685-690.

Knutson, B., Westdorp, A., Kaiser, E., and Hommer, D. (2000). FMRI visualization of brain activity during a monetary incentive delay task. *Neuroimage, 12,* 20-27.

Kotter, R. and Stephan, K. E. (2003). Network participation indices: characterizing component roles for information processing in neural networks. *Neural Netw., 16,* 1261-1275.

Kubicki, M., Westin, C. F., Maier, S. E., Mamata, H., Frumin, M., Ersner-Hershfield, H. et al. (2002). Diffusion tensor imaging and its application to neuropsychiatric disorders. *Harv.Rev.Psychiatry, 10,* 324-336.

Kuhnen, C. M. and Knutson, B. (2005). The neural basis of financial risk taking. *Neuron, 47,* 763-770.

Kwong, K. K., Belliveau, J. W., Chesler, D. A., Goldberg, I. E., Weisskoff, R. M., Poncelet, B. P. et al. (1992). Dynamic magnetic resonance imaging of human brain activity during primary sensory stimulation. *Proc.Natl.Acad.Sci.U.S.A, 89,* 5675-5679.

Lachman, H. M., Papolos, D. F., Saito, T., Yu, Y. M., Szumlanski, C. L., and Weinshilboum, R. M. (1996). Human catechol-O-methyltransferase

pharmacogenetics: description of a functional polymorphism and its potential application to neuropsychiatric disorders. *Pharmacogenetics, 6,* 243-250.

Latora, V. and Marchiori, M. (2001). Efficient behavior of small-world networks. *Phys.Rev.Lett., 87,* 198701.

LaVoie, D. J., Willoughby, L., and Faulkner, K. (2006). Frontal lobe dysfunction and false memory susceptibility in older adults. *Exp.Aging Res., 32,* 1-21.

Le Bihan, D. (2007). The 'wet mind': water and functional neuroimaging. *Phys.Med.Biol., 52,* R57-R90.

Le Bihan, D., Poupon, C., Amadon, A., and Lethimonnier, F. (2006a). Artifacts and pitfalls in diffusion MRI. *J.Magn Reson.Imaging, 24,* 478-488.

Le Bihan, D., Urayama, S., Aso, T., Hanakawa, T., and Fukuyama, H. (2006b). Direct and fast detection of neuronal activation in the human brain with diffusion MRI. *Proc.Natl.Acad.Sci.U.S.A, 103,* 8263-8268.

Le Bihan, D. (2003). Looking into the functional architecture of the brain with diffusion MRI. *Nat.Rev.Neurosci, 4,* 469-480.

Lerch, J. P., Worsley, K., Shaw, W. P., Greenstein, D. K., Lenroot, R. K., Giedd, J. et al. (2006). Mapping anatomical correlations across cerebral cortex (MACACC) using cortical thickness from MRI. *Neuroimage., 31,* 993-1003.

Logothetis, N. K. (2008). What we can do and what we cannot do with fMRI. *Nature, 453,* 869-878.

Logothetis, N. K. (2003). The underpinnings of the BOLD functional magnetic resonance imaging signal. *J.Neurosci., 23,* 3963-3971.

Logothetis, N. K., Pauls, J., Augath, M., Trinath, T., and Oeltermann, A. (2001). Neurophysiological investigation of the basis of the fMRI signal. *Nature, 412,* 150-157.

Lowe, M. J., Mock, B. J., and Sorenson, J. A. (1998). Functional connectivity in single and multislice echoplanar imaging using resting-state fluctuations. *Neuroimage., 7,* 119-132.

Lowe, M. J., Phillips, M. D., Lurito, J. T., Mattson, D., Dzemidzic, M., and Mathews, V. P. (2002). Multiple sclerosis: low-frequency temporal blood oxygen level-dependent fluctuations indicate reduced functional connectivity initial results. *Radiology, 224,* 184-192.

Luppino, G., Matelli, M., Camarda, R. M., Gallese, V., and Rizzolatti, G. (1991). Multiple representations of body movements in mesial area 6 and the adjacent cingulate cortex: an intracortical microstimulation study in the macaque monkey. *J.Comp Neurol., 311,* 463-482.

Lutcke, H., Merboldt, K. D., and Frahm, J. (2006). The cost of parallel imaging in functional MRI of the human brain. *Magn Reson.Imaging, 24,* 1-5.

Madden, D. J., Whiting, W. L., Huettel, S. A., White, L. E., MacFall, J. R., and Provenzale, J. M. (2004). Diffusion tensor imaging of adult age differences in cerebral white matter: relation to response time. *Neuroimage., 21,* 1174-1181.

Maguire, E. A., Woollett, K., and Spiers, H. J. (2006). London taxi drivers and bus drivers: a structural MRI and neuropsychological analysis. *Hippocampus, 16,* 1091-1101.

Makris, N., Kennedy, D. N., McInerney, S., Sorensen, A. G., Wang, R., Caviness, V. S., Jr. et al. (2005). Segmentation of subcomponents within the superior longitudinal fascicle in humans: a quantitative, in vivo, DT-MRI study. *Cereb.Cortex, 15,* 854-869.

Malonek, D., Dirnagl, U., Lindauer, U., Yamada, K., Kanno, I., and Grinvald, A. (1997). Vascular imprints of neuronal activity: relationships between the dynamics of cortical blood flow, oxygenation, and volume changes following sensory stimulation. Proc.Natl.Acad.Sci.U.S.A, 94, 14826-14831.

Marco-Pallares, J., Camara, E., Münte, T.F., Rodriguez-Fornells, A. Neuroimaging analysis I: Electroencephalography.In Millsap, RE. and Maydeu-Olivares, A. Handbook of Quantitative Methods in Psychology. SAGE (in press).

Marco-Pallares, J., Cucurell, D., Cunillera, T., Garcia, R., ndres-Pueyo, A., Munte, T. F. et al. (2008). Human oscillatory activity associated to reward processing in a gambling task. *Neuropsychologia, 46,* 241-248.

Marco-Pallares, J., Muller, S. V., and Munte, T. F. (2007). Learning by doing: an fMRI study of feedback-related brain activations. *Neuroreport, 18,* 1423-1426.

Markowitz, M. A., Gold, M., and Rice, T. (1991). Determinants of health insurance status among young adults. *Med.Care, 29,* 6-19.

Marner, L., Nyengaard, J. R., Tang, Y., and Pakkenberg, B. (2003). Marked loss of myelinated nerve fibers in the human brain with age. *J.Comp Neurol., 462,* 144-152.

Marota, J. J., Mandeville, J. B., Weisskoff, R. M., Moskowitz, M. A., Rosen, B. R., and Kosofsky, B. E. (2000). Cocaine activation discriminates dopaminergic projections by temporal response: an fMRI study in Rat. *Neuroimage., 11,* 13-23.

Matsumoto, M., Hidaka, K., Tada, S., Tasaki, Y., and Yamaguchi, T. (1996). Low levels of mRNA for dopamine D4 receptor in human cerebral cortex and striatum. *J.Neurochem., 66,* 915-919.

May, J. C., Delgado, M. R., Dahl, R. E., Stenger, V. A., Ryan, N. D., Fiez, J. A. et al. (2004). Event-related functional magnetic resonance imaging of reward-related brain circuitry in children and adolescents. *Biol.Psychiatry, 55,* 359-366.

McClure, S. M., York, M. K., and Montague, P. R. (2004). The neural substrates of reward processing in humans: the modern role of FMRI. *Neuroscientist., 10,* 260-268.

McDonald, A. J. (1998). Cortical pathways to the mammalian amygdala. *Prog.Neurobiol., 55,* 257-332.

McIntosh, A. R., Grady, C. L., Ungerleider, L. G., Haxby, J. V., Rapoport, S. I., and Horwitz, B. (1994). Network analysis of cortical visual pathways mapped with PET. *J.Neurosci., 14,* 655-666.

Meador-Woodruff, J. H., Damask, S. P., and Watson, S. J., Jr. (1994). Differential expression of autoreceptors in the ascending dopamine systems of the human brain. *Proc.Natl.Acad.Sci.U.S.A, 91,* 8297-8301.

Mechelli, A., Penny, W. D., Price, C. J., Gitelman, D. R., and Friston, K. J. (2002). Effective connectivity and intersubject variability: using a multisubject network to test differences and commonalities. *Neuroimage., 17,* 1459-1469.

Meier-Ruge, W., Ulrich, J., Bruhlmann, M., and Meier, E. (1992). Age-related white matter atrophy in the human brain. *Ann.N.Y.Acad.Sci., 673,* 260-269.

Mesulam, M. M. (1990). Large-scale neurocognitive networks and distributed processing for attention, language, and memory. *Ann.Neurol., 28,* 597-613.

Meyer-Lindenberg, A., Kohn, P. D., Kolachana, B., Kippenhan, S., Inerney-Leo, A., Nussbaum, R. et al. (2005). Midbrain dopamine and prefrontal function in humans: interaction and modulation by COMT genotype. *Nat.Neurosci., 8,* 594-596.

Middleton, F. A. and Strick, P. L. (2001). Cerebellar projections to the prefrontal cortex of the primate. *J.Neurosci., 21,* 700-712.

Mirenowicz, J. and Schultz, W. (1996). Preferential activation of midbrain dopamine neurons by appetitive rather than aversive stimuli. *Nature, 379,* 449-451.

Mitsuyasu, R., Gelman, R., Cherng, D. W., Landay, A., Fahey, J., Reichman, R. et al. (2007). The virologic, immunologic, and clinical effects of interleukin 2 with potent antiretroviral therapy in patients with moderately advanced human immunodeficiency virus infection: a randomized controlled clinical trial--AIDS Clinical Trials Group 328. *Arch.Intern.Med., 167,* 597-605.

Moore, C. J. and Price, C. J. (1999). A functional neuroimaging study of the variables that generate category-specific object processing differences. *Brain, 122 (Pt 5),* 943-962.

Mori, S. and van Zijl, P. C. (2002). Fiber tracking: principles and strategies - a technical review. *NMR Biomed., 15,* 468-480.

Morris, J. S., Scott, S. K., and Dolan, R. J. (1999). Saying it with feeling: neural responses to emotional vocalizations. *Neuropsychologia, 37,* 1155-1163.

Moseley, M. (2002). Diffusion tensor imaging and aging - a review. *NMR Biomed., 15,* 553-560.

Moseley, M. E., Cohen, Y., Kucharczyk, J., Mintorovitch, J., Asgari, H. S., Wendland, M. F. et al. (1990). Diffusion-weighted MR imaging of anisotropic water diffusion in cat central nervous system. *Radiology, 176,* 439-445.

Moscovitch, M., 1999. False recall and false recognition: anexamination of the effects of selective and combined lesions to the medial temporal lobe/diencephalon and frontal lobe structures. Cogn. Neuropsychol. 16, 343-359.

Mrzljak, L., Bergson, C., Pappy, M., Huff, R., Levenson, R., and Goldman-Rakic, P. S. (1996). Localization of dopamine D4 receptors in GABAergic neurons of the primate brain. *Nature, 381,* 245-248.

Mukamel, R., Gelbard, H., Arieli, A., Hasson, U., Fried, I., and Malach, R. (2005). Coupling between neuronal firing, field potentials, and FMRI in human auditory cortex. *Science, 309,* 951-954.

Muller, S. V., Moller, J., Rodriguez-Fornells, A., and Munte, T. F. (2005). Brain potentials related to self-generated and external information used for performance monitoring. *Clinical Neurophysiology, 116,* 63-74.

Nieuwenhuis, S., Slagter, H. A., von Geusau, N. J. A., Heslenfeld, D. J., and Holroyd, C. B. (2005). Knowing good from bad: differential activation of human cortical areas by positive and negative outcomes. *European Journal of Neuroscience, 21,* 3161-3168.

Norman, K. A. and Schacter, D. L. (1997). False recognition in younger and older adults: exploring the characteristics of illusory memories. *Mem.Cognit., 25,* 838-848.

Nusbaum, A. O., Tang, C. Y., Buchsbaum, M. S., Wei, T. C., and Atlas, S. W. (2001a). Regional and global changes in cerebral diffusion with normal aging. *AJNR Am.J.Neuroradiol., 22,* 136-142.

Nusbaum, A. O., Tang, C. Y., Buchsbaum, M. S., Wei, T. C., and Atlas, S. W. (2001b). Regional and global changes in cerebral diffusion with normal aging. *AJNR Am.J.Neuroradiol., 22,* 136-142.

Nusbaum, A. O., Tang, C. Y., Buchsbaum, M. S., Wei, T. C., and Atlas, S. W. (2001c). Regional and global changes in cerebral diffusion with normal aging. *AJNR Am.J.Neuroradiol., 22,* 136-142.

O'Doherty, J., Kringelbach, M. L., Rolls, E. T., Hornak, J., and Andrews, C. (2001). Abstract reward and punishment representations in the human orbitofrontal cortex. *Nat.Neurosci., 4,* 95-102.

O'Doherty, J. P., Deichmann, R., Critchley, H. D., and Dolan, R. J. (2002). Neural responses during anticipation of a primary taste reward. *Neuron, 33,* 815-826.

O'Sullivan, M., Jones, D. K., Summers, P. E., Morris, R. G., Williams, S. C., and Markus, H. S. (2001). Evidence for cortical "disconnection" as a mechanism of age-related cognitive decline. *Neurology, 57,* 632-638.

Ogawa, S., Lee, T. M., Nayak, A. S., and Glynn, P. (1990). Oxygenation-sensitive contrast in magnetic resonance image of rodent brain at high magnetic fields. *Magn Reson.Med., 14,* 68-78.

Okuyama, Y., Ishiguro, H., Nankai, M., Shibuya, H., Watanabe, A., and Arinami, T. (2000). Identification of a polymorphism in the promoter region of DRD4 associated with the human novelty seeking personality trait. *Mol.Psychiatry, 5,* 64-69.

Okuyama, Y., Ishiguro, H., Toru, M., and Arinami, T. (1999). A genetic polymorphism in the promoter region of DRD4 associated with expression and schizophrenia. *Biochem.Biophys.Res.Commun., 258,* 292-295.

Pajevic, S. and Pierpaoli, C. (1999). Color schemes to represent the orientation of anisotropic tissues from diffusion tensor data: application to white matter fiber tract mapping in the human brain. *Magn Reson.Med., 42,* 526-540.

Papadakis, N. G., Xing, D., Huang, C. L., Hall, L. D., and Carpenter, T. A. (1999). A comparative study of acquisition schemes for diffusion tensor imaging using MRI. *J.Magn Reson., 137,* 67-82.

Parker, G. J., Haroon, H. A., and Wheeler-Kingshott, C. A. (2003). A framework for a streamline-based probabilistic index of connectivity (PICo) using a structural interpretation of MRI diffusion measurements. *J.Magn Reson.Imaging, 18,* 242-254.

Parkin, A. J., Bindschaedler, C., Harsent, L., and Metzler, C. (1996). Pathological false alarm rates following damage to the left frontal cortex. *Brain Cogn, 32,* 14-27.

Passingham, R. E., Stephan, K. E., and Kotter, R. (2002). The anatomical basis of functional localization in the cortex. *Nat.Rev.Neurosci., 3,* 606-616.

Paulus, M. P., Rogalsky, C., Simmons, A., Feinstein, J. S., and Stein, M. B. (2003). Increased activation in the right insula during risk-taking decision making is related to harm avoidance and neuroticism. *Neuroimage., 19,* 1439-1448.

Paus, T. (2000). Functional anatomy of arousal and attention systems in the human brain. *Prog.Brain Res., 126,* 65-77.

Payne, J. D., Jackson, E. D., Ryan, L., Hoscheidt, S., Jacobs, J. W., and Nadel, L. (2006). The impact of stress on neutral and emotional aspects of episodic memory. *Memory., 14,* 1-16.

Paz-Alonso, P. M., Ghetti, S., Donohue, S. E., Goodman, G. S., and Bunge, S. A. (2008). Neurodevelopmental Correlates of True and False Recognition. *Cereb.Cortex.*

Phan, K. L., Wager, T. D., Taylor, S. F., and Liberzon, I. (2004). Functional neuroimaging studies of human emotions. *CNS.Spectr., 9,* 258-266.

Phelps, E. A. and LeDoux, J. E. (2005). Contributions of the amygdala to emotion processing: from animal models to human behavior. *Neuron, 48,* 175-187.

Phillips, M. L., Young, A. W., Scott, S. K., Calder, A. J., Andrew, C., Giampietro, V. et al. (1998). Neural responses to facial and vocal expressions of fear and disgust. *Proc.Biol.Sci., 265,* 1809-1817.

Pierpaoli, C. and Basser, P. J. (1996). Toward a quantitative assessment of diffusion anisotropy. *Magn Reson.Med., 36,* 893-906.

Platt, M. L. and Glimcher, P. W. (1999). Neural correlates of decision variables in parietal cortex. *Nature, 400,* 233-238.

Poldrack, R. A. and Gabrieli, J. D. (2001). Characterizing the neural mechanisms of skill learning and repetition priming: evidence from mirror reading. *Brain, 124,* 67-82.

Poldrack, R. A. (2000). Imaging brain plasticity: conceptual and methodological issues--a theoretical review. *Neuroimage., 12,* 1-13.

Polyn, S. M., Natu, V. S., Cohen, J. D., and Norman, K. A. (2005). Category-specific cortical activity precedes retrieval during memory search. *Science, 310,* 1963-1966.

Poupon, C., Clark, C. A., Frouin, V., Regis, J., Bloch, I., Le, B. D. et al. (2000). Regularization of diffusion-based direction maps for the tracking of brain white matter fascicles. *Neuroimage., 12,* 184-195.

Powell, H. W., Parker, G. J., Alexander, D. C., Symms, M. R., Boulby, P. A., Wheeler-Kingshott, C. A. et al. (2006). Hemispheric asymmetries in language-related pathways: a combined functional MRI and tractography study. *Neuroimage., 32,* 388-399.

Preuschoff, K. and Bossaerts, P. (2007). Adding prediction risk to the theory of reward learning. *Ann.N.Y.Acad.Sci., 1104,* 135-146.

Preuschoff, K., Quartz, S. R., and Bossaerts, P. (2008). Human insula activation reflects risk prediction errors as well as risk. *J.Neurosci., 28,* 2745-2752.

Price, C. J., Crinion, J., and Friston, K. J. (2006). Design and analysis of fMRI studies with neurologically impaired patients. *J.Magn Reson.Imaging, 23,* 816-826.

Putnam, M. C., Wig, G. S., Grafton, S. T., Kelley, W. M., and Gazzaniga, M. S. (2008). Structural organization of the corpus callosum predicts the extent and impact of cortical activity in the nondominant hemisphere. *J.Neurosci, 28,* 2912-2918.

Ramnani, N., Elliott, R., Athwal, B. S., and Passingham, R. E. (2004). Prediction error for free monetary reward in the human prefrontal cortex. *Neuroimage., 23,* 777-786.

Ranganath, C., Heller, A., Cohen, M. X., Brozinsky, C. J., and Rissman, J. (2005). Functional connectivity with the hippocampus during successful memory formation. *Hippocampus, 15,* 997-1005.

Raz, N., Rodrigue, K. M., Kennedy, K. M., and Acker, J. D. (2004). Hormone replacement therapy and age-related brain shrinkage: regional effects. *Neuroreport, 15,* 2531-2534.

Rees, G., Friston, K., and Koch, C. (2000). A direct quantitative relationship between the functional properties of human and macaque V5. *Nat.Neurosci., 3,* 716-723.

Resnick, S. M., Pham, D. L., Kraut, M. A., Zonderman, A. B., and Davatzikos, C. (2003b). Longitudinal magnetic resonance imaging studies of older adults: a shrinking brain. *J.Neurosci., 23,* 3295-3301.

Resnick, S. M., Pham, D. L., Kraut, M. A., Zonderman, A. B., and Davatzikos, C. (2003a). Longitudinal magnetic resonance imaging studies of older adults: a shrinking brain. *J.Neurosci., 23,* 3295-3301.

Reynolds, S. M. and Zahm, D. S. (2005). Specificity in the projections of prefrontal and insular cortex to ventral striatopallidum and the extended amygdala. *J.Neurosci., 25,* 11757-11767.

Riba J., Krämer U.M., Heldmann M., Richter S., Münte T.F. (2008) Dopamine Agonist Increases Risk Taking but Blunts Reward-Related Brain Activity. PLoS ONE 3:6: e2479.

Rissman, J., Gazzaley, A., and D'Esposito, M. (2004). Measuring functional connectivity during distinct stages of a cognitive task. *Neuroimage., 23,* 752-763.

Roediger, H. L. and McDermott, K. B. (1995). Creating false memories: remembering words not presented in lists. *J.Exp.Psychol.Learn.Mem.Cogn., 21,* 803-814.

Roediger, H. L., III, Watson, J. M., McDermott, K. B., and Gallo, D. A. (2001). Factors that determine false recall: a multiple regression analysis. *Psychon.Bull.Rev., 8,* 385-407.

Rogers, B. P., Carew, J. D., and Meyerand, M. E. (2004). Hemispheric asymmetry in supplementary motor area connectivity during unilateral finger movements. *Neuroimage., 22,* 855-859.

Rogers, B. P., Morgan, V. L., Newton, A. T., and Gore, J. C. (2007). Assessing functional connectivity in the human brain by fMRI. *Magn Reson.Imaging*.

Rolls, E. T. (2000). The orbitofrontal cortex and reward. *Cereb.Cortex, 10,* 284-294.

Rolls, E. T. (1996). The orbitofrontal cortex. *Philos.Trans.R.Soc.Lond B Biol.Sci., 351,* 1433-1443.

Ronai, Z., Szekely, A., Nemoda, Z., Lakatos, K., Gervai, J., Staub, M. et al. (2001). Association between Novelty Seeking and the -521 C/T polymorphism in the promoter region of the DRD4 gene. *Mol.Psychiatry, 6,* 35-38.

Rossi, D. J. (2006). Another BOLD role for astrocytes: coupling blood flow to neural activity. *Nat.Neurosci., 9,* 159-161.

Rubinstein, M., Phillips, T. J., Bunzow, J. R., Falzone, T. L., Dziewczapolski, G., Zhang, G. et al. (1997). Mice lacking dopamine D4 receptors are supersensitive to ethanol, cocaine, and methamphetamine. *Cell, 90,* 991-1001.

Rykhlevskaia, E., Gratton, G., and Fabiani, M. (2008). Combining structural and functional neuroimaging data for studying brain connectivity: a review. *Psychophysiology, 45,* 173-187.

Salat, D. H., Buckner, R. L., Snyder, A. Z., Greve, D. N., Desikan, R. S., Busa, E. et al. (2004). Thinning of the cerebral cortex in aging. *Cereb.Cortex, 14,* 721-730.

Salat, D. H., Tuch, D. S., Greve, D. N., van der Kouwe, A. J., Hevelone, N. D., Zaleta, A. K. et al. (2005). Age-related alterations in white matter micro-structure measured by diffusion tensor imaging. *Neurobiol.Aging, 26,* 1215-1227.

Salin, P. A. and Bullier, J. (1995). Corticocortical connections in the visual system: structure and function. *Physiol Rev., 75,* 107-154.

Salinas, J. A. and White, N. M. (1998). Contributions of the hippocampus, amygdala, and dorsal striatum to the response elicited by reward reduction. *Behav.Neurosci., 112,* 812-826.

Salvador, R., Suckling, J., Coleman, M. R., Pickard, J. D., Menon, D., and Bullmore, E. (2005). Neurophysiological architecture of functional magnetic resonance images of human brain. *Cereb.Cortex, 15,* 1332-1342.

Sanyal, S. and Van Tol, H. H. (1997). Review the role of dopamine D4 receptors in schizophrenia and antipsychotic action. *J.Psychiatr.Res., 31,* 219-232.

Sauvage, M. M., Fortin, N. J., Owens, C. B., Yonelinas, A. P., and Eichenbaum, H. (2008). Recognition memory: opposite effects of hippocampal damage on recollection and familiarity. *Nat.Neurosci, 11,* 16-18.

Schacter, D. L., Curran, T., Galluccio, L., Milberg, W. P., and Bates, J. F. (1996). False recognition and the right frontal lobe: a case study. *Neuropsychologia, 34,* 793-808.

Schacter, D. L., Reiman, E., Curran, T., Yun, L. S., Bandy, D., McDermott, K. B. et al. (1996a). Neuroanatomical correlates of veridical and illusory recognition memory: evidence from positron emission tomography. *Neuron, 17,* 267-274.

Schacter, D. L., Verfaellie, M., and Pradere, D. (1996b). The neuropsychology of memory illusions: false recall and recognition in amnesic patients. J.Mem.Lang., 35, 319-344.

Schacter, D. L., Verfaellie, M., and Anes, M. D. (1997). Illusory memories in amnesic patients: conceptual and perceptual false recognition. *Neuropsychology., 11,* 331-342.

Schacter, D. L., Verfaellie, M., Anes, M. D., and Racine, C. (1998). When true recognition suppresses false recognition: evidence from amnesic patients. *J.Cogn Neurosci., 10,* 668-679.

Schinka, J. A., Letsch, E. A., and Crawford, F. C. (2002). DRD4 and novelty seeking: results of meta-analyses. *Am.J.Med.Genet., 114,* 643-648.

Schmahmann, J. D., Pandya, D. N., Wang, R., Dai, G., D'Arceuil, H. E., de Crespigny, A. J. et al. (2007). Association fibre pathways of the brain: parallel observations from diffusion spectrum imaging and autoradiography. *Brain, 130,* 630-653.

Schonberg, T., Pianka, P., Hendler, T., Pasternak, O., and Assaf, Y. (2006). Characterization of displaced white matter by brain tumors using combined DTI and fMRI. *Neuroimage., 30,* 1100-1111.

Schott, B. H., Richardson-Klavehn, A., Henson, R. N., Becker, C., Heinze, H. J., and Duzel, E. (2006). Neuroanatomical dissociation of encoding processes related to priming and explicit memory. *J.Neurosci., 26,* 792-800.

Schott, B. H., Sellner, D. B., Lauer, C. J., Habib, R., Frey, J. U., Guderian, S. et al. (2004). Activation of midbrain structures by associative novelty and the formation of explicit memory in humans. *Learn.Mem., 11,* 383-387.

Schultz, W. (2002). Getting formal with dopamine and reward. *Neuron, 36,* 241-263.

Schultz, W. (2007). Behavioral dopamine signals. *Trends Neurosci., 30,* 203-210.

Schultz, W. (1998). Predictive reward signal of dopamine neurons. *J.Neurophysiol., 80,* 1-27.

Schultz, W., Dayan, P., and Montague, P. R. (1997). A neural substrate of prediction and reward. *Science, 275,* 1593-1599.

Seeman, P. and Van Tol, H. H. (1994). Dopamine receptor pharmacology. *Trends Pharmacol.Sci., 15,* 264-270.

Seger, C. A. and Cincotta, C. M. (2005). The roles of the caudate nucleus in human classification learning. *J.Neurosci., 25,* 2941-2951.

Sell, L. A., Morris, J. S., Bearn, J., Frackowiak, R. S., Friston, K. J., and Dolan, R. J. (2000). Neural responses associated with cue evoked emotional states and heroin in opiate addicts. *Drug Alcohol Depend., 60,* 207-216.

Shmuel, A., Augath, M., Oeltermann, A., and Logothetis, N. K. (2006). Negative functional MRI response correlates with decreases in neuronal activity in monkey visual area V1. *Nat.Neurosci., 9,* 569-577.

Sirevaag, A. M. and Greenough, W. T. (1991). Plasticity of GFAP-immunoreactive astrocyte size and number in visual cortex of rats reared in complex environments. *Brain Res., 540,* 273-278.

Skare, S., Hedehus, M., Moseley, M. E., and Li, T. Q. (2000). Condition number as a measure of noise performance of diffusion tensor data acquisition schemes with MRI. *J.Magn Reson., 147,* 340-352.

Slotnick, S. D. and Schacter, D. L. (2004). A sensory signature that distinguishes true from false memories. *Nat.Neurosci., 7,* 664-672.

Smith, S. M., Jenkinson, M., Johansen-Berg, H., Rueckert, D., Nichols, T. E., Mackay, C. E. et al. (2006). Tract-based spatial statistics: voxelwise analysis of multi-subject diffusion data. *Neuroimage., 31,* 1487-1505.

Spiegel, D. (1997). Trauma, dissociation, and memory. *Ann.N.Y.Acad.Sci., 821,* 225-237.

Spiegel, I., Adamsky, K., Eisenbach, M., Eshed, Y., Spiegel, A., Mirsky, R. et al. (2006). Identification of novel cell-adhesion molecules in peripheral nerves using a signal-sequence trap. *Neuron Glia Biol., 2,* 27-38.

Sporns, O., Tononi, G., and Edelman, G. M. (2000). Theoretical neuroanatomy: relating anatomical and functional connectivity in graphs and cortical connection matrices. *Cereb.Cortex, 10,* 127-141.

Staempfli, P., Reischauer, C., Jaermann, T., Valavanis, A., Kollias, S., and Boesiger, P. (2008). Combining fMRI and DTI: a framework for exploring the limits of fMRI-guided DTI fiber tracking and for verifying DTI-based fiber tractography results. *Neuroimage., 39,* 119-126.

Stanberry, L., Nandy, R., and Cordes, D. (2003). Cluster analysis of fMRI data using dendrogram sharpening. *Hum.Brain Mapp., 20,* 201-219.

Stein, T., Moritz, C., Quigley, M., Cordes, D., Haughton, V., and Meyerand, E. (2000). Functional connectivity in the thalamus and hippocampus studied with functional MR imaging. *AJNR Am.J.Neuroradiol., 21,* 1397-1401.

Stevens, B., Porta, S., Haak, L. L., Gallo, V., and Fields, R. D. (2002). Adenosine: a neuron-glial transmitter promoting myelination in the CNS in response to action potentials. *Neuron, 36,* 855-868.

Stejskal EO, Tanner JE. Spin diffusion measurements: spin echoes in the presence of time-dependent field gradient. Journal of Chemical Physics 1965;42(1):288-292.

Strange, P. G. (1993). New insights into dopamine receptors in the central nervous system. *Neurochem.Int., 22,* 223-236.

Sugrue, L. P., Corrado, G. S., and Newsome, W. T. (2004). Matching behavior and the representation of value in the parietal cortex. *Science, 304,* 1782-1787.

Sullivan, E. V. and Pfefferbaum, A. (2003). Diffusion tensor imaging in normal aging and neuropsychiatric disorders. *Eur.J.Radiol., 45,* 244-255.

Sun, F. T., Miller, L. M., and D'Esposito, M. (2004). Measuring interregional functional connectivity using coherence and partial coherence analyses of fMRI data. *Neuroimage., 21,* 647-658.

Sutton R, Barto A (1998). Reinforcement Learning: An Introduction. MIT Press.

Takano, T., Tian, G. F., Peng, W., Lou, N., Libionka, W., Han, X. et al. (2006). Astrocyte-mediated control of cerebral blood flow. *Nat.Neurosci., 9,* 260-267.

Thakkar, K. N., Polli, F. E., Joseph, R. M., Tuch, D. S., Hadjikhani, N., Barton, J. J. et al. (2008). Response monitoring, repetitive behaviour and anterior cingulate abnormalities in ASD. *Brain*.

Talairach, J. and Tournoux, P. (1988). *Co-Planar Sterotaxic Atlas of the Human Brain: An Approach to Medical Cerebral Imaging*. New York: Thieme Medical Publishers.

Thulborn, K. R., Waterton, J. C., Matthews, P. M., and Radda, G. K. (1982). Oxygenation dependence of the transverse relaxation time of water protons in whole blood at high field. *Biochim.Biophys.Acta, 714,* 265-270.

Tom, S. M., Fox, C. R., Trepel, C., and Poldrack, R. A. (2007). The neural basis of loss aversion in decision-making under risk. *Science, 315,* 515-518.

Toosy, A. T., Ciccarelli, O., Parker, G. J., Wheeler-Kingshott, C. A., Miller, D. H., and Thompson, A. J. (2004). Characterizing function-structure relationships in the human visual system with functional MRI and diffusion tensor imaging. *Neuroimage., 21,* 1452-1463.

Tovar-Moll, F., Moll, J., de Oliveira-Souza, R., Bramati, I., Andreiuolo, P. A., and Lent, R. (2007). Neuroplasticity in human callosal dysgenesis: a diffusion tensor imaging study. *Cereb.Cortex, 17,* 531-541.

Tuch, D. S., Salat, D. H., Wisco, J. J., Zaleta, A. K., Hevelone, N. D., and Rosas, H. D. (2005a). Choice reaction time performance correlates with diffusion anisotropy in white matter pathways supporting visuospatial attention. *Proc.Natl.Acad.Sci U.S.A, 102,* 12212-12217.

Tuch, D. S., Wisco, J. J., Khachaturian, M. H., Ekstrom, L. B., Kotter, R., and Vanduffel, W. (2005b). Q-ball imaging of macaque white matter architecture. *Philos.Trans.R.Soc.Lond B Biol.Sci., 360,* 869-879.

Tulving, E. (1985). Memory and consciousness. Canadian Psychologist, 26, 1-12.

Turner, R., Le, B. D., Moonen, C. T., Despres, D., and Frank, J. (1991). Echo-planar time course MRI of cat brain oxygenation changes. *Magn Reson.Med., 22,* 159-166.

Ungerleider, L. G., Gaffan, D., and Pelak, V. S. (1989). Projections from inferior temporal cortex to prefrontal cortex via the uncinate fascicle in rhesus monkeys. *Exp.Brain Res., 76,* 473-484.

Uylings, H. B. and de Brabander, J. M. (2002). Neuronal changes in normal human aging and Alzheimer's disease. *Brain Cogn, 49,* 268-276.

Van Veen, V., Holroyd, C. B., Cohen, J. D., Stenger, V. A., and Carter, C. S. (2004). Errors without conflict: Implications for performance monitoring theories of anterior cingulate cortex. *Brain and Cognition, 56,* 267-276.

Verfaellie, M., Rapcsak, S. Z., Keane, M. M., and Alexander, M. P. (2004). Elevated false recognition in patients with frontal lobe damage is neither a general nor a unitary phenomenon. *Neuropsychology., 18,* 94-103.

Virta, A., Barnett, A., and Pierpaoli, C. (1999). Visualizing and characterizing white matter fiber structure and architecture in the human pyramidal tract using diffusion tensor MRI. *Magn Reson.Imaging, 17,* 1121-1133.

Vogt, O. Vogt, C. 1919 Ergebnisse unserer Hirnforshung (Results of our neuroscience). J. Psychologicol. Neurol. 25, 277-462.

Volkow, N. D., Fowler, J. S., Wang, G. J., Swanson, J. M., and Telang, F. (2007). Dopamine in drug abuse and addiction: results of imaging studies and treatment implications. *Arch.Neurol., 64,* 1575-1579.

Volkow, N. D., Wang, G. J., Fowler, J. S., Hitzemann, R., Angrist, B., Gatley, S. J. et al. (1999). Association of methylphenidate-induced craving with changes in right striato-orbitofrontal metabolism in cocaine abusers: implications in addiction. *Am.J.Psychiatry, 156,* 19-26.

Volterra, A. and Meldolesi, J. (2005). Astrocytes, from brain glue to communication elements: the revolution continues. *Nat.Rev.Neurosci., 6,* 626-640.

Voorn, P., Jorritsma-Byham, B., Van, D. C., and Buijs, R. M. (1986). The dopaminergic innervation of the ventral striatum in the rat: a light- and electron-microscopical study with antibodies against dopamine. *J.Comp Neurol., 251,* 84-99.

Wakana, S., Jiang, H., Nagae-Poetscher, L. M., van Zijl, P. C., and Mori, S. (2004c). Fiber tract-based atlas of human white matter anatomy. *Radiology, 230,* 77-87.

Walters, N. B., Egan, G. F., Kril, J. J., Kean, M., Waley, P., Jenkinson, M. et al. (2003). In vivo identification of human cortical areas using high-resolution MRI: an approach to cerebral structure-function correlation. *Proc.Natl.Acad.Sci.U.S.A, 100,* 2981-2986.

Walton, M. E., Bannerman, D. M., Alterescu, K., and Rushworth, M. F. (2003). Functional specialization within medial frontal cortex of the anterior cingulate for evaluating effort-related decisions. *J.Neurosci., 23,* 6475-6479.

Wang, G. J., Volkow, N. D., Fowler, J. S., Cervany, P., Hitzemann, R. J., Pappas, N. R. et al. (1999). Regional brain metabolic activation during craving elicited by recall of previous drug experiences. *Life Sci., 64,* 775-784.

Watson, J. M., Bunting, M. F., Poole, B. J., and Conway, A. R. (2005). Individual differences in susceptibility to false memory in the Deese-Roediger-McDermott paradigm. *J.Exp.Psychol.Learn.Mem.Cogn, 31,* 76-85.

Waxman, S. G. and Bennett, M. V. (1972). Relative conduction velocities of small myelinated and non-myelinated fibres in the central nervous system. *Nat.New Biol., 238,* 217-219.

Welchew, D. E., Honey, G. D., Sharma, T., Robbins, T. W., and Bullmore, E. T. (2002). Multidimensional scaling of integrated neurocognitive function and schizophrenia as a disconnexion disorder. *Neuroimage., 17,* 1227-1239.

Werring, D. J., Clark, C. A., Barker, G. J., Miller, D. H., Parker, G. J., Brammer, M. J. et al. (1998). The structural and functional mechanisms of motor recovery: complementary use of diffusion tensor and functional magnetic resonance

imaging in a traumatic injury of the internal capsule. *J.Neurol.Neurosurg.Psychiatry, 65,* 863-869.

Werring, D. J., Clark, C. A., Parker, G. J., Miller, D. H., Thompson, A. J., and Barker, G. J. (1999). A direct demonstration of both structure and function in the visual system: combining diffusion tensor imaging with functional magnetic resonance imaging. *Neuroimage., 9,* 352-361.

Westlye, L. T., Walhovd, K. B., Bjornerud, A., Due-Tonnessen, P., and Fjell, A. M. (2008). Error-Related Negativity is Mediated by Fractional Anisotropy in the Posterior Cingulate Gyrus--A Study Combining Diffusion Tensor Imaging and Electrophysiology in Healthy Adults. *Cereb.Cortex.*

Wise, R. A. (2002). Brain reward circuitry: insights from unsensed incentives. *Neuron, 36,* 229-240.

Wittmann, B. C., Schiltz, K., Boehler, C. N., and Duzel, E. (2008). Mesolimbic interaction of emotional valence and reward improves memory formation. *Neuropsychologia, 46,* 1000-1008.

Wittmann, B. C., Schott, B. H., Guderian, S., Frey, J. U., Heinze, H. J., and Duzel, E. (2005). Reward-related FMRI activation of dopaminergic midbrain is associated with enhanced hippocampus-dependent long-term memory formation. *Neuron, 45,* 459-467.

Woods, R. P., Grafton, S. T., Holmes, C. J., Cherry, S. R., and Mazziotta, J. C. (1998). Automated image registration: I. General methods and intrasubject, intramodality validation. *J.Comput.Assist.Tomogr., 22,* 139-152.

Worsley, K. J., Chen, J. I., Lerch, J., and Evans, A. C. (2005). Comparing functional connectivity via thresholding correlations and singular value decomposition. *Philos.Trans.R.Soc.Lond B Biol.Sci., 360,* 913-920.

Worsley, K. J. and Friston, K. J. (1995). Analysis of fMRI time-series revisited--again. *Neuroimage., 2,* 173-181.

Worsley, K. J., Poline, J. B., Vandal, A. C., and Friston, K. J. (1995). Tests for distributed, nonfocal brain activations. *Neuroimage., 2,* 183-194.

Wrase, J., Kahnt, T., Schlagenhauf, F., Beck, A., Cohen, M. X., Knutson, B. et al. (2007). Different neural systems adjust motor behavior in response to reward and punishment. *Neuroimage., 36,* 1253-1262.

Xiong, J., Parsons, L. M., Gao, J. H., and Fox, P. T. (1999). Interregional connectivity to primary motor cortex revealed using MRI resting state images. *Hum.Brain Mapp., 8,* 151-156.

Yacoub, E., Shmuel, A., Pfeuffer, J., Van De Moortele, P. F., Adriany, G., Ugurbil, K. et al. (2001). Investigation of the initial dip in fMRI at 7 Tesla. *NMR Biomed., 14,* 408-412.

Yacubian, J., Glascher, J., Schroeder, K., Sommer, T., Braus, D. F., and Buchel, C. (2006). Dissociable systems for gain- and loss-related value predictions and errors of prediction in the human brain. *Journal of Neuroscience, 26,* 9530-9537.

Yacubian, J., Sommer, T., Schroeder, K., Glascher, J., Kalisch, R., Leuenberger, B. et al. (2007). Gene-gene interaction associated with neural reward sensitivity. *Proc.Natl.Acad.Sci.U.S.A, 104,* 8125-8130.

Yonelinas, A. P., Otten, L. J., Shaw, K. N., and Rugg, M. D. (2005). Separating the brain regions involved in recollection and familiarity in recognition memory. *J.Neurosci, 25,* 3002-3008.

Zilles, K., zur, N. K., Schleicher, A., and Traber, J. (1990). A new method for quenching correction leads to revisions of data in receptor autoradiography. *Histochemistry, 94,* 569-578.

1. Summary (in Catalan Language)

Introducció

Un dels principals interessos de la neurociència cognitiva és la neuroanatomia funcional. Els estudis amb animals i pacients amb lesions cerebrals ja mostraven com dèficits en determinades funcions cognitives estaven relacionats amb la localització de la lesió cerebral. Posteriorment, els estudis de neuroimatge han permès identificar definitivament com funcions cognitives específiques s' associaven amb diferents regions cerebrals. Molts dels avenços en aquesta direcció han sorgit gràcies a la ressonància magnètica funcional (fMRI) , tècnica no-invasiva que mitjançant el que es coneix com efecte BOLD (*Blood-oxigenation-level-dependent*) (Logothetis, 2003) permet relacionar mecanismes d' activitat neuronal amb canvis locals en el consum d' oxigen Combinant aquesta mesura induïda de l' activitat neuronal amb dissenys experimentals enginyosos és possible determinar quines són les àrees del cervell involucrades en una tasca o procés cognitiu concret (Buckner et al., 1996). No obstant, malgrat la importància de poder localitzar diferents unitats funcionals a l'escorça cerebral, s'ha de tenir present que aquestes regions no participen aïlladament, i per tant, s' ha d' estudiar tant la ubicació d' aquestes unitats funcionals així com la dinàmica i les complexes interaccions que suporten els sistemes neuronals del que aquestes en formen part (Catani and ffytche, 2005).

En el cervell humà concorren dos principis complementaris d'organització funcional, segregació i integració. Les primeres teories anatomistes de Gall ja feien referència al

concepte de segregació funcional, on determinades funcions cognitives s'ubicaven en regions cerebrals concretes. Així, la mirada clàssica dels estudis funcionals és localitzacionista, és a dir, es centra en l'associació de funcions específiques segons la seva ubicació en el cervell. Tot i això, a partir d'estudis de lesions cerebrals i de registres d'activitat elèctrica cerebral, tant intracortical com en el cuir cabellut, s'ha pogut observar que aquestes regions no operen de forma independent, sinó que interactuen les unes amb unes altres creant circuits neuronals que depenen d'un context determinat.

Un estudi més complert dels processos cognitius implicaria tant una descripció a nivell regional com la descripció de les interaccions que s'estableixen entre les diferents regions involucrades en el seu processament. La inherent naturalesa multivariant de la ressonància magnètica funcional permet tant la descripció tradicional modular utilitzant anàlisis univariants així com l'estudi de les seves interaccions.

Els estudis de connectivitat funcional assumeixen que aquelles regions que pertanyen a un mateix sistema funcional presenten patrons d'activació similars i per tant, a partir de mesures de covariància, es pot inferir la connectivitat funcional entre diferents regions. Per exemple, a partir de les correlacions (o correlacions parcials) entre diferents regions cerebrals podem explicar l'activitat d'una àrea determinada en funció dels altres elements del sistema (terme conegut com *functional connectivity*, (Friston et al., 1993).

Tot i això, aquest estudis generalment no donen informació sobre la dinàmica existent entre les diferents àrees del cervell. En canvi, els estudis de connectivitat efectiva incorporen causalitat en l' anàlisi, essent possible la descripció i la quantificació de les

influències que una regió exerceix sobre una altra. En particular, permet mesurar quines influències exerceix un sistema neuronal concret sobre un altre (*effective connectivity,* (Friston et al., 1993). Amb aquest propòsit s'han descrit diferents models per tal de poder avaluar les inferències causals existents entre les diferents unitats funcionals involucrades en les xarxes neuronals, com ara els models d'equacions estructurals (Goncalves and Hall, 2003) o de relacions dinàmiques causals (Friston et al., 2003). Tot i això, aquests darrers representen anàlisis de connectivitat cerebral que computacionalment són més complexos que els clàssics, però permeten modelar determinats processos cognitius des d'una vessant més pròxima, donant-li un punt de visat més biològic.

No obstant, un model en el qual diferents unitats funcionals s'integrin a través de relacions causals requereix un suport anatòmic que permeti i moduli les interaccions entre les diferents regions. La connectivitat anatòmica generalment fa referència a l'estudi de la substància blanca, que és la que es pressuposa com a principal font de la connexió i unió entre les diferents regions. Malauradament, un estudi detallat d'aquestes connexions no és fàcil d'obtenir degut a la gran complexitat del cervell i la diferència espacial que hi ha entre els nivells neuronals i la resolució que s' obté en els estudis de neuroimatge de forma no-invasiva. Tanmateix, la introducció i desenvolupament de les imatges de difusió suposa una nova aproximació, molt interesant i prometedora, per a l'estudi de l' arquitectura neuronal que sustenta els diferents processons cognitius.

Així, amb l'objectiu de conèixer l'estructura anatòmica subjacent a aquestes unitats funcionals, sorgeix la importància de la tècnica de *Diffusion Tensor Imaging* (DTI). A través del moviment tèrmic de les molècules d'aigua, aquesta tècnica, relativament

nova, ens permet obtenir informació estructural dels diferents teixits neuronals. A nivell microscòpic els teixits neuronals presenten estructures diferenciades, principalment generades per les membranes cel·lulars, que direccionen el moviment de les molècules d'aigua en funció d'aquestes barreres. El moviment de les molècules d'aigua flueix seguint preferentment l'orientació dels feixos neuronals, i per tant, el recorregut es veu modulat segons els obstacles que ofereix l'estructura tissular. Per exemple, presenten patrons *isotròpics* aquelles regions on l'aigua no segueix cap direcció privilegiada, mentre que aquelles regions que presenten una direcció preferent s'anomenaran regions anisotròpiques (Beaulieu, 2002). Així, una quantificació del moviment de l' aigua, en funció dels índexs que mesuren les influències direccionals que exerceix el medi, permet caracteritzar diferents propietats tissulars.

En aquest marc i mitjançant la combinació d' imatges de fMRI i DTI, l'objectiu d'aquesta tesi doctoral és integrar funció i estructura cerebrals per tal d'obtenir un coneixement més acurat de les funcions cognitives. Per a tal fi, ens centrarem en l'estudi de les diferents unitats funcionals (efectes regionals i les seves possibles interaccions funcionals), així com de les possibles interaccions estructurals (relacions entre funció i micro-estructura).

Experiments

La tesi doctoral consta de cinc experiments cadascun dels quals és independent per ell mateix i pretén donar visions complementàries en l' estudi del cervell humà.

Experiment 1: Aproximació funcional clàssica

Double dissociation of the effects of COMT and dopamine receptor D4 genotypes on brain activations related to valence and magnitude of rewards

La teoria d' aprenentatge per reforçament proposa l' existència d'un sistema intern de predicció d'errors que s'amplifica en aquelles situacions on la resposta obtinguda és pitjor que l' esperada. Aquest senyal influenciaria la nostra resposta en futures decisions modificant les expectatives associades a aquest estímul, i la nostra conducta s' adaptaria a aquella que permetés una recompensa òptima (Sutton and Barto, 1998). No obstant, s'han descrit diferències individuals en aquesta resposta a l'error o al càstig.

Una qüestió interessant que se'ns planteja al respecte és saber en quin grau les diferències individuals observades en el sistema de reforçament són degudes a diferències de la resposta del sistema dopaminèrgic. S'ha proposat que diferents polimorfismes associats a la funció dopaminèrgica podrien explicar parcialment la variabilitat observada (Yacubian et al., 2007). Concretament, dos gens espec
Catechol-o-methyltransferase (COMT) i el receptor dopaminèrgic D4 (DRD4
descrit com especialment rellevants en aquest processament, degut a la seva

importància en la regulació dopamina en les àrees associades a la recompensa (principalment àrees prefrontals i estriatals).

En aquest marc, l'objectiu d'aquest experiment és avaluar possibles influències dels polimorfirmes COMT i DRD4 en el processament del sistema de recompensa a través d'imatges de ressonància magnètica funcional utilitzant una aproximació univariant en una tasca de joc d'apostes. Més concretament, a partir d'una tasca de joc on la recompensa (pèrdues i guanys) es produeix bàsicament a l'atzar, (tasca de *gambling*, Figura 1 adaptada de (Gehring and Willoughby, 2002), es va analitzar el processament de guanys i pèrdues així com possibles diferències individuals associades als polimorfismes COMT Val108Met i DRD4 SNP-521.

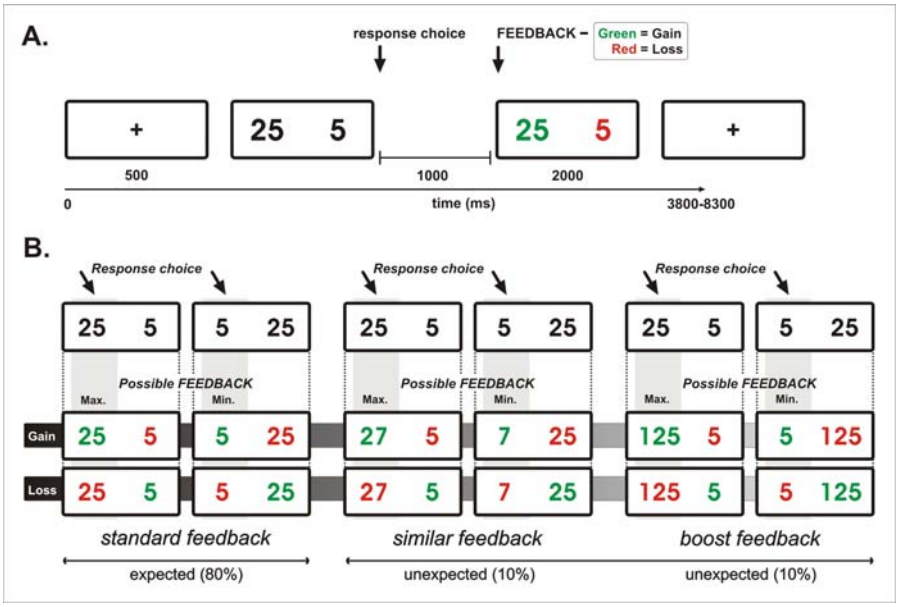

Figura 1: A. Seqüència d'estímuls i respostes utilitzada en la tasca de gambling. Després d'un senyal d' alerta, un parell de números ([5 25] o [25 5]) es presentaven en pantalla. Els participants havien de seleccionar una de les dues opcions prement el botó de la mà dreta o de la mà esquerra. Un segon després de l'elecció, un dels números es convertia en vermell mentre que l'altre es tornava verd (feedback) indicant un guany (verd) o una pèrdua (vermell) de la corresponent quantitat de diners en cèntims d' Euro. B. En la condició de *standard feedback* els participants guanyaven o perdien la mateixa quantitat de diners que ells apostaven. En la condició inesperada de boost feedback la magnitud de la recompensa era molt més gran que la que ells esperaven (10 % probabilitat). En la condició de *similar feedback* la magnitud canviava lleugerament. Aquesta última condició permetia dissociar els efectes de magnitud i de la probabilitat de la recompensa.

Els resultats mostraren que sistemàticament, guanys i pèrdues, activaven el mateix circuit fronto-estriatal-límbic funcional. No obstant, les activacions eren més grans en la condició de guanys que en la de pèrdues, resultats que són congruents amb estudis previs (Nieuwenhuis et al., 2005). A nivell de diferències individuals associades a diferències genètiques, els efectes més importants es van trobar associats al polimorfisme COMT en diverses regions relacionades amb el sistema de recompensa (veure Figura 2).

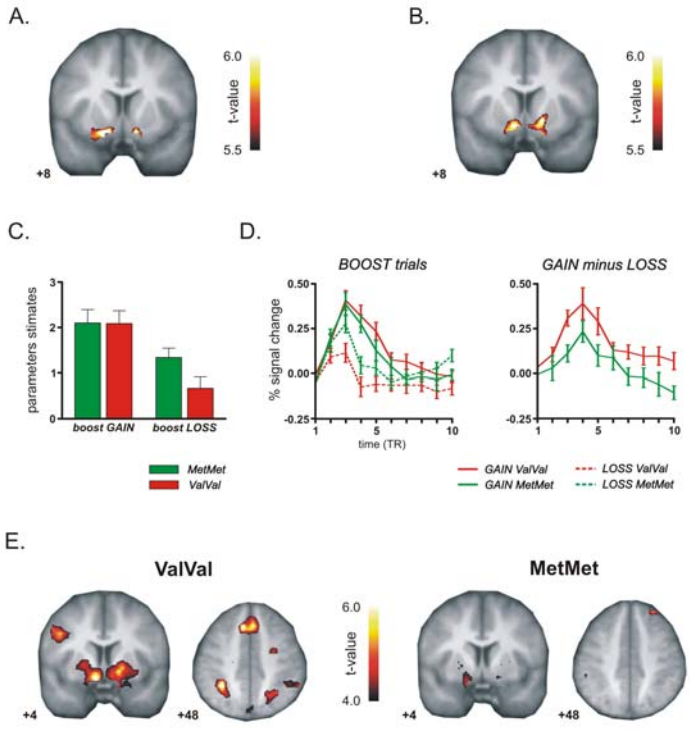

Figura 2: Efectes de valència. Talls coronals del promitjat de grup mostrant els contrast de Guany vs. Pèrdua sobreposat en una imatge estructural de grup en l' espai estereotàctic (els valors de *t* estan indicats després d' haver estat corregit per comparacions múltiples a nivell de tot el cervell, $P < 0.05$). Tant els standard trials (A) (pic *x*, *y*, *z*: -24, 4,-12 mm), com els boost trials (B), (pic, -8, 4, -8 mm), mostraven un increment de l' activitat en l' estriat ventral dret i esquerre. C. Activacions relacionades al sistema de recompensa en la condició de boost (Guanys i Pèrdues) i cada grup COMT. Es mostra un efecte en la reducció de l' activitat en la condició de pèrdua i boost pel grup ValVal. D. BOLD time-course en el pic d' activació del nucli accumbens representat de forma separada pels dos grups COMT (costat esquerra). E. El contrast de Guany i Pèrdua per cada grup COMT (valor de *t*, $P < 0.001$ no corregit). Podem veure que en aquest contrast l' activació en el NAcc, ACC i el IPL en el grup ValVal és molt dèbil en el grup MetMet.

Experiment 2: Aproximació de connectivitat funcional

Functional brain connectivity of reward processing in humans

Mentre que els estudis univariants de ressonància magnètica funcional mos diferències regionals relacionades amb un processament cognitiu concret, els estudis de connectivitat pretenen aportar informació sobre la dinàmica que sustenta i integra les diferents regions modulars activades. Estudis previs suporten la idea que el mateix circuit neuronal processa tant guanys com pèrdues però amb un nivell diferencial d'activitat (Nieuwenhuis et al., 2005). Per contra, altres línies d' investigació suggereixen que són dos circuits diferenciats els que processarien les recompenses i els càstigs (Wrase et al., 2007; Yacubian et al., 2006).

En aquest experiment, utilitzant la mateixa tasca de *gambling* que en l' experiment anterior (Figura 1), es pretén estudiar el processament de guanys i pèrdues en funció de diferències en els patrons de connectivitat funcional utilitzant el mètode proposat per Rissman et al.(Rissman et al., 2004).

L' estudi clàssic univariant funcional mostra que un circuit molt semblant fronto-subcortical-parietal s' activa tant pel processament de guanys com pel de pèrdues. En canvi, examinant els patrons de connectivitat amb l' estriat ventral s' observa un cicuit subcortical-limbic anterior prefrontal diferenciat de l' anàlisi clàssic modular. Ambdós patrons (guanys i pèrdues) presenten una distribució similar que difereixen en el còrtex orbito-frontal per la condició de boost (Figure 3). Aquest estudi mostra que els estudis de connectivitat funcional complementen els estudis funcional univariants.

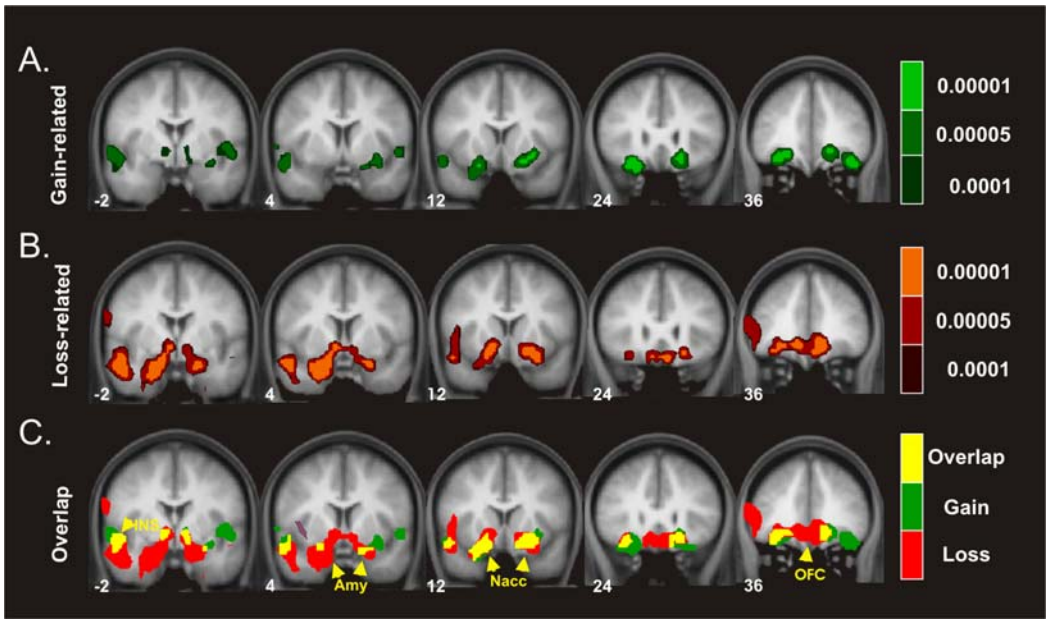

Figure 3: Talls coronals de la mitjana de grup del cervell mostrant les diferents interaccions interregionals entre el estriat ventral i la resta del cervell sobreposat en una imatge estructural de grup en espai estereotàctic (valors de *t* mostrats). La connectivitat funcional s' examina en el sistema de recompensa (A), i en el de càstig (B) utilitzant diferents nivells estadístics (p < 0.0001; p < 0.0005; p < 0.001). Els patrons de guanys i pèrdues es mostren simultàniament a (C): Guany verd; p < 0.001, Pèrdua (vermell; p < 0.001), i conjunció Guany ∩ Pèrdua (groc; P < 0.001 i p < 0.001).

Experiment 3: Aproximació anatòmica utilitzant DTI

Age-related water diffusion changes in human brain:

a voxel-based approach

Els circuits funcionals descrits en els dos experiments anteriors mostren com diferents unitats funcionals segregades anatòmicament participen en el processament de guanys i pèrdues. La presència de feixos neuronals específics que permetin el flux d'informació entre les diferents regions és, per tant, essencial per la seva integració. En aquesta direcció, un coneixement més detallat i exhaustiu sobre els feixos de substància blanca, tal i com ens permetria la tècnica de difusió, pot ser clau per la caracterització de l'arquitectura que conforma la dinàmica cerebral. En aquest context, l'estudi de conceptes com difusió i anisotropia són absolutament bàsics per tal d'interpretar els resultats obtinguts a partir de les imatges de DTI. Coneixements metodològics en l'adquisició de les imatges de DTI així com el seu anàlisi són també eines claus pel seu desenvolupament pràctic.

Considerant la novetat de la tècnica i des d' un punt de vista de familiarització, aquest experiment forma part del procés d' aprenentatge de la tècnica de DTI. En aquest experiment es realitza un anàlisi morfomètric on es mostren correlacions significatives entre l' edat i la substància blanca en diferents regions cerebrals (Figure 4).

En aquest experiment s' emfatitza la part metodològica que requereixen els anàlisis de difusió, així com la importància d' un bon control tècnic a l' hora de la interpretació de les dades. Mostrem la importància d' un bon procés de normalització reportant efectes significatius deguts a problemes metodològics i alhora, es brinden noves consideracions

en les comparatives d'estudis longitudinals utilitzant un anàlisi vòxel a vòxel (*voxel based*). Concretament, es proposa un procediment d' emmascarament per tal de poder distingir diferències micro-estructurals i morfomètriques globals en els estudis d'envelliment (Camara et al., 2007).

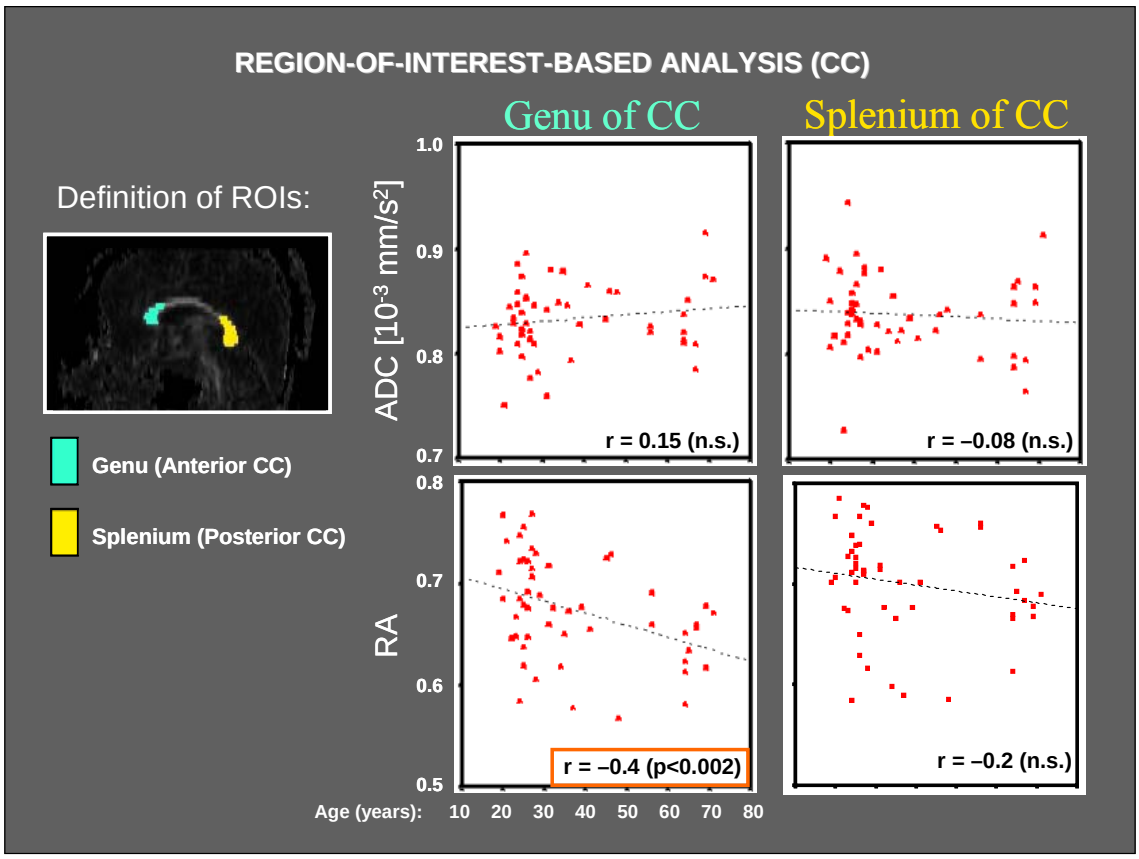

Figura 4: Correlacions entre anisotropia (RA) (a) i coeficient aparent de difusió (b) vs. l' edat en dos regions del cos callós.

Experiment 4: Una aproximació combinada fMRI-DTI en el processament del guany i la pèrdua

Structural white matter brain differences predict functional hemodynamic responses in a reward processing task

La relació entre funció i estructura és una qüestió fonamental en neurociència cognitiva, encara avui en dia oberta, ja que es coneix l'existència de relacions entre funció i estructura a diferents nivells d' organització cerebral però es desconeix quin és el seu paper en l'expressió de les funcions cognitives. Noves línies d' investigació suggereixen interaccions entre connectivitat funcional i estructural, suposant modulacions de les de la resposta funcional en funció de la natura de les seves connexions de substància blanca.

En aquest experiment utilitzant, la mateixa tasca de recompensa que la corresponent als experiments previs (Figura 1), s' avalua la hipòtesi que les diferències individuals en la resposta BOLD en l'estriat ventral podrien ser degudes a diferències en les seves connexions anatòmiques extrínseques. En aquest experiment, correlacionant la resposta diferencial BOLD entre guanys i pèrdues en l'estriat ventral amb les imatges d'anisotropia dels mateixos participants, es va trobar una correlació significativa negativa entre aquests dos paràmetres al fascicle uncinat inferior/ fronto-occipital (Figura 5).

El fascicle uncinat ja s' havia relacionat prèviament amb el feix que connecta el còrtex orbito-frontal i l'estriat ventral (Ungerleider et al., 1989), donant consistència als resultats de connectivitat funcional prèviament mostrats. En aquesta línia, avui en dia no hi ha molts estudis que hagin reportat una correlació directa entre micro-estructura i funció (Rykhlevskaia et al., 2008; Cohen et al., 2008). Aquest experiment obre noves perspectives en l' estudi de la integració entre funció i estructura.

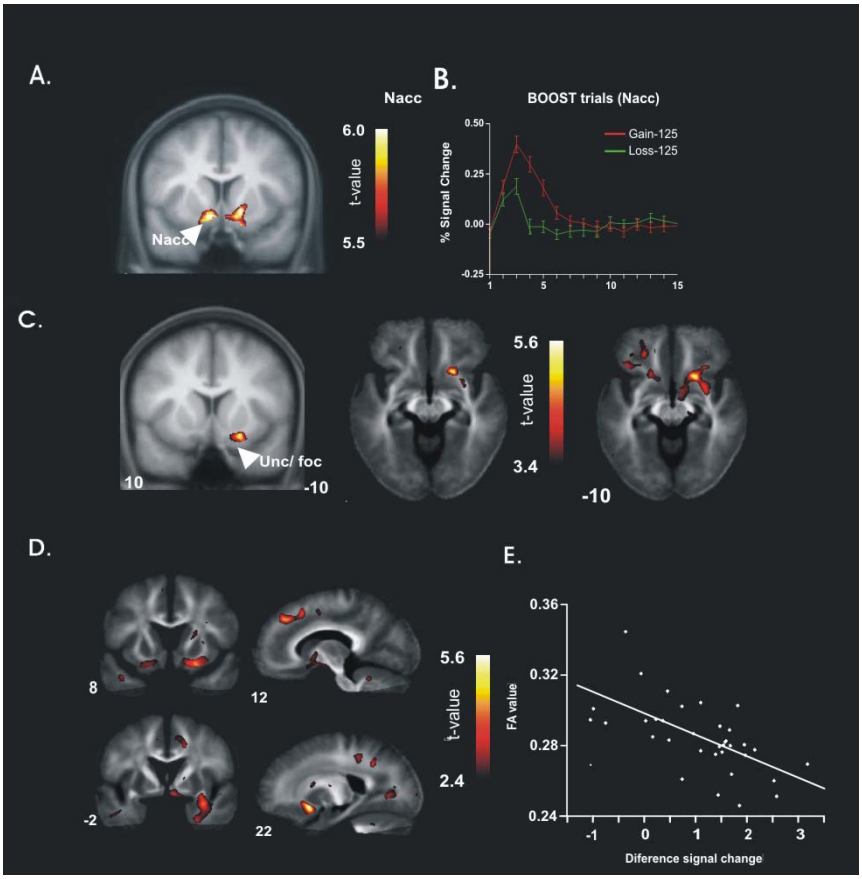

Figura 5:: A. Patró de correlació DTI-fMRI: Es mostra una correlació negativa obtinguda després de correlacionar la diferència dels valors de beta que se'n deriven del contrast guany i pèrdua en la condició de boost (panel B) i els corresponents valors d'anisotropia ($P < 0.001$), (pic 22, 11, -12). Els valors de t estan sobreposat en imatges estructurals coronals de grup en coordenades estereotàctiques MNI B. Imatges addicionals de la correlació entre DTI-fMRI correlacions amb nivells de significació menys conservadors ($P > 0.01$) C. Gràfic on es mostra la correlació entre el valor de beta i l'anisotropia en el mateix pic ($r = 0.613$, $P < 0.00001$).

Experiment 5: Una aproximació combinada fMRI-DTI en la generació de falses memòries

False memories are related to micro-structure of brain white matter

Actualment, molts estudis investiguen possibles relacions funcionals associades a determinats processos cognitius. Així, la relació existent entre la resposta BOLD i l'execució de determinades tasques ha estat una de les mesures més emprades per tal de relacionar funció i cognició. En canvi, des d'un punt de vista micro-estructural aquests efectes no han estat tan estudiats. Tot i això, alguns estudis previs ja mostren que algunes diferències individuals a nivell d' execució d'algunes tasques es pot explicar també a nivell micro-estructural (Toosy et al., 2004; Madden et al., 2004). En aquest experiment proposem que diferències individuals en la recuperació de memòria podrien estar sostingudes per correlats estructurals.

A vegades tenim la sensació de recordar coses que realment no vam passar (falses memòries) (Loftus, 2003) i que no podem diferenciar d'aquelles que són un record real. Dos sistemes de recuperació de memòria diferenciats s'han relacionat en un i un altre procés. Així, s' ha proposat que les memòries reals provindrien d'un accés directe a la informació recuperada, mentre que les falses memòries es generarien en un procés de recuperació semàntica (Brainerd and Reyna, 2002; Schacter et al., 1996). En aquesta mateixa línia, diversos estudis de fMRI han donat suport a aquesta mateixa distinció mostrant que les memòries reals estarien representades per un circuit medial-temporal, mentre que la recuperació de falses memòries tindria una codificació fronto-parietal. (Dennis et al., 2008; Kim and Cabeza, 2007). Tot i això, actualment no hi ha evidències que diferències individuals en la recuperació de memòries viscudes i les

falses puguin ser explicades en termes de diferències anatòmiques. En aquest estudi mostrem que diferències micro-estructurals en els feixos de substància blanca permeten predir diferències en la generació de falses memòries. Concretament, el nivell d' anisotropia del fascicle longitudinal inferior correlacionava amb la recuperació de memòries prèviament viscudes, mentre que els participants que presentaven més tendència a crear falses memòries presentaven valors d' anisotropia més alta en el fascicle longitudinal superior.

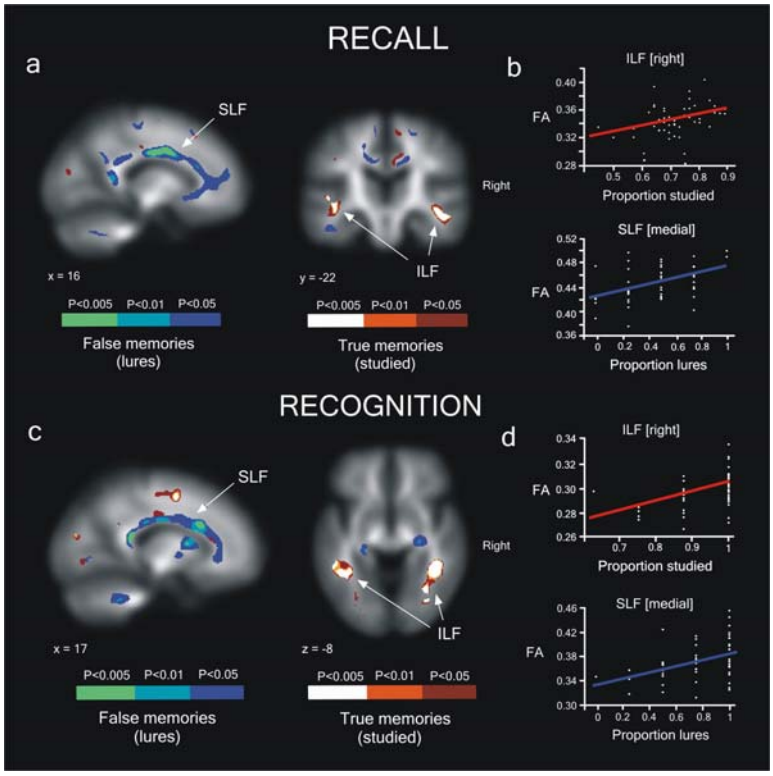

Figura 6: Diferències individuals en correctes i falses memòries (TM/FM) quan es recordaven lliurament i quan es reconeixien associades a diferències en canvis de substància blanca (Fractional Anisotropy, FA). (a) Es mostren els conjunts de voxels que mostraven una correlació significativa entre substància blanca i TM i FM sobreposat amb la imatge d' anisotropia mitjana de grup (P < 0.005). Els mateixos resultats es mostren amb una significació menys conservadora per tal de visualitzar el feix de substància blanca (P < 0.01; P < 0.05;). (b) Gràfics de la mitjana de FA per cada participant en les dues regions d' interès per TM (dreta ILF, pic 46 -25 -13) i FM (dreta SLF, pic 17 -1 34). (c) Els conjunts de voxels de substància blanca més significantiss estan correlacionats amb les puntuacions de reconeixement de TM i FM (P < 0.005; P < 0.05; P < 0.01). (d) Valor mig de FA per cada participant en les regions d' interès més significants per TM (dreta ILF, pic 40 -46 -6) i reconeixement de FM (dreta SFL, pic 21 15 22).

Conclusions

En aquesta tesi hem pogut evidenciar com l'estructura cerebral, i sobretot, la interconnectivitat cerebral, esdevé un factor clau a l'hora d'interpretar, estudiar i caracteritzar el processament cognitiu. Les diferències funcionals observades entre els anàlisis regionals clàssics i els de connectivitat cerebral emfatitzen la importància d'utilitzar les dues informacions com a complementàries en l' estudi dels correlats funcional. A més a més, les correlacions anatòmiques observades tant amb la resposta BOLD com amb mesures conductuals i els nivells d'anisotropia, mostren la importància de traçar l' arquitectura funcional cerebral.

Creiem que els resultats que presentem aporten informació que serà clau a l'hora d'entendre el lligam entre les estructures cerebrals i la resposta funcional de determinades àrees del cervell, mesurada amb la resposta BOLD. Finalment comentar també que els resultats obtinguts en t ermes de diferències individuals obren noves línies d'exploració sobre la relació que existeix entre l'arquitectura cerebral i les funciones mentals.